

LESSONS FROM THE TAYLOR ENERGY OIL SPILL: HISTORY, SEASONALITY, AND
NUTRIENT LIMITATION

by

SARAH JOSEPHINE HARRISON

(Under the Direction of Samantha B. Joye)

ABSTRACT

In 2004, Hurricane Ivan destroyed Taylor Energy platform 23051 in the northern Gulf of Mexico, and oil has leaked from this site into the marine environment since the platform was destroyed, resulting in the nation's longest ongoing offshore oil spill. This thesis explores this site's history and environmental context using publicly available records and field observations. Oil slicks observed at this site are longer and more frequently observed in summer months, coinciding with seasonal wind and riverine discharge patterns. This seasonal nature of the region is further manifested in the biogeochemistry of surface water from the site, with higher nutrient concentrations in the summer compared to fall; hydrocarbon oxidation rates suggest both a seasonally dynamic and persistent community of oil degrading microorganisms in surface water. Lessons learned from the Taylor Energy site can be applied to future oil spill response efforts in the Gulf and beyond.

INDEX WORDS: Oil; Biogeochemistry; Taylor Energy; Gulf of Mexico; Season; Surface Waters; Chemical Dispersant; Inorganic Nutrients

LESSONS FROM THE TAYLOR ENERGY OIL SPILL: HISTORY, SEASONALITY, AND
NUTRIENT LIMITATION

by

SARAH JOSEPHINE HARRISON

A Thesis Submitted to the Graduate Faculty of the University of Georgia in Partial

Fulfillment of the Requirements for the Degree

MASTER OF SCIENCE

ATHENS, GEORGIA

2017

© 2017

Sarah Josephine Harrison

All Rights Reserved

LESSONS FROM THE TAYLOR ENERGY OIL SPILL: HISTORY, SEASONALITY, AND
NUTRIENT LIMITATION

by

SARAH JOSEPHINE HARRISON

Major Professor: Samantha B. Joye

Committee: Patricia M. Medeiros

Mary Ann Moran

Electronic Version Approved

Suzanne Barbour
Dean of the Graduate School
The University of Georgia
December 2017

ACKNOWLEDGMENTS

Many hands helped bring this project over the finish line. I would like to sincerely thank my advisor, Mandy Joye, and committee, Patricia Medeiros and Mary Ann Moran, for their support, advice, and encouragement to finish both my thesis and pursue an internship with the National Oceanic and Atmospheric Administration during my final year of graduate school. I would especially like to thank Mandy Joye for demonstrating that it is possible to research, educate about, and advocate for the ocean.

This project would not have been possible without the support of my lab mates, both past and present; many thanks go out to Mary Kate Rogener, Andy Montgomery, Ryan Sibert, Guangchao Zhang, Cathrine Sheperd, Hannah Chao, Joy Battles, Sarah Herschede, Jessica Washington, Samantha Waters, Sairah Malkin, Lindsey Fields, Lisa Nigro, Matt Saxton, and Kim Hunter. I would also like to thank the science party and crew of Endeavor cruise EN559, especially Leigha Peterson, Kelsey Rogers, and the Montoya Lab from Georgia Tech, for their efforts in collecting the 2015 samples from the Taylor Site. Sincere thanks to the MacDonald Lab at Florida State University for the collection of the 2014 samples.

I would also like the Apalachicola Riverkeeper for connecting me with the Tulane Environmental Law Clinic and Mabelle Hall, who generously provided background documents detailing the site history of the Taylor Energy oil spill. Science does not unfold on a blank stage, and thank you sincerely for allowing me to examine this site through a historical and legal lens.

No part of me would still be standing were it not for the support of my family and friends. My parents, Nat and Tammy, have always encouraged me to follow my dreams and blaze whatever medium I need to make my own way on my own terms, and my sister, Natalie Harrison, has always lent a listening ear and alternative perspective to my own narrow one.

Funding for this research and support for my graduate education has been generously provided by the University of Georgia Graduate School, the Gulf of Mexico Research Initiative's ECOGIG consortium, and the National Science Foundation's Graduate Research Fellowship Program.

This work is dedicated in loving memory of three of the best teachers I ever had: Gale Petronis, Robert Germany, and Vladimir Samarkin.

TABLE OF CONTENTS

	Page
ACKNOWLEDGEMENTS.....	iv
LIST OF FIGURES.....	ix
LIST OF TABLES	xv
CHAPTER	
1. INTRODUCTION.....	1
1.1 Taylor Energy Site History.....	1
1.2 Oil at the Sea Surface	7
1.3 Aims, Objectives, and Thesis Overview	13
References.....	15
2. HISTORICAL EXAMINATION OF SEASONAL VARIATION AT THE TAYLOR ENERGY SITE IN THE NORTHERN GULF OF MEXICO	20
2.1 Introduction.....	20
2.2 Description of the Data	21
2.3 Results	26
2.4 Synthesizing Oil Slick Observations with Meteorological and Riverine Observations from the Taylor Energy Site.....	48
References	53

3	A TALE OF TWO TAYLORS: COMPARISON OF THE TAYLOR ENERGY SITE WITH TWO SEASONALLY DISTINCT TRANSECTS.....	54
	3.1 Introduction.....	54
	3.2 Methods	55
	3.3 Results.....	65
	3.4 Discussion.....	75
	3.5 Conclusion.....	82
	References.....	83
4	AVAILABILITY OF DISSOLVED NUTRIENTS AND CHEMICAL DISPERSANT IMPACTS MICROBIAL COMMUNITES AND POTENTIAL HYDROCARBON OXIDATION RATES IN SURFACE WATER FROM THE TAYLOR ENERGY SITE	85
	4.1 Introduction.....	85
	4.2 Methods and Materials.....	87
	4.3 Results.....	96
	4.4 Discussion.....	107
	4.5 Conclusion.....	111
	References.....	113
5	LESSONS FROM THE TAYLOR ENERGY SITE.....	117
	5.1 Take Home Lessons from this Study.....	117
	5.2 Recognizing a Dynamic and Changing Gulf of Mexico.....	118
	References.....	121

APPENDIX

1. List of Abbreviations.....	123
2. Statistical Analyses.....	125
3. Equations.....	126

LIST OF FIGURES

- Figure 1.1:** The Taylor Energy site in the northern Gulf of Mexico lies southeast of the Mississippi River’s bird-foot delta (a) and is the site where Taylor Energy platform 23051 (b) once stood in Mississippi Canyon lease block 20 (MC20), before being destroyed by an underwater mudslide, triggered by Hurricane Ivan (c). Oil has leaked from the site since the platform fell in 2004.....2
- Figure 1.2** Schematic of the Taylor Energy debris field, before and after Hurricane Ivan toppled the Taylor Energy platform in September 2004. Adapted from BSEE and TEC documents; not drawn to scale.....3
- Figure 1.3.** Photos from the days the platform deck (a) and jacket (b) were removed from the seafloor in 2011. The removal process required several weeks of preparation by divers to excavate and prepare the submerged debris for lifting prior to removal from the seafloor. Images from TEC.....6
- Figure 2.1** NDBC stations in the northern Gulf of Mexico.....24
- Figure 2.2** Reported oil slick length (2.2a) and width (2.2b) at the Taylor Energy site from 2004 to 2016. Each dot represents the reported length or width of a slick attributed to Taylor Energy Company in the northern Gulf of Mexico.....26

Figure 2.3 Reported oil slick length at the Taylor Energy site from 2008-2016 (a). Dot color indicates the month the slick was observed at the Taylor Energy site. The black line is a LOESS curve, a non-parametric locally weighted regression curve. Box plots of reported slick length at the Taylor Energy site from 2008-2016, binned by month (b) and by meteorological seasons (c).....28

Figure 2.4 Reported oil slick frequencies were tabulated monthly, with the total number of days with oil slicks reported divided by the number of days in the month, and plotted over the same period, June 2008- December 2016 (a). Box plots of slick frequency by month (b) and by season (c).....31

Figure 2.5 Taylor Energy Site History from 2004 to 2016. Top panel is the timeline of events documented to have happened at or near the Taylor Energy site that could potentially influence the ability of observers to document oil at the Taylor Energy site. The bottom panel is a plot of the monthly slick frequencies over the site history.....33

Figure 2.6 Photos from TEC following successful removal of Taylor Energy platform 23051 (a) and platform jacket (b) from the seafloor in July and August 2011. Images from TEC.....34

Figure 2.7 Slick frequency data excluding summers 2010 and 2011 (a). Box plots of slick frequency by month (b) and by season (c) with the summers of 2010 and 2011 excluded.....35

Figure 2.8 Box plots of observed (a) oil slick lengths by year (a), estimated oil slick areas by year (b), and reported slick frequencies by year (c) at the Taylor Energy site.....38

Figure 2.9 Wind speed data from BURL1 buoy plotted by day, colored by month, and fitted with a Loess line (a). Wind speed data binned by month (b) and season (c).....40

Figure 2.10 Atmospheric pressure data from PSTL buoy plotted by day, colored by month, and fitted with a Loess line (a). Pressure data binned by month (b) and season (c).....42

Figure 2.11 Wind direction data from PSTL buoy plotted by day, colored by month, and fitted with a Loess line (a). Wind direction binned by month (b) and season (c).....44

Figure 2.12 Data from USGS 07374000 station plotting riverine discharge of the Mississippi River at Baton Rouge through time (a). Each dot represents the average daily value for each variable, colored to represent the month in which that data point was collected. The black line is a Loess curve, a non-parametric locally weighted regression curve. Discharge data by month (b) and season (c).....46

Figure 2.13 Data from USGS 07374000 station plotting dissolved NO_x concentrations of the Mississippi River at Baton Rouge through time (a). Each dot represents the average daily value for each variable, colored to represent the month in which that data point was collected. The black line is a Loess curve, a non-parametric locally weighted regression curve. NO_x data by month (b) and season (c).....47

Figure 2.14 Correlogram of all variables from the publicly available record using a Spearman's Rank Correlation Analysis between each variable.....49

Figure 2.15 Schematic of how oil slicks change across seasons at the Taylor Energy site, with summer on the left, winter on the right.....52

Figure 3.1	Map of (a) the northern Gulf of Mexico, (b) the Taylor Energy site, just 11 miles southeast of the Bird Foot Delta, a slick progressing from the northeast to southwest, and (c) locations of the stations along the 2014 and 2015 transects.....	56
Figure 3.2	Structures of ^{14}C substrates used to quantify hydrocarbon turnover in surface waters. [1- ^{14}C]-n-hexadecane (a) was used as a model linear alkane, and [1,4,5,8- ^{14}C] naphthalene was used as a model aromatic compound (b).....	60
Figure 3.3	Schematic of hydrocarbon oxidation rate method developed by Kleindienst et al. (2015) and Sibert et al. (2016).....	61
Figure 3.4	Average dissolved nutrient concentrations in surface water for each station.....	66
Figure 3.5	GC-FID chromatograms of surface slick samples from each of the stations along the fall 2014 transect.....	68
Figure 3.6	Potential hexadecane oxidation rates by station, yellow bars are from the 2014 transect, green from the 2015 transect.....	69
Figure 3.7	Potential naphthalene oxidation rates by station, yellow bars are from the 2014 transect, green from the 2015 transect.....	71
Figure 3.8	Box plots of the potential hexadecane oxidation rate (a) and potential naphthalene oxidation rate (b) aggregated by transect.....	72
Figure 3.9	Rate constants for hexadecane oxidation, plus or minus the standard deviation among the radiotracer replicates. Bars are colored according to the year the sample was taken.....	73

Figure 3.10	Rate Constants for naphthalene oxidation, plus or minus the standard deviation among the radiotracer replicates.....	74
Figure 3.11	Correlogram of all rates and geochemical parameters from the <i>in situ</i> sampling regime of the Taylor Energy site, using a Spearman's rank correlation test.....	81
Figure 4.1	Map of the Taylor Energy Site in the northern Gulf of Mexico. Regional overview from Google Maps (left); satellite image of the site with oil emanating from the source, demarcated with an X (top right); and a map of surface water sampling locations (shades of blue) featured in this chapter (bottom right).....	88
Figure 4.2	Schematic of experimental design (a) and sampling design (b).....	89
Figure 4.3	Structures of ¹⁴ C substrates used to quantify hydrocarbon turnover in surface waters. [1- ¹⁴ C]-n-hexadecane (a) was used as a model linear alkane, and [1,4,5,8- ¹⁴ C] naphthalene was used as a model aromatic compound (b).....	92
Figure 4.4	Schematic of hydrocarbon oxidation rate method developed by Kleindienst et al. (2015) and Sibert et al. (2016).....	93
Figure 4.5	Bar plots of the dissolved nitrogen species grouped by treatments and shaded by station after incubation for 24h with each respective treatment.....	97
Figure 4.6	Bar plots of ammonium drawdown (a) and total dissolved nitrogen drawdown (b) grouped by treatments and shaded by sites after incubation for 24h with each respective treatment.....	97

Figure 4.7	Bar plots of the dissolved organic carbon (DOC) and dissolved organic nitrogen (DON) concentrations following 24h incubation with each respective treatment. Plots are grouped by treatments and shaded by site.....	99
Figure 4.8	Bar plots of phosphate (a) and total dissolved phosphate (TDP) species (b) grouped by treatments and shaded by site.....	100
Figure 4.9	Bar plots of the phosphate drawdown grouped by treatments and shaded by site.....	100
Figure 4.10	Bar plots of the cell counts (a) and virus like particles (b) grouped by treatments and shaded by site.....	102
Figure 4.11	Bar plots of the potential hexadecane oxidation grouped by treatments and shaded by site.....	103
Figure 4.12	Bar plots of potential naphthalene oxidation rates grouped by treatments and shaded by site.....	105
Figure 4.13	Structure of naphthalene from above and the side with the sp^2 hybrid orbitals in view.....	106
Figure 5.1	Map of oil production platforms and pipelines in the northern Gulf of Mexico; Taylor Energy platform 23051 is marked as a red triangle, while other production platforms are marked as green dots and pipelines as green lines.....	119
Figure 5.2	Comparison of annual oil fluxes from various sources in the Gulf of Mexico in barrels of oil per year.....	121

LIST OF TABLES

Table 2.1	Summary of the Wilcoxon Rank Sum Tests for differences in observed oil slick length by season.....	40
Table 2.2	Summary of the Wilcoxon Rank sum tests for differences in wind speed by season.	
Table 2.3	Summary of the Wilcoxon Rank sum tests for differences in atmospheric pressure by season for PSTL station.....	42
Table 2.4	Summary of the Wilcoxon Rank sum tests for differences in wind direction by season for PSTL station.....	44
Table 2.5	Spearman's Rank Correlation Coefficients (ρ) for slick length data and all other significant metadata from the site.....	50
Table 3.1	Coordinates for the 2014 transect and 2015 transects.....	56
Table 3.2	Table of DNA concentrations for surface water samples from the two Taylor Energy transects and the amplicon barcodes assigned to each sample using the protocol developed by Kozich et al. (2013).....	64
Table 3.3	Table summarizing extractable hydrocarbons for surface water samples from the two Taylor Energy transects.....	67
Table 4.1	Table of potential rates in Kleindienst <i>et al.</i> (2015) and this study.....	108

CHAPTER 1

INTRODUCTION

1.1 Taylor Energy Site History

The Taylor Energy site refers to the area in the northern Gulf of Mexico where Taylor Energy Company (TEC) platform 23051 once stood (Figure 1.1a). The site is 17.7 kilometers southeast of the Mississippi River's bird-foot delta at a depth of 150 meters. The fixed, 8-pile structure (Figure 1.1b) was constructed in 1984, with 28 oil and gas wells extending from the structure into the seafloor, down to reservoirs as deep as 3.35 km deep.

On September 16, 2004, Hurricane Ivan approached Gulf Shores, Alabama as a strong category 3 storm on the Saffir-Simpson scale (Figure 1.1c). The eye of the storm passed 100 km to the east of the Taylor Energy site, inundating the platform with extensive wind and wave action. The storm and subsequent storm surge destabilized the seafloor beneath TEC platform 23051, resulting in an underwater regional slope failure, e.g. an underwater mudslide. As the 8-pile platform fell to the seafloor, its legs twisted and bent, and the platform and jacket were carried to rest 170 m down slope and southeast of its original location. The event buried the deck, jacket, and tangle of pipelines and 28 wells under 30 m of mud and sediment (MMS, 2004). Many of the wells were significantly damaged. Some of the wells were permanently plugged during the

platform's destruction and subsequent journey across the seafloor, while nine of the wells survived and were capable of flow in the immediate aftermath of the platform's destruction.



Figure 1.1 The Taylor Energy site in the northern Gulf of Mexico lies southeast of the Mississippi River's bird-foot delta (a) and is the site where Taylor Energy platform 23051 (b) once stood in Mississippi Canyon lease block 20 (MC20), before being destroyed by an underwater mudslide, triggered by Hurricane Ivan (c). Oil has leaked from the site since the platform fell in 2004, as pictured in the grey box of (a).

Oil was first sighted at the sea surface around the Taylor Energy site and reported to the US Coast Guard (USCG) the day after the hurricane passed through the region, on September 17, 2004 (NRC; SEQNOS ID: 735409). Oil and gas emanated from the seafloor at three discrete locations across the ~30,000 m² debris field: oil Plumes A and B were close to the site of the partially buried jacket and deck, while gas Plume C emanated from the platform's original location (Figure 1.2; FRACE, 2014).

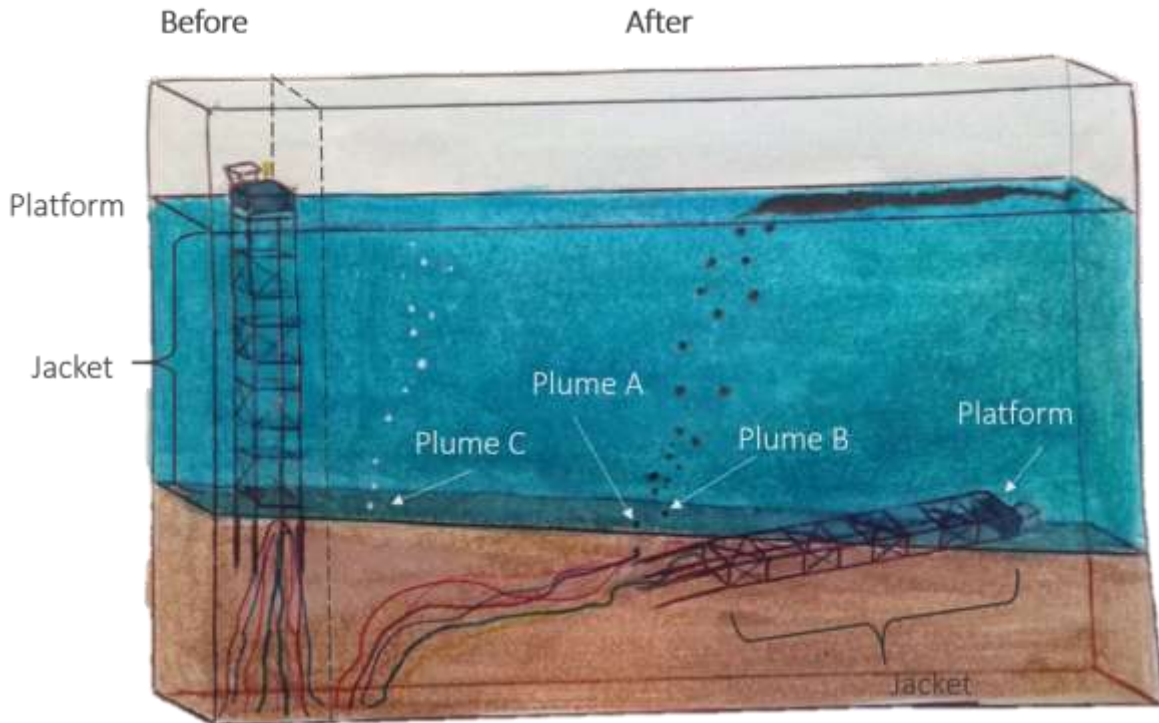


Figure 1.2 Schematic of the Taylor Energy debris field, before (left) and after (right) Hurricane Ivan toppled the Taylor Energy platform in September 2004. Adapted from BSEE and TEC documents; not drawn to scale.

Per the Oil Pollution Act of 1990 (OPA), TEC, the responsible party, is required to pay for the cost of responding to, containing, and/or removing any oil discharged, or taking other actions “as may be necessary to minimize or mitigate damage to the public health or welfare, including, but not limited to, fish, shellfish, wildlife, and public and private property, shorelines, and beaches” (OPA, 1990), regardless of intent. In March 2008, nearly four years after the platform fell, TEC and the Minerals Management Service (MMS) entered into a trust agreement to begin the well decommissioning process. Shortly thereafter, USCG established a Unified Command (UC) comprised of the TEC, USCG, and MMS to oversee response efforts at the site. MMS ordered TEC to plug all wells by June 2008, but TEC failed to meet these demands, claiming that the technology needed to plug the wells at the site did not yet—and still does not—exist. In this

unprecedented type of oil spill, TEC had few options for stopping the flow of oil at the site, and, much like BP in the aftermath of the 2010 *Deepwater Horizon* blowout, TEC pursued a variety of previously untested options for oil well intervention and well containment to stop the flow of oil and gas. Significant efforts were also made to monitor the site for slicks and sheens from mid-2008 onward.

Well Intervention

Dredging the site to access the wells was deemed too much of an environmental hazard and safety risk, and so UC pursued alternative intervention strategies. In August 2008, UC capped nearby pipelines that had been damaged by the storm. Between March 2009 and March 2011, TEC plugged and abandoned nine wells (wells 1, 4, 10, 11, 13, 16, 17, 19, and 21), all of which were capable of flow after the platform collapsed (FRACE, 2014). These efforts eliminated the source of Plume A and Plume B (FRACE, 2014). Drilling intervention wells for the remaining seventeen wells was deemed too risky for both environmental and health standpoints, and only four of the remaining wells were deemed capable of flow (wells 2, 3, 8, and 18). By 2013, UC concluded that intervention activities had stemmed the flow of the nine wells that were capable of leaking oil after the platform fell, preventing the release of 13-500 barrels of oil per day, or 2050-79,500 L of oil per day (FRACE, 2014).

Containment

UC also explored the plausibility of subsea containment systems as early as mid-2008 to address the leaking oil while well intervention operations continued. After a brief design period, three containment domes were installed on the seafloor on May 23, 2009, one over oil Plume A,

another over gas Plume C, and the third over a small gas seep adjacent to Plume C. These containment systems were designed to sit on the seafloor and shunt any leaking oil into a containment vessel that could be tapped from the surface, collected, and disposed of properly onshore. In early 2010, Plume A was eliminated through well intervention activities, yet the containment dome over Plume A's site continued to yield oily water. Controversy remained over whether this oil was from a continued leak or from improper cleaning of the containment dome collection apparatus between deployments. UC concluded that the persistent oil in the containment drum was most likely emanating from oil-soaked sediments at the site, but there is little public data to support or refute this claim.

Clearing the debris field

In early 2010, UC prepared to lift platform debris out from under the sediment and off the seafloor. This endeavor was completed in the summer of 2011 in several steps, first with the recovery of the platform deck in early July 2011 (Figure 1.3a), followed by the jacket several weeks later (Figure 1.3b).

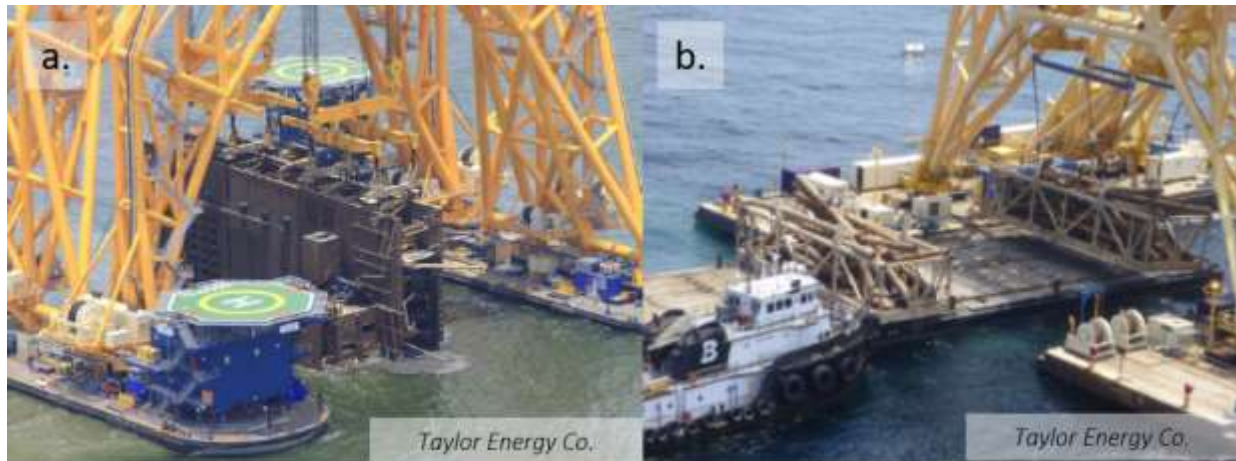


Figure 1.3. Photos from the days the platform deck (a) and jacket (b) were removed from the seafloor in 2011. The removal process required several weeks of preparation by divers to excavate and prepare the submerged debris for lifting prior to removal from the seafloor. Images from TEC.

Site Monitoring

In 2008, as part of the response activities, TEC embarked on an extensive oil slick monitoring program with twice daily overflights of the site. These oil slick sightings were reported to the National Response Center (NRC), operated by USCG. The NRC is the designation point of contact across the U.S. and U.S. territories to report all chemical, radioactive, and/or biological discharges into the environment, including maritime oil spills. The reported information is publicly available, and contains information about the size of the oil slick, wind direction, sea conditions, and information on the party responsible for the spill. From 2004 to 2016, there are over 2,100 discrete NRC reports from the Taylor Energy site where TEC was the designated responsible party (NRC).

The Future of the Taylor Energy spill

As of 2014, TEC has spent an estimated \$435 million on decommissioning activities at the Taylor Energy site. Despite all well intervention and containment efforts to stymie the flow of oil

and gas from the Taylor Energy site, oil slicks at the site persist to this day, and are visible on satellite images of the area (Figure 1.1a). TEC officials contend that the ongoing source of oil at the site is from the oil-soaked sediment at the site, while the natural gas at the site is biogenic in origin (FRACE, 2014). BSEE officials estimate that the volume of oil leaking from this site ranges from 1 barrel of oil to 55 barrels of oil per day and that oil will continue to leak from the site for 100 years (BSEE, 2017).

1.2 Oil at the Sea Surface

The fate of oil in the northern Gulf of Mexico has been intensely studied in the wake of the 2010 *Deepwater Horizon* oil spill, and yet, questions remain about the fate of oil in the marine environment. The Taylor Energy site offers investigators the opportunity to understand how oil moves and is biologically processed through marine waters.

As soon as oil is released into the environment, it undergoes a myriad of processes, collectively referred to as weathering. These processes ultimately transform its chemical composition and dictate the oil's fate in the environment. To determine the fate of oil in the environment and to better respond to future oil spills, these weathering processes must be further characterized and constrained.

With a lighter density than water, oil released into the marine environment usually makes its way to the sea surface, forming oil sheens, slicks, or emulsions of gas, water, and oil commonly referred to as 'mousse'. There are weathering processes unique to surface waters and the euphotic zone, including photo-oxidation, evaporation, and emulsification of oil. The combined

forces of biodegradation and photo-oxidation are the principle drivers of oil's transformation in the marine environment⁷, but very little effort has been put forth to constrain these forces or to set biodegradation into the larger context of the surface water ecosystem, where organic matter and inorganic nutrients are cycled rapidly by microbial communities (Azam *et al.* 2007; Pomeroy *et al.* 1995).

Composition of oil

Petroleum is formed over millions of years from buried organic material subjected to high temperatures and pressures beneath the Earth's surface. This process creates a vastly dynamic mixture that includes solid, liquid, and gaseous hydrocarbons, collectively referred to as petroleum, and thousands of discrete compounds. The liquid phase is better known as crude oil and is comprised of four classes of hydrocarbons: saturates, aromatics, resins, and asphaltenes. The saturated fraction comprises the largest fraction of crude oil by mass, and includes linear, branched, and cyclic alkanes. The aromatic fraction includes benzene and its alkylated sister compounds, toluene, ethylbenzene, and xylene (BTEX), as well as polycyclic aromatic hydrocarbons (PAHs). Although PAHs comprise only a small fraction of oil by mass, these compounds remain some of the most well studied within oil, as known notorious persistent organic pollutants, carcinogens (Guengerich *et al.* 2000), and some have been found to disrupt cardiac function in fish (Incardona *et al.* 2004; Brette *et al.* 2017). The two remaining fractions, resins and asphaltenes, are complex mixtures within themselves. Both fractions contain high molecular weight heteroatomic molecules that have yet to be fully described, but are distinguished functionally by polarity (Peters *et al.* 2005). The asphaltene fraction is readily

precipitated from crude oil upon the addition of a nonpolar solvent, while the resin fraction remains in solution.

Elementally, oil is predominantly carbon and hydrogen, but may also contain quantities of sulfur, oxygen, and nitrogen within organic compounds, particularly in the heteroatomic-rich resin and asphaltene fractions. Oil is also known to contain trace metals, including iron, nickel, vanadium, aluminum, sodium, calcium, copper, and uranium (Peters *et al.* 2005; Spiro *et al.* 2012).

Weathering of Oil

As stated earlier, it is now accepted that oil's composition is not static as it moves through the environment. In the wake of the *Deepwater Horizon* oil spill much research characterized weathered oil found in the sub-tropical, marine and coastal environments (Aeppli *et al.* 2014; Hall *et al.* 2013; Aeppli *et al.* 2012; Kiruri *et al.* 2013; White *et al.* 2016). Within the water column, these weathering processes include degradation by microorganisms, dissolution of the polar fraction, and sedimentation of insoluble constituents. Once at the surface, oil continues to evolve, losing volatile species to the atmosphere, aromatic species via photooxidative processes, and microbial degradation of the oil continues. The oil undergoes a predictable succession, with the disappearance of short chain alkanes and volatile PAHs within a few days. While whole compounds disappear, new functional groups emerge, including carboxylic acids, esters, and ketones and the overall oxygen content of the oil increases (Kiruri *et al.* 2013; Charrie-Duhaut *et al.* 2000).

Satellite data of oil emanating from natural seeps in the Gulf of Mexico has revealed that oil slicks at the sea surface are ephemeral, with a mean residence time of 12 hours and a range of 8-24 hours (MacDonald *et al.* 1993). Once spilled oil reaches the shore, however, it can persist for months (Liu *et al.* 2012; Mendelsohn *et al.* 2012; Turner *et al.* 2014) or decades once buried in the sediment (Reddy *et al.* 2002). Herein lies the oil paradox: oil in surface waters is ephemeral, yet if it arrives onshore, it can persist for a very long time. Understanding the processes and controls on surface slicks will better illuminate the long-term fate of oil in the marine and coastal environments.

Biodegradation of Oil

The study of hydrocarbon degrading microorganisms dates to the early twentieth century, in the infancy of the oil industry and microbiology (Zobell, 1946). Some of the earliest studies of hydrocarbon degradation were conducted in surface waters. By the latter half of the twentieth century, researchers began to understand the ecological context of these microbial metabolisms. Wyndham and Costerton (1982) described adhesion by hydrocarbon degrading bacteria to the underside of surface slicks, resulting in the formation of transparent extracellular polysaccharides (TEP). Recent studies have sought to characterize the formation of these TEPs in the Gulf of Mexico, as TEPs are believed to initiate the formation of marine snow, aggregated matrices of bacteria, phytoplankton, micro-zooplankton, fecal pellets, and other detritus in the water column, and may play an important role in the global carbon cycle (Ziervogel *et al.* 2014; Gutierrez *et al.* 2013).

Controls on hydrocarbon degradation in surface waters remain poorly constrained. Malkin and coauthors demonstrated the important role dissolved nutrients play in regulating hydrocarbon degrading microbial communities in surface waters (Malkin *et al.* in prep). Furthermore, the percolation of oil from the seafloor at natural seeps may also bring dissolved nutrients up to the surface from deeper, nutrient rich waters (D'souza *et al.* 2016). Ziervogel *et al.* (2014) observed the disappearance of short chain alkanes (n-C₁₂ to n-C₂₁) characteristic of fresh oil and enrichment of long chain alkanes (>n-C₂₂) after just four days in the northern Gulf, consistent with what has been observed previously in slightly cooler temperatures (Dutta *et al.* 2000). The rapid and predictable removal of n-alkanes is not surprising considering the recent discovery that strains of the most abundant cyanobacteria, *Prochlorococcus* and *Synechococcus*, intracellularly produce and store linear alkanes (Lea-Smith *et al.* 2015). Some have even speculated that there is a symbiotic relationship between alkanogenic cyanobacteria and hydrocarbon degrading microorganisms in surface waters, which may serve as a reservoir for hydrocarbon degrading microorganisms (Valentine and Reddy, 2015).

Photooxidation of Oil

The saturated fraction of oil has long thought to be resistant to photooxidation, while the aromatic fraction of oil is particularly susceptible to photooxidation, owing to the abundance of delocalized electrons on either side of planar aromatic compounds (Garrett *et al.* 1998). The susceptibility to photooxidation increases with increasing molecular weight and increasing alkyl substitution (Ehrhardt *et al.* 1992; King *et al.* 2014). This process is dramatic and rapid, as demonstrated by King *et al.* (2014)'s work that tracked the disappearance of 80-90% of high molecular weight PAHs after just 12 hours of simulated sunlight. The transformed products of

photooxidation can then enter the DOC pool, where they have been found to be acutely toxic to the common brine shrimp, *Artemia* (Maki *et al.* 2001). Gros *et al.* (2014) demonstrated that photo-oxidation could enrich an oil in the resin-like compounds and in sulfur-containing moieties, while decreasing the abundance of nitrogen-containing species.

Synergistic Weathering Processes and the Fate of Oil in the Environment

Environmental sampling in the wake of the *Deepwater Horizon* oil spill revealed that fate of oil in the marine environment is complex and multifaceted. Work on sand patties found along Gulf Coast beaches has revealed novel oxyhydrocarbons formed from synergistic weathering processes, including the photooxidation of saturated hydrocarbons, a fraction long considered to be photo-resistant (Hall *et al.* 2013). Not all oil that made it to shore evolved into this extremely weathered matrix, as demonstrated by the work of Turner *et al.* (2014) in the oiled marshes of southern Louisiana, which found alkanes and PAHs characteristic of fresh oil in marsh sediment.

Furthermore, there is evidence that much of the oil returned to the seafloor through synergistic weathering processes. Specifically, the biodegradation of oil in surface slicks led to the accumulation of TEPs, triggering the formation of marine oil snow (MOS), which transported at a minimum 14% of the oil discharged during the *Deepwater Horizon* release back to the seafloor in what has been called the Marine Oil Snow Sedimentation and Flocculent Accumulation (MOSSFA) event (Daly *et al.* 2016; Valentine *et al.* 2014). This underwater snowstorm resulted in a footprint of petrocarbon and 17- α -21- β -hopane on the seafloor (Chanton *et al.* 2015; Valentine *et al.* 2014). The impact of this oil deposition is poorly understood, but one study found Macondo oil within a brown flocculent matrix on deep sea corals 11 km southwest of the

blown out well (White *et al.* 2012) and there is evidence a similar deposition occurred in the wake of other major oil spills, including the 1979 IXTOC spill in the southern Gulf of Mexico (Vonk *et al.* 2015). The sedimented petrocarbon on the seafloor may be so weathered that it is no longer within the analytical window of the parent oil it originated from, as evidenced from the work of Stout *et al.* in the years after the Macondo blowout (Stout *et al.* 2016a; Stout *et al.* 2016b).

1.3 Aims, Objectives, and Overview

The Taylor Energy site offers a rare opportunity to explore the impact of oil in surface waters across a dynamic range of biogeochemistry conditions. The first chapter explores the history of the site through careful examination of the public record of slick sightings at the Taylor Energy site, as well as the metadata from the surrounding northern Gulf of Mexico region. This chapter aims to understand the nature oil at the site, as well as understanding potential controls on the fate of oil in surface waters at the site. The next chapter is a biogeochemical comparison of two transects conducted at different times of the year. In the fall of 2014 and the summer of 2015, surface water was collected from four stations approaching the site of the felled platform and assessed for dissolved nutrients, microbial community composition, and capacity for degrading petroleum hydrocarbons using a radiotracer technique. This chapter aims to understand the interseasonal dynamics and controls of hydrocarbon oxidation and community structure in the surface waters near this on-going oil spill. The final chapter of this thesis is an amendment experiment conducted with water from the summer 2015 transect. Water was amended with excess inorganic nutrients (N and P), with Corexit 9500A, a common chemical dispersant, and with a combination of the two to examine how oil spill mitigation efforts might alter the capacity

for the microbial community to degrade petroleum hydrocarbons. The ultimate goal of this project is to shed light on the dynamics and drivers for microbial degradation of oil in surface waters, so that we may be able to better understand and respond to oil spills like the Taylor Energy oil spill.

References

- Aeppli, C.; Carmichael, C. A.; Nelson, R. K.; Lemkau, K. L.; Graham, W. M.; Redmond, M. C.; Valentine, D. L.; Reddy, C. M. Oil Weathering after the Deepwater Horizon Disaster Led to the Formation of Oxygenated Residues. *Environ. Sci. Technol.* **2012**, *46* (16), 8799–8807 DOI: 10.1021/es3015138.
- Aeppli, C.; Nelson, R. K.; Radovic, J. R.; Carmichael, C. A.; Valentine, D. L.; Reddy, C. M. Recalcitrance and Degradation of Petroleum Biomarkers upon Abiotic and Biotic Natural Weathering of Deepwater Horizon Oil. *Environ. Sci. Technol.* **2014**, *48*, 6726–6734.
- Azam, F.; Malfatti, F. Microbial Structuring of Marine Ecosystems. *Nat. Rev. Microbiol.* **2007**, *5* (10), 782–791 DOI: 10.1038/nrmicro1798.
- Brette, F.; Shiels, H. A.; Galli, G. L. J.; Cros, C.; Incardona, J. P.; Scholz, N. L.; Block, B. A. A Novel Cardiotoxic Mechanism for a Pervasive Global Pollutant. *Sci. Rep.* **2017**, *7*, 41476 DOI: 10.1038/srep41476.
- Bureau of Safety and Environmental Enforcement (BSEE) and Bureau of Ocean Energy Management (BOEM). Incident Archive- Taylor Energy Oil Discharge at MC-20 Site and Ongoing Response Efforts. Retrieved 5/1/2017 from <https://www.bsee.gov/newsroom/library/incident-Archive/taylor-Energy-Mississippi-Canyon/ongoing-Response-Efforts>. **2017**.
- Chanton, J.; Zhao, T.; Rosenheim, B. E.; Joye, S. B.; Bosman, S.; Brunner, C.; Yeager, K. M.; Diercks, A. R.; Hollander, D. Using Natural Abundance Radiocarbon To Trace the Flux of Petrocarbon to the Seafloor Following the Deepwater Horizon Oil Spill. *Environ. Sci. Technol.* **2015**, *49*, 847–854 DOI: 10.1021/es5046524.
- Charrie-Duhaut, A.; Lemoine, S.; Adam, P.; Connan, J.; Albrecht, P. Abiotic Oxidation of Petroleum Bitumens under Natural Conditions. *Org. Geochem.* **2000**, *31*, 977–1003.
- D'souza, N. A.; Subramaniam, A.; Juhl, A. R.; Hafez, M.; Chekalyuk, A.; Phan, S.; Yan, B.; MacDonald, I. R.; Weber, S. C.; Montoya, J. P. Elevated Surface Chlorophyll Associated with Natural Oil Seeps in the Gulf of Mexico. *Nat. Geosci.* **2016**, *9* (January), 1–4 DOI: 10.1038/ngeo2631.
- Daly, K. L.; Passow, U.; Chanton, J.; Hollander, D. Assessing the Impacts of Oil-Associated Marine Snow Formation and Sedimentation during and after the Deepwater Horizon Oil Spill. *Anthropocene* **2016** DOI: 10.1016/j.ancene.2016.01.006.
- Dutta, T. K.; Harayama, S. Fate of Crude Oil by the Combination of Photooxidation and Biodegradation. *Environ. Sci. Technol.* **2000**, *34*, 1500–1505.

- Ehrhardt, M. G.; Burns, K. A.; Bicego, M. C. Sunlight-Induced Compositional Alterations in the Seawater-Soluble Fraction of a Crude Oil. *Mar. Chem.* **1992**, *37* (1–2), 53–64 DOI: 10.1016/0304-4203(92)90056-G.
- Garrett, R. M.; Pickering, I. J.; Haith, C. E.; Prince, R. C. Photooxidation of Crude Oils. *Environ. Sci. Technol.* **1998**, *32* (23), 3719–3723 DOI: 10.1021/es980201r.
- Gros, J.; Reddy, C. M.; Aeppli, C.; Nelson, R. K.; Carmichael, C. A.; Arey, J. S. Resolving Biodegradation Patterns of Persistent Saturated Hydrocarbons in Weathered Oil Samples from the Deepwater Horizon Disaster. *Environ. Sci. Technol.* **2014**, *48*, 1628–1637.
- Guengerich, F. P. Metabolism of Chemical Carcinogens. *Carcinogenesis* **2000**, *21* (3), 345–351.
- Gutierrez, T.; Berry, D.; Yang, T.; Mishamandani, S.; McKay, L.; Teske, A.; Aitken, M. D. Role of Bacterial Exopolysaccharides (EPS) in the Fate of the Oil Released during the Deepwater Horizon Oil Spill. *PLoS One* **2013**, *8* (6), e67717 DOI: 10.1371/journal.pone.0067717.
- Hall, G. J.; Frysinger, G. S.; Aeppli, C.; Carmichael, C. a; Gros, J.; Lemkau, K. L.; Nelson, R. K.; Reddy, C. M. Oxygenated Weathering Products of Deepwater Horizon Oil Come from Surprising Precursors. *Mar. Pollut. Bull.* **2013**, *75* (1–2), 140–149 DOI: 10.1016/j.marpolbul.2013.07.048.
- Incardona, J. P.; Collier, T. K.; Scholz, N. L. Defects in Cardiac Function Precede Morphological Abnormalities in Fish Embryos Exposed to Polycyclic Aromatic Hydrocarbons. *Toxicol. Appl. Pharmacol.* **2004**, *196* (2), 191–205 DOI: 10.1016/j.taap.2003.11.026.
- King, S. M.; Leaf, P. a; Olson, A. C.; Ray, P. Z.; Tarr, M. a. Photolytic and Photocatalytic Degradation of Surface Oil from the Deepwater Horizon Spill. *Chemosphere* **2014**, *95* (2014), 415–422 DOI: 10.1016/j.chemosphere.2013.09.060.
- Kiruri, L. W.; Dellinger, B.; Lomnicki, S. M. Tar Balls from Deep Water Horizon Oil Spill - Environmentally Persistent Free Radicals (EPFR) Formation During Crude Weathering. *Environ. Sci. Technol.* **2013** DOI: 10.1021/es305157w.
- Kleindienst, S.; Seidel, M.; Ziervogel, K.; Grim, S.; Loftis, K.; Harrison, S.; Malkin, S. Y.; Perkins, M. J.; Field, J.; Sogin, M. L.; Dittmar, T.; Passow, U.; Medeiros, P. M.; Joye, S. B. Chemical Dispersants Can Suppress the Activity of Natural Oil-Degrading Microorganisms. *Proc. Natl. Acad. Sci.* **2015**, *112* (48) DOI: 10.1073/pnas.1507380112.
- Lea-Smith, D. J.; Biller, S. J.; Davey, M. P.; Cotton, C. a. R.; Perez Sepulveda, B. M.; Turchyn, A. V.; Scanlan, D. J.; Smith, A. G.; Chisholm, S. W.; Howe, C. J. Contribution of

- Cyanobacterial Alkane Production to the Ocean Hydrocarbon Cycle. *Proc. Natl. Acad. Sci.* **2015**, 201507274 DOI: 10.1073/pnas.1507274112.
- Liu, Z.; Liu, J.; Zhu, Q.; Wu, W. The Weathering of Oil after the Deepwater Horizon Oil Spill: Insights from the Chemical Composition of the Oil from the Sea Surface, Salt Marshes and Sediments. *Environ. Res. Lett.* **2012**, 7 (3), 35302 DOI: 10.1088/1748-9326/7/3/035302.
- MacDonald, I. R.; Guinasso, N. L.; Ackleson, S. G.; Amos, J. F.; Duckworth, R.; Sassen, R.; Brooks, J. M. Natural Oil Slicks in the Gulf of Mexico Visible from Space. *J. Geophys. Res.* **1993**, 98 (C9), 16351 DOI: 10.1029/93JC01289.
- MacFayden, A.; Wei, E.; Warren, C.; Henry, C.; Watabayashi, G. Utilization of the Northern Gulf Operational Forecast System to Predict Trajectories of Surface Oil from a Persistent Source Offshore of the Mississippi River Delta. In *2014 International Oil Spill Conference*; 2014; Vol. 53, pp 1689–1699.
- Maki, H.; Sasaki, T.; Harayama, S. Photo-Oxidation of Biodegraded Crude Oil and Toxicity of the Photo-Oxidized Products. *Chemosphere* **2001**, 44 (5), 1145–1151.
- Mendelssohn, I. A.; Andersen, G. L.; Baltz, D. M.; Caffey, R. H.; Carman, K. R.; Fleeger, J. W.; Joye, S. B.; Lin, Q.; Maltby, E.; Overton, E. B. Oil Impacts on Coastal Wetlands: Implications for the Mississippi River Delta Ecosystem after the Deepwater Horizon Oil Spill. *Bioscience* **2012**, 62 (6), 562–574 DOI: 10.1525/bio.2012.62.6.7.
- Pomeroy, L. R.; Sheldon, J. E.; Sheldon, W. M.; Peters, F. C. Limits to Growth and Respiration of Bacterioplankton in the Gulf of Mexico. *Mar. Ecol. Prog. Ser.* **1995**, 117, 259–268.
- Reddy, C. M.; Eglinton, T. I.; Hounshell, A.; White, H. K.; Xu, L.; Gaines, R. B.; Frysinger, G. S. The West Falmouth Oil Spill after Thirty Years: The Persistence of Petroleum Hydrocarbons in Marsh Sediments. *Environ. Sci. Technol.* **2002**, 36 (22), 4754–4760.
- Sibert, R. J.; Harrison, S. J.; Joye, S. B. Protocols for Radiotracer Estimation of Primary Hydrocarbon Oxidation in Oxygenated Seawater. In *Hydrocarbon and Lipid Microbiology Protocols*; McGenity, T. J., Timmis, K. N., Nogales, B., Eds.; Humana Press, 2016; pp 263–276.
- Simister, R. L.; Poutasse, C. M.; Thurston, A. M.; Reeve, J. L.; Baker, M. C.; White, H. K. Degradation of Oil by Fungi Isolated from Gulf of Mexico Beaches. *Mar. Pollut. Bull.* **2015**, 100 (1), 327–333 DOI: 10.1016/j.marpolbul.2015.08.029.
- Spiro, T. G.; Purvis-Roberts, K. L.; Stigliani, W. M. *Chemistry of the Environment*; University Science Books, 2012.

- Stout, S. A.; Payne, J. R. Macondo Oil in Deep-Sea Sediments: Part 1 -- Sub-Sea Weathering of Oil Deposited on the Seafloor. *Mar. Pollut. Bull.* **2016**, *111* (1–2), 365–380 DOI: 10.1016/j.marpolbul.2016.07.036.
- Stout, S. A.; Payne, J. R.; Ricker, R. W.; Baker, G.; Lewis, C. Macondo Oil in Deep-Sea Sediments: Part 2 -- Distribution and Distinction from Background and Natural Oil Seeps. *Mar. Pollut. Bull.* **2016**, *111* (1–2), 381–401 DOI: 10.1016/j.marpolbul.2016.07.041.
- Taylor Energy Company LLC MC20. FRACE: Final Risk Assessment and Cost Estimate. Unified Command Summary. March 25-26, **2014**.
- Taylor Energy Company, LLC. v United States Department of the Interior , No. 09-1029, Mem. Op. (Washington, D.C. Aug. 31, 2010). **2010**.
- The Biomarker Guide*; Peters, K. E., Walters, C. C., Moldowan, J. M., Eds.; Cambridge University Press, 2005; Vol. 1.
- Turner, R. E.; Overton, E. B.; Meyer, B. M.; Miles, M. S.; McClenachan, G.; Hooper-Bui, L.; Engel, A. S.; Swenson, E. M.; Lee, J. M.; Milan, C. S.; Gao, H. Distribution and Recovery Trajectory of Macondo (Mississippi Canyon 252) Oil in Louisiana Coastal Wetlands. *Mar. Pollut. Bull.* **2014**, *87* (1–2), 57–67 DOI: 10.1016/j.marpolbul.2014.08.011.
- United States Department of Interior, Minerals Management Service. MMS Updates Damage Assessment from Hurricane Ivan. (New Orleans, Oct. 8, 2004). Retrieved 4/27/2017 from <https://www.bsee.gov/sites/bsee.gov/files/news/news-item/mms-press-release-1008a.pdf>. 2004.
- Valentine, D. L.; Fisher, G. B.; Bagby, S. C.; Nelson, R. K.; Reddy, C. M.; Sylva, S. P.; Woo, M. a. Fallout Plume of Submerged Oil from Deepwater Horizon. *Proc. Natl. Acad. Sci.* **2014** DOI: 10.1073/pnas.1414873111.
- Valentine, D. L.; Reddy, C. M. Latent Hydrocarbons from Cyanobacteria. *Proc. Natl. Acad. Sci.* **2015**, *112* (12), 201518485 DOI: 10.1073/pnas.1518485112.
- Vonk, S. M.; Hollander, D. J.; Murk, A. T. J. Was the Extreme and Wide-Spread Marine Oil-Snow Sedimentation and Flocculent Accumulation (MOSSFA) Event during the Deepwater Horizon Blow-out Unique? *Mar. Pollut. Bull.* **2015**, No. February 2016 DOI: 10.1016/j.marpolbul.2015.08.023.
- White, H.; Hsing, P.-Y.; Cho, W.; Shank, T. M.; Cordes, E. E.; Quattrini, A. M.; Nelson, R. K.; Camilli, R.; Demopoulos, A. W. J.; German, C. R.; Brooks, J. M.; Roberts, H. H.; Shedd, W.; Reddy, C. M.; Fisher, C. R. Impact of the Deepwater Horizon Oil Spill on a Deep-Water Coral Community in the Gulf of Mexico. *PNAS* **2012**, 1–6 DOI: 10.1073/pnas.1118029109.

Wyndham, R. C.; Costerton, J. W. Bacterioneston Involved in the Oxidation of Hydrocarbons at the Air-Water Interface. *J. Great Lakes Res.* **1982**, 8 (2), 316–322 DOI: 10.1016/S0380-1330(82)71972-0.

Ziervogel, K.; D'Souza, N.; Sweet, J.; Yan, B.; Passow, U. Natural Oil Slicks Fuel Surface Water Microbial Activities in the Northern Gulf of Mexico. *Front. Microbiol.* **2014**, 5 (May), 188 DOI: 10.3389/fmicb.2014.00188.

Zobell, C. E. Action of Microorganisms on Hydrocarbons. *Bacteriol Rev.* **1946**, 10 (1–2), 1–49.

CHAPTER 2

HISTORICAL EXAMINATION OF SEASONAL VARIATION AT THE TAYLOR ENERGY SITE IN THE NORTHERN GULF OF MEXICO

2.1 Introduction

In September 2004, Hurricane Ivan destroyed Taylor Energy platform 23051, an 8-pile structure originally built 17.7 km southeast of the Mississippi River's bird-foot delta in the northern Gulf of Mexico. The destruction of the platform and its 28 operational wells has led to pervasive oil slicks at the site since the platform fell thirteen years ago. Despite the duration of this oil spill, very little has been done to assess the magnitude of this oil spill or its impact of this oil on coastal waters in the Gulf of Mexico.

The northern Gulf of Mexico is no stranger to seasonal oscillations. This region experiences seasonal variations in freshwater inputs from the Mississippi River plume as well as variations in atmospheric conditions, including wind speed, direction, and rainfall. One prominent example of how these riverine and meteorological conditions manifest to alter the nature of the water column is in the annual hypoxic event known as 'The Dead Zone' (Rabalais *et al.* 2002). Nutrient loading from the Mississippi and Atchafalaya rivers in the spring delivers large amounts of inorganic nutrients and labile riverine carbon to offshore microbial communities, which rapidly utilize these inputs in the shallow coastal water column. This nutrient loading in the spring is followed by periods of stable atmospheric pressure in the summer, which minimizes surface

water mixing within the shallow (<100 m) water column. These riverine, atmospheric, and marine processes converge to deplete the supply of dissolved oxygen in the water column to hypoxic levels (< 2 mg/L). The 2017 ‘Dead Zone’ was the largest on record, stretching over 22,700 km², an area the size of the state Connecticut.

This location offers investigators a rare opportunity to explore the impact of oil in surface waters across a dynamic range of biogeochemical and seasonal conditions. This chapter will collect and describe all publicly available data on the Taylor Energy site and explore how oil slicks and other variables change seasonally at this highly dynamic site. The goal is to put these data in environmental context, describing how atmospheric and riverine influences converge to shape the fate of oil in the marine environment. This effort will better inform stakeholders and first responders to future oil spills in the northern Gulf of Mexico.

2.2 Description of the Data

The data included below was collected from a variety of public sources, including the U.S. Geological Survey (USGS), U.S. Coast Guard (USCG), and the National Oceanographic and Atmospheric Administration (NOAA).

2.2.1 *Oil Slick Observational Data*

Oil slick data was collected from the National Response Center and is presently housed by the U.S. Coast Guard (USCG)'s Maritime Information Exchange (CGMIX). The National Response Center is a massive database, including every reported chemical spill across the entire U.S. and

its territories, including both federal and state waterways. This data repository is comprised of voluntary reports from individuals after witnessing a chemical spill and/or fire to which might require emergency response, much like a 9-1-1 emergency line. Reports filed with the NRC can include precise coordinates of the slick, a quantitative slick description (length, width, area, etc.), qualitative slick descriptions (e.g. "silvery", "rainbow", etc.), and various levels of meteorological and maritime observations (wind speed, direction, sea state, etc.), along with number of injured persons, responsible party, and fire details.

For this study, only oil slick records that included the Taylor Energy Company (TEC) as the responsible party and located in the region of the felled oil platform in MC20 were included. The record of observed oil slicks is inconsistent in its coverage, because the information was collected for regulatory rather than research purposes.

Oil slick dimensions were extracted from the database, converted into kilometers from the various reporting units, and ordered so that if a difference in length versus width was reported, length was always greater than the width. For days with multiple filed NRC reports, the average of all observations were used to describe a slick to not oversample the data. For days in the record where no slick was reported, value is "N/A" rather than assumed to be zero, as it cannot be assumed the site was surveyed for oil.

A Shapiro-Wilk normality test concluded that the slick length data does not have a normal distribution ($p\text{-value} < 2.2 \times 10^{-16}$), and so non-parametric modes of analysis were used to analyze the variance of the slick length data. Kruskal Wallis rank sum tests were used to analyze for variance of populations, and Wilcoxon rank sum tests were used to test for significant differences between populations.

2.2.2 Buoy Data and Atmospheric Observations

Information on atmospheric conditions was explored using data collected from nearby observational buoys. The National Data Buoy Center (NDBC) is a unique part of the National Oceanic and Atmospheric Administration (NOAA)'s National Weather Service (NWS). The NDBC oversees, designs, and operates a global array of data collecting buoys and coastal stations, including many stations in the lower Mississippi River and the northern Gulf of Mexico. Six candidate stations were selected from the NDBC database to gather data from as many stations surrounding the Taylor Energy site, including other offshore stations (Figure 2.1). However, there was either no accessible or usable data from the closest offshore stations, including the KMIS station (operated by the Federal Aviation Administration) or either of the stations operated by private organizations (Stone Energy platform and CGCL, operated by Shell). Instead data was curated from the three observation stations in and near the bird-foot delta.

For this study, buoy data from three NDBC stations were examined: BURL1, PSTL, and PILL1 (Figure 2.1).

1. Station BURL1 is located due Southwest of the Southwest Pass, LA and is owned and maintained by National Data Buoy Center. BURL1 Coordinates: 28.905 N 89.428 W (28°54'18" N 89°25'42" W). The buoy located at sea level. Data collected 2009-2016.
2. Station PSTL1 (Buoy ID: 8760922) is located at Pilot's Station East, Southwest Pass, LA, and is owned and maintained by NOAA's National Ocean Service Water Level Observation Network. PSTL1 coordinates: 28.932 N 89.407 W (28°55'56" N 89°24'25" W). The site is located 3.6 m above mean sea level. Data collected 2006-2016.

- Station PILL1 (Buoy ID: 8760721) in Pilottown, LA is owned and maintained by NOAA's National Ocean Service Water Level Observation Network. PILL1 coordinates: 29.179 N 89.259 W (29°10'45" N 89°15'32" W). The site is located 2.3 m above sea-level. Data collected 2011-2016.



Figure 2.1 NDBC stations in the northern Gulf of Mexico. Buoys with records featured in this discussion are in red. Candidate buoys without abundant or accessible data are in pink. The coordinates of the Taylor Energy site are demarcated by a black diamond.

Buoys featured in this study collected data on wind direction, wind speed, maximum sustained gust, barometric pressure, air temperature, and water temperature, however, only wind speed, barometric pressure, and wind direction are discussed in this study. Data was extracted from these sources, manually aligned, and averaged into daily average values, as many of these observations were collected at variable intervals, ranging from every five minutes to once per day.

2.2.3 Mississippi River Data

Another important component of this region of the northern Gulf of Mexico is the Mississippi River, the largest river in North America. The river has seasonal variations with respect to discharge rates (flow) and nutrient loading. The U.S. Geological Survey (USGS) collects data on rivers through their National Water Information System program. USGS Station 07374000 is located at 30°26'44.4", 91°11'29.6" near Baton Rouge, LA and is operated by the USGS Baton Rouge Field Station, home of the Lower Mississippi—Gulf Water Science Center.

Although this station is 80 km upriver from the Gulf of Mexico, the station is one of the most well documented in the Lower Mississippi River. Observations from this station include water temperature, river discharge, river gage height, specific conductivity at 25°C, pH, salinity, stream level, turbidity, and dissolved NO_x^- (sum of $\text{NO}_3^- + \text{NO}_2^-$ in water). For this study, only temperature, discharge, and NO_x^- are discussed.

2.3 Results

2.3.1 Oil Slick Observations

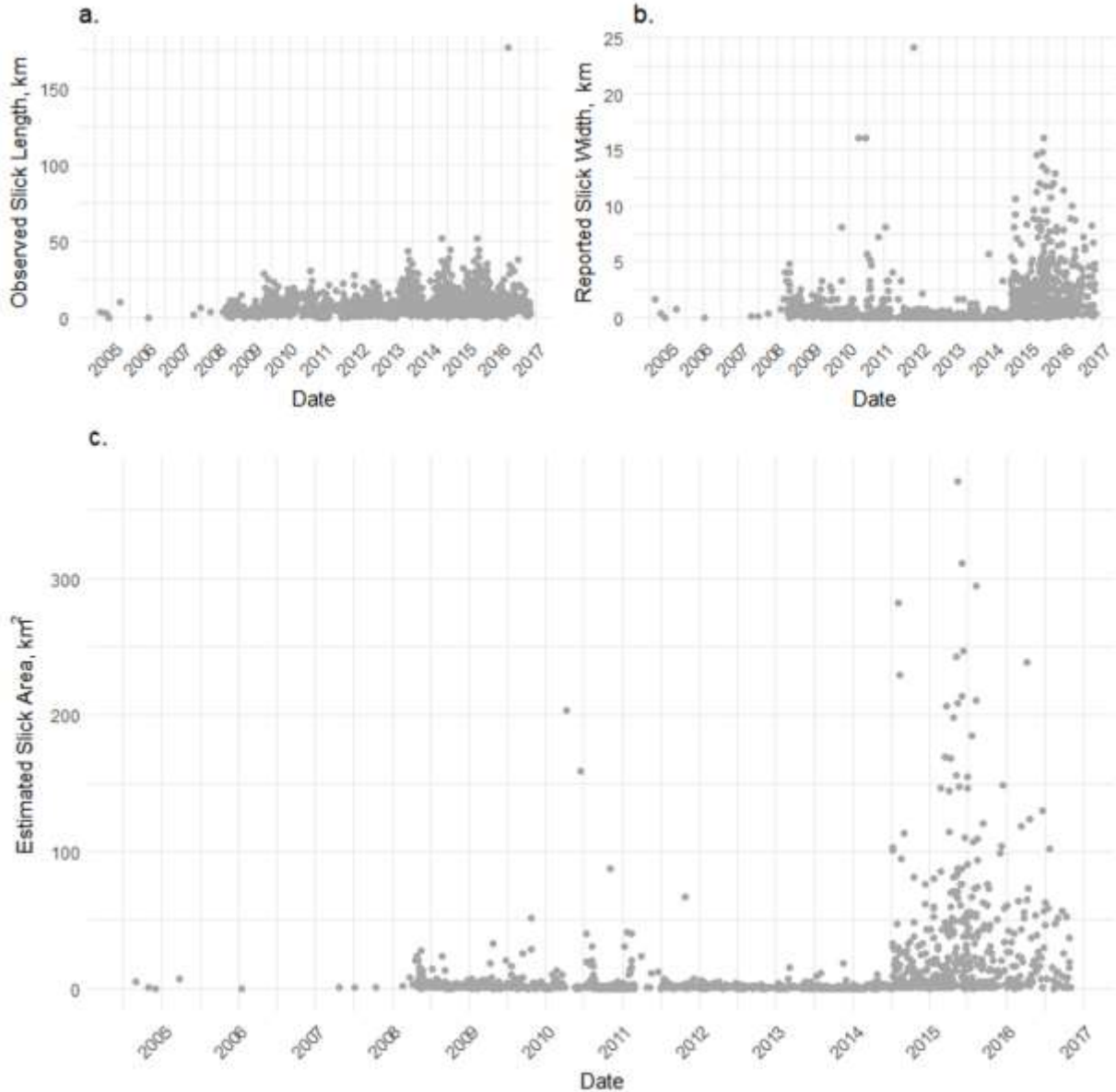


Figure 2.2 Reported oil slick length (2.2a) and width (2.2b) at the Taylor Energy site from 2004 to 2016. Each dot represents the reported length or width of a slick attributed to Taylor Energy Company in the northern Gulf of Mexico. All slick lengths were converted into kilometers from the reported unit(s). The oil slick surface area values (2.2c) are an estimation that uses the reported slick length and width to calculate the area of an ellipse as the total surface area of the slick $((\text{Length}/2) \times (\text{Width}/2) \times \pi)$.

The first oil slick sighting attributed to Taylor Energy was recorded on September 14, 2004. From September 14, 2004 to December 31, 2016, there were 2,083 days out of the 4445 day record with observed oil slicks in the vicinity of the felled platform and which the CGMIX database listed TEC as the responsible party (Figure 2.2). This amounts to an average of 0.468 slicks sighted per day or 1 oil slick every 2.14 days. The reported slick length values range from 0.27 m to 176 km; observed slick widths vary from 1.2 m to 24 km. To better ascertain the relative size of these slicks through time, the length and width values were used to calculate the area of an ellipse, a more conservative estimate than a rectangular surface area (Fig 2.2c). These estimated areas range from 0.000016700 to 471.78989 km². Historic profiles of slick width (Figure 2.2b) and slick area (Figure 2.2c) have the similar profiles, indicating that the upward trend through time in surface area and overall variance of the surface area data set is driven by the values of the reported slick widths. There is also a sharp increase in the reported values for the oil slick width in mid-2014.

2.3.1.1 Observed Oil Slick Length at the Taylor Energy Site

The slick length data can be used to explore intra- and inter-annual variation of oil slicks at the Taylor Energy Site. Although the record stretches back to September 2004 (Fig 2.1), the frequency of reports increased steeply in mid-2008, when the USCG established a Unified Command (UC) to respond to the ongoing oil sightings at the Taylor Energy site (FRACE, 2014). The data for the following section, thus, will only contain data from June 1, 2008-December 31, 2016. A closer look of the reported slick length reveals that length of the oil slick sighted varies sinusoidally through time (Figure 2.3a).

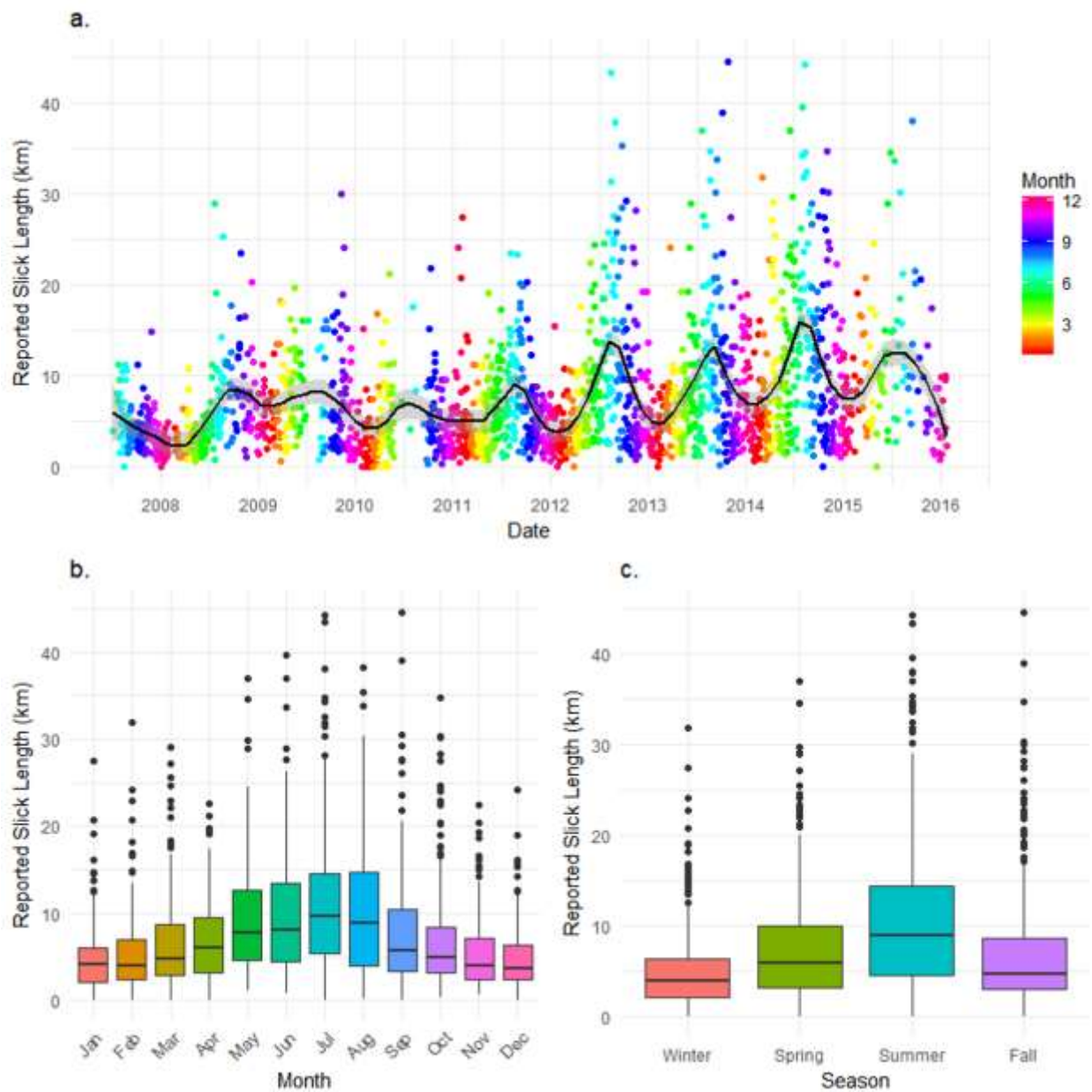


Figure 2.3 Reported oil slick length at the Taylor Energy site from 2008-2016 (a). Dot color indicates the month the slick was observed at the Taylor Energy site. The black line is a Loess curve, a non-parametric locally weighted regression curve. Box plots of reported slick length at the Taylor Energy site from 2008-2016, binned by month (b) and by meteorological seasons (c). Note the y-scale has been limited to 0-45 km to highlight the seasonal trend, but no data has been omitted from the period.

A pair of Kruskal-Wallis rank sum tests found that the population of oil slick length observations varies significantly between months (Kruskal-Wallis chi-squared = 248.22, df = 11, p-value < 2.2e-16) and between meteorological seasons (Kruskal-Wallis chi-squared = 203.66, df = 3, p-value < 2.2e-16). Examination between seasonal pairings with a series of Wilcoxon Rank sum tests detected significant differences between all seasonal pairings (Table 2.1)

Table 2.1 Summary of the Wilcoxon Rank Sum Tests for differences in observed oil slick length by season.

	Spring	Summer	Fall	Winter
Spring	<i>n/a</i>			
Summer	W = 103440, p-value = 1.214e-11	<i>n/a</i>		
Fall	W = 138360, p-value = 0.002871	W = 103020, p-value < 2.2e-16	<i>n/a</i>	
Winter	W = 154930, p-value = 1.839e-15	W = 178150, p-value < 2.2e-16	W = 160950, p-value = 5.315e-08	<i>n/a</i>

These data provide substantial evidence that there is a seasonal variation with respect to the observed oil slick length at the Taylor Energy site in the northern Gulf of Mexico. There are significantly longer slicks observed in the summer months compared to the spring and fall months, and the smallest slicks are observed in the winter months. However, the way that the slick length data was collected is not listed on the CGMIX webpage or documented in any way, and so the value of these data should be taken with caution and may not reflect a true seasonal oscillation of slick size at the Taylor Energy site. Additionally, the observed seasonal oscillation does not necessarily reflect a seasonal oscillation in the rate of oil leaking from the Taylor Energy site.

2.3.1.2 Observation Frequency of Oil Slicks at the Taylor Energy Site

To circumvent the questionable quality of the observational oil slick data, the frequency of oil slick sightings can be used to examine the seasonal difference in the number of days with an oil slick(s) reported at the Taylor Energy site. The data included in this section uses the same data as the previous section, but instead of taking the value of the observation, this section examines the number of reports per month, reported as Slick Frequency (Equation 2.1).

$$F_s = \frac{[\textit{number of days with reported slick(s) in the month}]}{[\textit{total number of days in the month}]} = n_s/n_{total}$$

Equation 2.1

The seasonal oscillations are not immediately apparent in this examination of the dataset (Figure 2.4a), nor did statistical tests detect differences in slick frequency by month or by season. The seasonal trend is somewhat apparent when examining the data by season (Figure 2.4c), and much less apparent when examining the data by calendar month (Figure 2.4b). This is driven by high amounts of variance of slick sighting frequency for May, June, July, and August months compared to all other months.

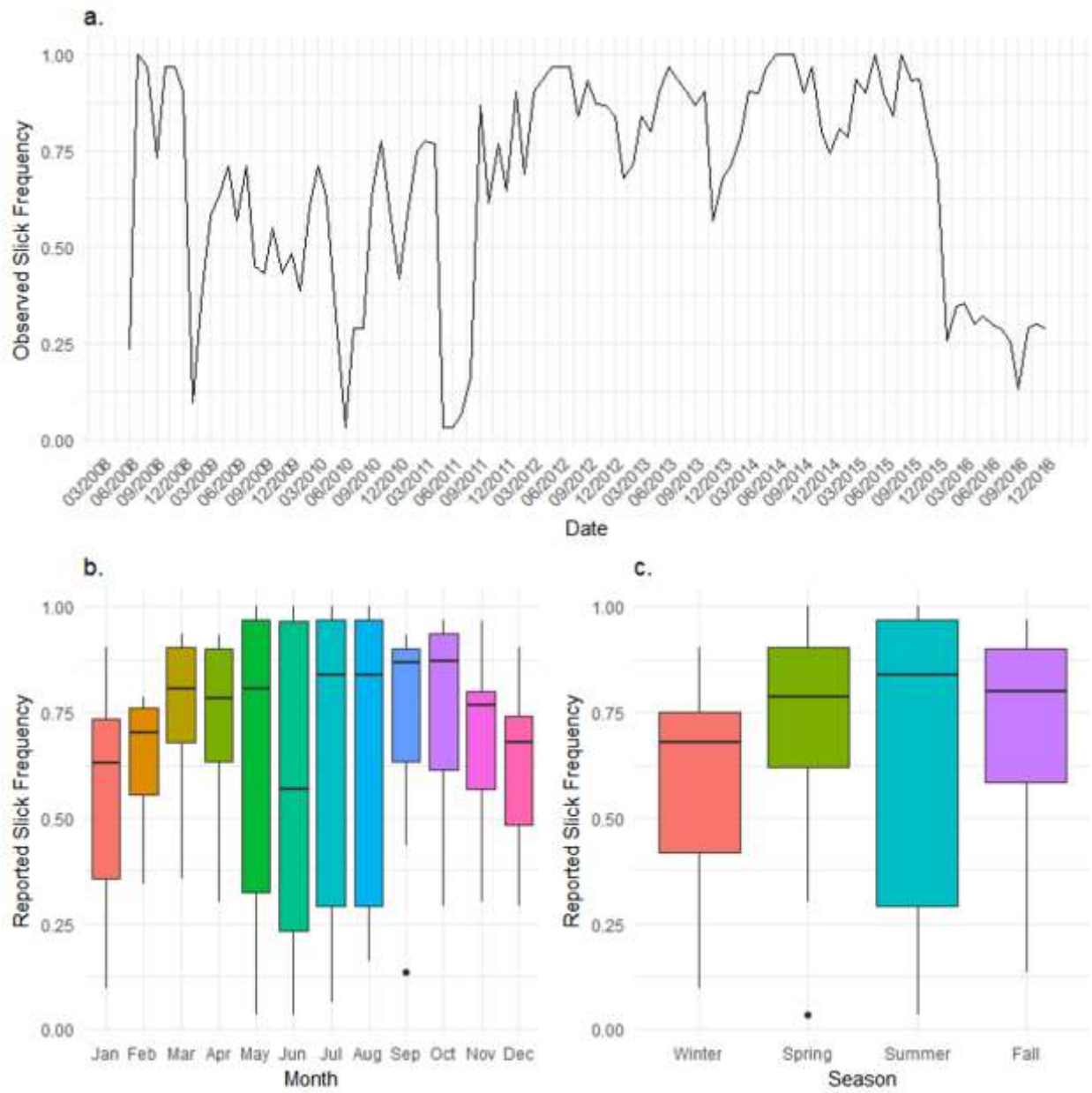


Figure 2.4 Reported oil slick frequencies were tabulated monthly, with the total number of days with oil slicks reported divided by the number of days in the month, and plotted over the same period, June 2008-December 2016 (a). Box plots of slick frequency by month (b) and by season (c).

To understand the sources of this variance, we must examine the entire record of data (Figure 2.1), which contains three substantial data gaps, which can be better understood if we consider the complex site history of the Taylor Energy site (Figure 2.5).

The first major gap is from September 2004 to June 2008, when a total of 11 oil slicks were reported at the site in approximately 3.75 years. This sparse record reflects the fact that the Unified Command to coordinate the joint industry and federal response effort for the Taylor Energy oil spill was not established until mid-2008. This process formally began in March 2008, when the Department of Interior's Minerals Management Service (MMS) entered a trust agreement with Taylor Energy Company to pay for the response effort (FRACE, 2014).

The second major gap in the data set extends from May 2010 to August 2010. This gap coincides with the *Deepwater Horizon* accident, the largest offshore oil spill in U.S. history. The spill began on April 20, 2010 and lasted until July 15, 2010, when BP successfully plugged the Macondo well. This spill occurred in Mississippi Canyon Lease Block 252 (MC252), only 62 km to the southeast of the site of Taylor Energy platform 23051 in Mississippi Canyon Lease Block 20 (MC20). It is likely that many of the oil slicks reported during this time were mistakenly attributed to the *Deepwater Horizon* oil spill.

Finally, the third gap in the data set occurred from May to August 2011 and coincided with the TEC's efforts to remove debris from the seafloor at the Taylor Energy site. This multi-year effort culminated with the recovery of the platform deck in early July 2011 and the platform jacket in August 2011. Images from the Taylor Energy Company reflect that the site was heavily occupied during these months, thereby obscuring observational efforts during this period (Figure 2.6).

Incorporating information about the Taylor Energy site history allows us to better understand potential sources of the observation variance. Let us look again at the observed slick frequency data, but this time removing months where slicks could have been misattributed to the *Deepwater Horizon* oil spill (May 2010-July 2010) or where the site was not monitored (May-August 2011).

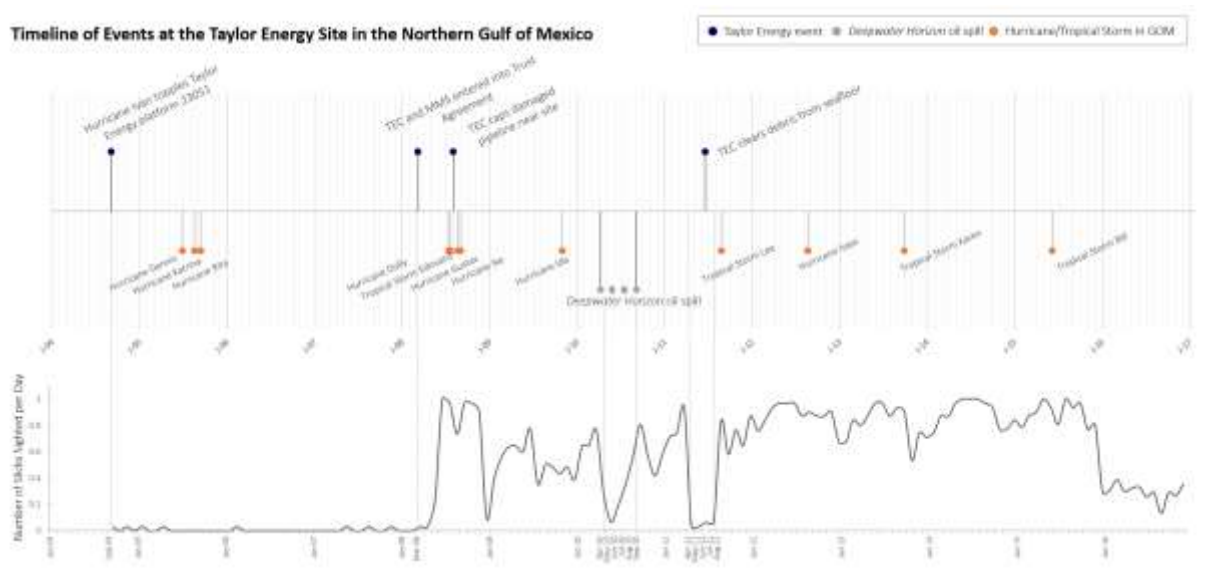


Figure 2.5 Taylor Energy Site History from 2004 to 2016. Top panel is the timeline of events documented to have happened at or near the Taylor Energy site that could potentially influence the ability of observers to document oil at the Taylor Energy site. The bottom panel is a plot of the monthly slick frequencies over the site history.

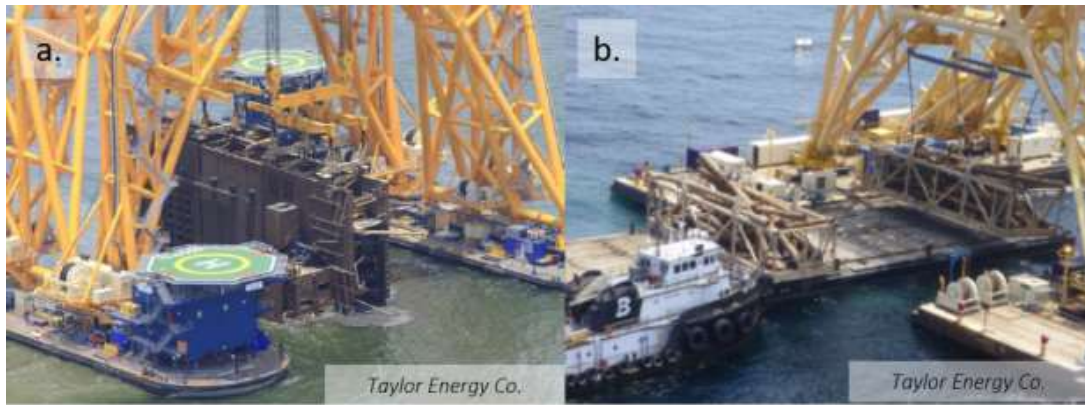


Figure 2.6 Photos from TEC following successful removal of Taylor Energy platform 23051 (a) and platform jacket (b) from the seafloor in July and August 2011. Images from TEC.

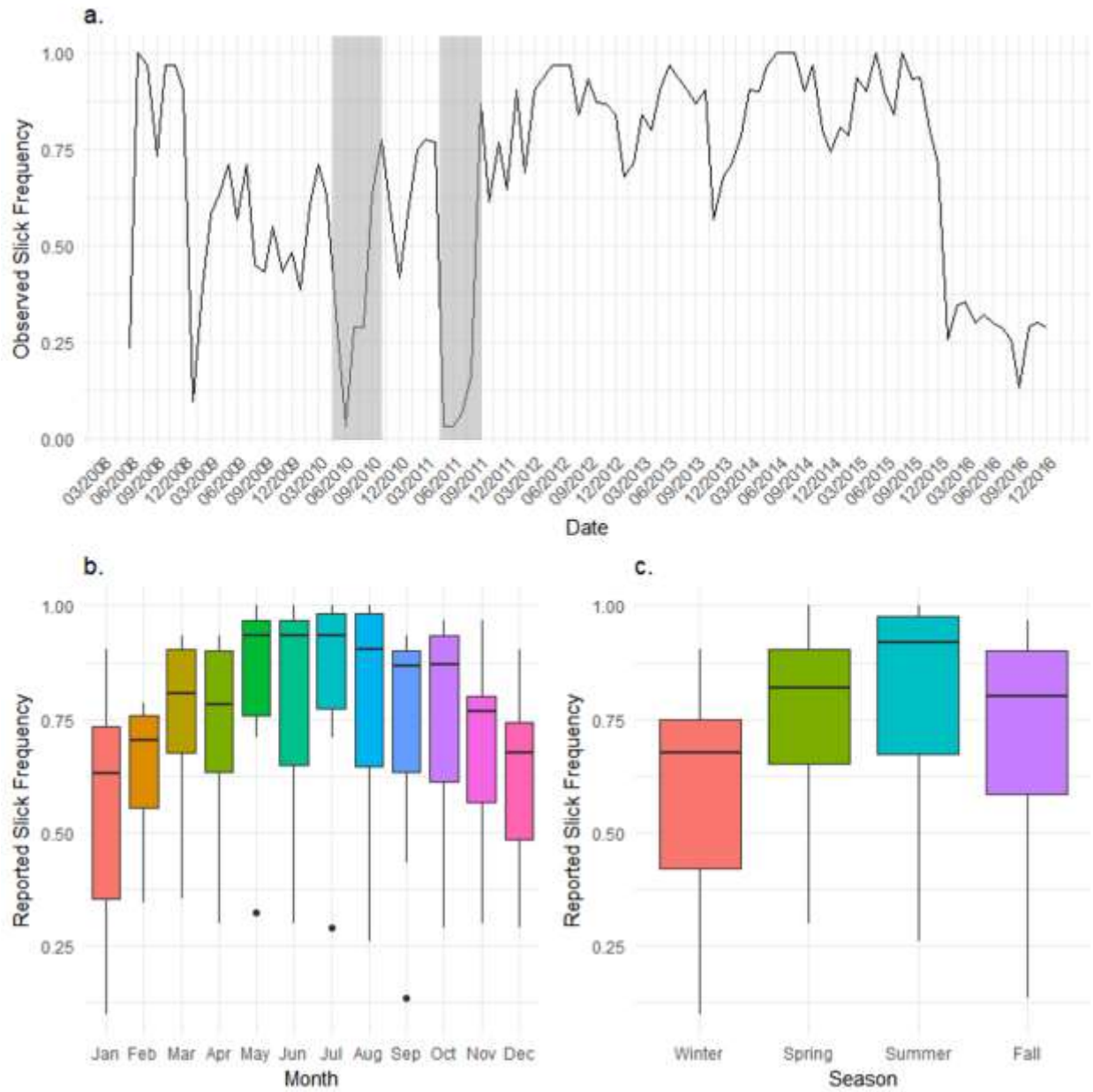


Figure 2.7 Slick frequency data excluding summers 2010 and 2011 (a). Box plots of slick frequency by month (b) and by season (c) with the summers of 2010 and 2011 excluded. Summer 2010 is excluded because of the confluence of the Deepwater Horizon oil spill, located 62 km to the southeast of the Taylor Energy site. Summer 2011 is excluded due to the response activities happening at the Taylor Energy Site.

Excluding these time periods (May 2010-July 2010 and May-August 2011) restores some of the seasonal oscillation observed with the slick length (Figure 2.3). Within this trimmed data set of slick observations, there was no significant difference in the monthly populations of slick frequencies (Kruskal-Wallis chi-squared = 15.229, df = 11, p-value = 0.1723). There was, however a difference in the variance by meteorological season (Kruskal-Wallis chi-squared = 12.376, df = 3, p-value = 0.0062).

Using the Wilcoxon rank sum test to test for differences in the frequency of slick observations by seasons, no significant differences between summer and spring ($W = 174$, p-value = 0.1217) or summer and fall ($W = 184$, p-value = 0.06544) were detected. However, a significant difference between summer and winter was detected ($W = 379$, p-value = 0.003295). The significant difference between summer and winter months underscores the seasonal oscillation of oil at the Taylor Energy site. The reason for this seasonal variation could stem from seasonal sampling bias (more traffic or observations made in the summer) or could reflect seasonal differences favoring slick formation in summer months compared to other times of the year.

2.3.1.3 Interannual Variation of Oil at the Taylor Energy Site

BOEM and BSEE have classified the persistent leaking oil from the Taylor Energy site as a ‘passive spill’ (BOEM and BSEE, 2016), but many questions remain about how the spill has changed over its 13-year history. Given the paucity of data collected in the first four years after the platform was destroyed, we can only examine the record since the site has been monitored in mid-2008.

A series of Kruskal Wallis rank sum tests examined the slick length and width, by year from mid-2008 to 2016, and rejected the null hypothesis that these data originated from identical

populations (Slick dimensions: Kruskal-Wallis chi-squared = 217.36, df = 8, p-value < 2.2e-16). Furthermore, this significance is unchanged if we exclude the farthest outlier of recorded slick lengths (Kruskal-Wallis chi-squared = 216.14, df = 8, p-value < 2.2e-16). Slick frequencies, excluding summers 2010 and 2011, were also found to originate from non-identical populations by year (Slick frequency: Kruskal-Wallis chi-squared = 67.824, df = 8, p-value = 1.331e-11).

A Spearman's Rank Correlation test detected a moderate positive, and statistically significant relationship between the observed slick length and the year ($S = 1073100000$, p-value < 2.2e-16, $\rho = 0.2957745$). A similar correlation is observed between estimated slick area and year ($S = 1186400000$, p-value < 2.2e-16, $\rho = 0.2213926$), suggesting that the observed oil slicks are growing larger through time (Figure 2.8 a and b). The slick frequency, however, does not have the same trend over the entire 8.5-year record examined ($S = 142750$, p-value = 0.7644, $\rho = -0.03132876$). Excluding 2016, a clear outlier of the record, however, a Spearman's Rank correlation coefficient test detected a positive correlation between slick frequency and time ($S = 51355$, p-value = 3.362e-05, $\rho = 0.4410686$), suggesting that the frequency of observed slicks is increasing through time, up until 2016 (Figure 2.8c).

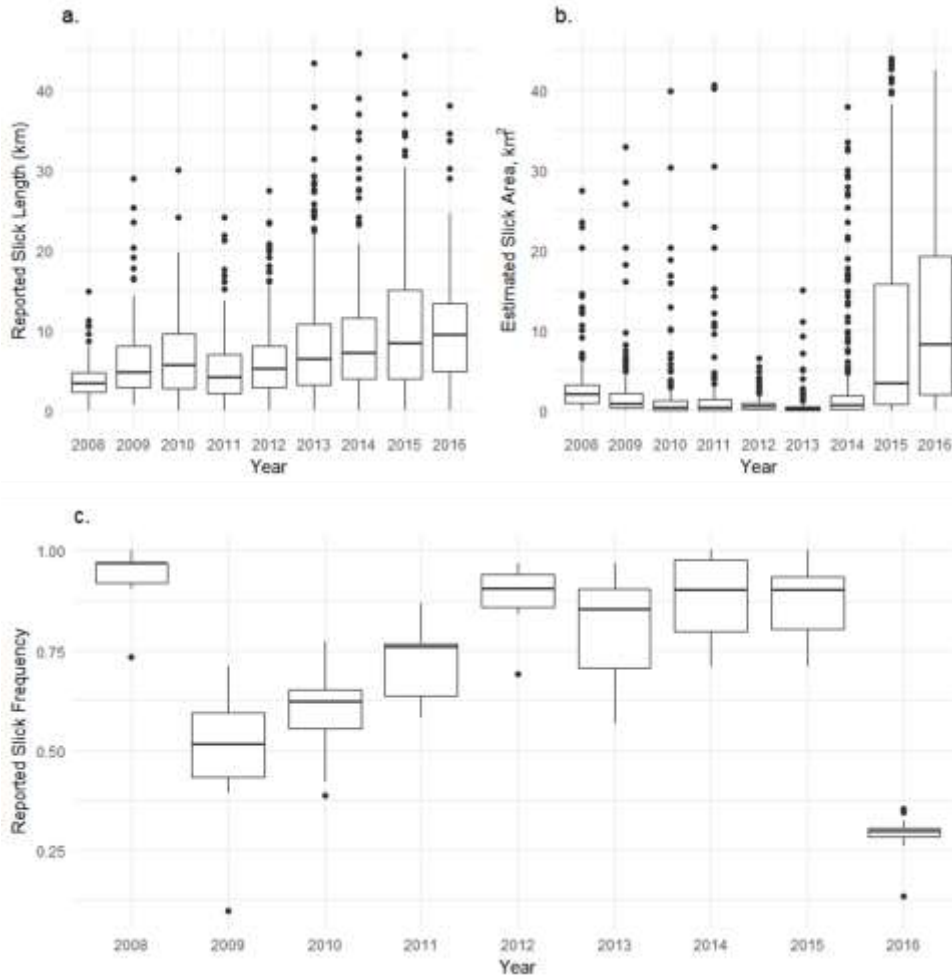


Figure 2.8 Box plots of observed (a) oil slick lengths by year (a), estimated oil slick areas by year (b), and reported slick frequencies by year (c) at the Taylor Energy site. Note that the frequency data (c) does not include summers 2010 and 2011.

2.3.2 Seasonal Variations in Meteorological Observations

2.3.2.1 Wind Speed Data

There are substantial seasonal variations with respect to wind speed in the northern Gulf of Mexico region. The average daily wind speed is highest in the winter months and lowest in the early summer months. There was strong agreement and significant correlation between all three stations included in the study, but for simplification, only BURL1 is discussed here. BURL1 had significant variance by both month and meteorological season.

The sinusoidal oscillation of wind speed at the BURL1 station is even more apparent after examining the results of the Wilcoxon rank sum tests, which finds significant differences across all seasons, except for the Spring and Fall ($W = 223730$, $p\text{-value} = 0.4683$), which have statistically indistinct wind speeds from one another.

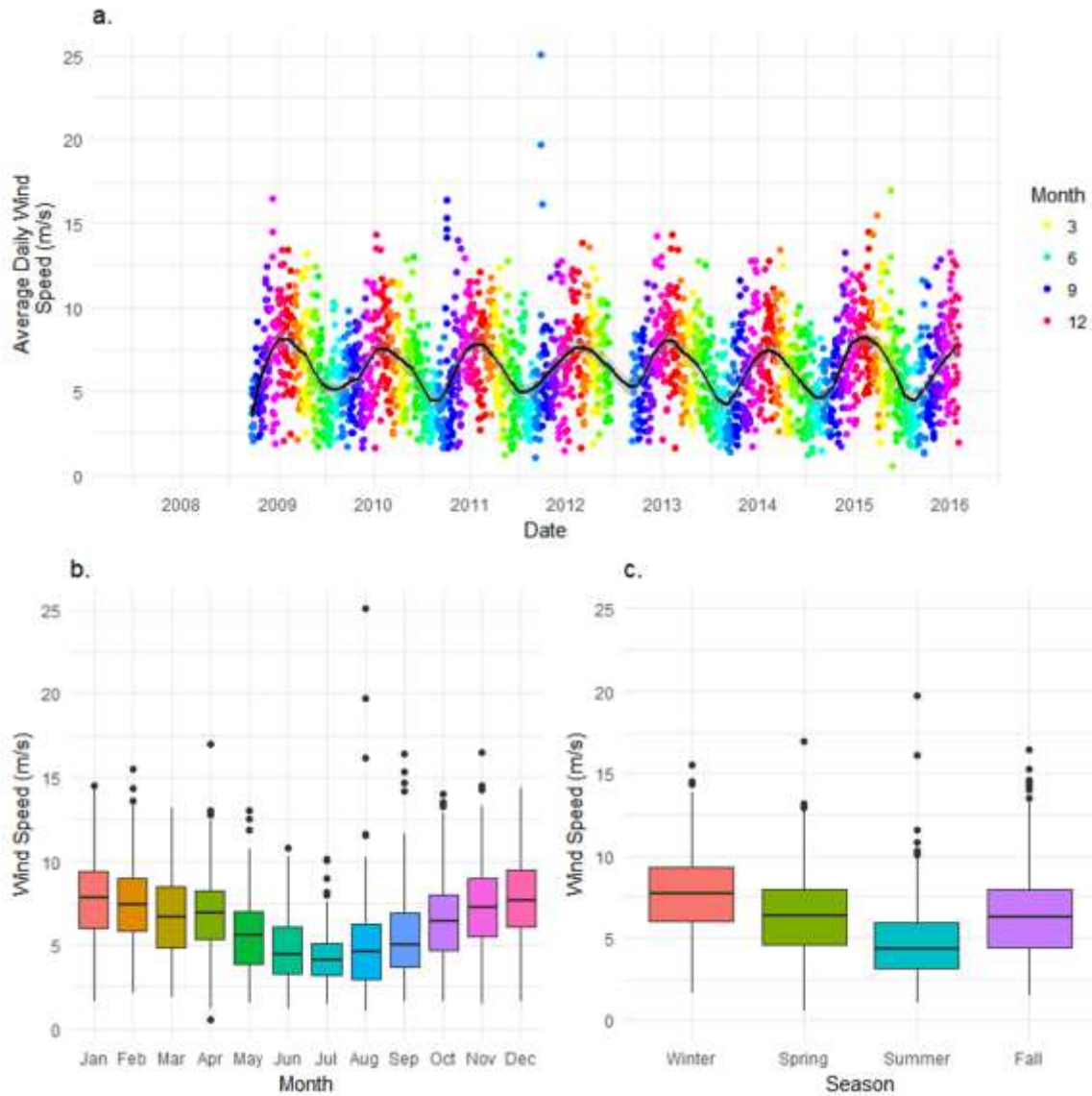


Figure 2.9 Wind speed data from BURL1 buoy plotted by day, colored by month, and fitted with a Loess line (a). Wind speed data binned by month (b) and season (c). No data has been excluded from these figures.

Table 2.2 Summary of the Wilcoxon Rank sum tests for differences in wind speed by season.

	Spring	Summer	Fall	Winter
Spring	n/a			
Summer	W = 264380, p-value < 2.2e-16	n/a		
Fall	W = 223730, p-value = 0.4683	W = 298730, p-value < 2.2e-16	n/a	
Winter	W = 146540, p-value < 2.2e-16	W = 66499, p-value < 2.2e-16	W = 168140, p-value < 2.2e-16	n/a

2.3.1.2. Atmospheric Pressure Data

Atmospheric pressure also varies significantly within the span of a year, with significantly higher pressures recorded in the winter compared to summer months. What may be more important for the Taylor Energy site, however, is the seasonal variance of atmospheric pressure. The variance of atmospheric pressure is much greater in winter months compared to the summer months, reflecting greater variation in weather systems are moving through the region. The sinusoidal oscillation of atmospheric pressure at the PSTL station is even more apparent after examining the results of the Wilcoxon rank sum test, which found significant differences across all seasons (p-values $< 1 \text{ e-}11$), except for the Spring and Fall (p-value = 0.3263), which have statistically indistinct atmospheric pressures from one another. Similar results were obtained examining the offshore BURL station, but were excluded for brevity.

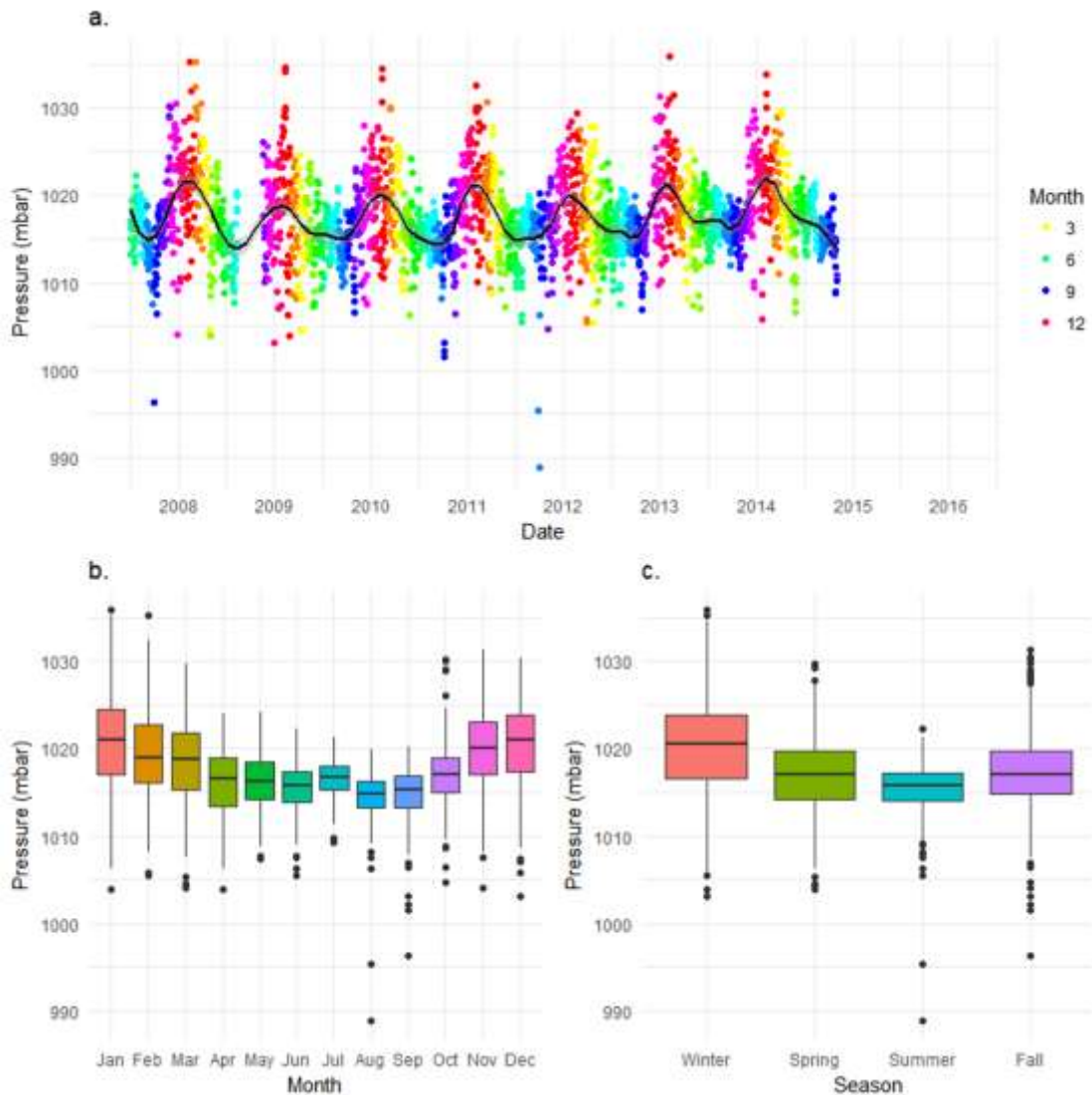


Figure 2.10 Atmospheric pressure data from PSTL buoy plotted by day, colored by month, and fitted with a Loess line (a). Pressure data binned by month (b) and season (c). No data has been excluded from these figures.

Table 2.3 Summary of the Wilcoxon Rank sum tests for differences in atmospheric pressure by season for PSTL station.

	Spring	Summer	Fall	Winter
Spring	<i>n/a</i>			
Summer	W = 266320, p-value = 4.133e-11	<i>n/a</i>		
Fall	W = 193180, p-value = 0.3263	W = 248910, p-value = 2.2e-14	<i>n/a</i>	
Winter	W = 126300, p-value < 2.2e-16	W = 93185, p-value < 2.2e-16	W = 120210, p-value < 2.2e-16	<i>n/a</i>

2.3.1.3 Wind Direction Data

MacFayden *et al.* (2014), the only other published study on the Taylor Energy site to date, observed that oil slicks emanating from the Taylor Energy site range from 0.5-2 km x 10-30 km in size and vary with respect to the wind conditions. Winds from the south advect oil slicks to the east from mid-spring to mid-fall, while winds from the north and northeast transport oil slicks to the west in the fall and winter (MacFayden *et al.* 2014). Examining the wind direction data from the three buoy stations confirms the seasonal oscillation of winds, which results in the seasonal oscillation of where the oil is advected. In the summer months, the wind is predominantly blowing from the southwest ($\sim 225^\circ$), and for the remainder of the year, the wind blows from the southeast ($\sim 135^\circ$) (Figure 2.11). This oscillating wind direction reflects that throughout the year, the oil is likely to be advected in different directions, further underscoring the dynamic nature of the Taylor Energy site.

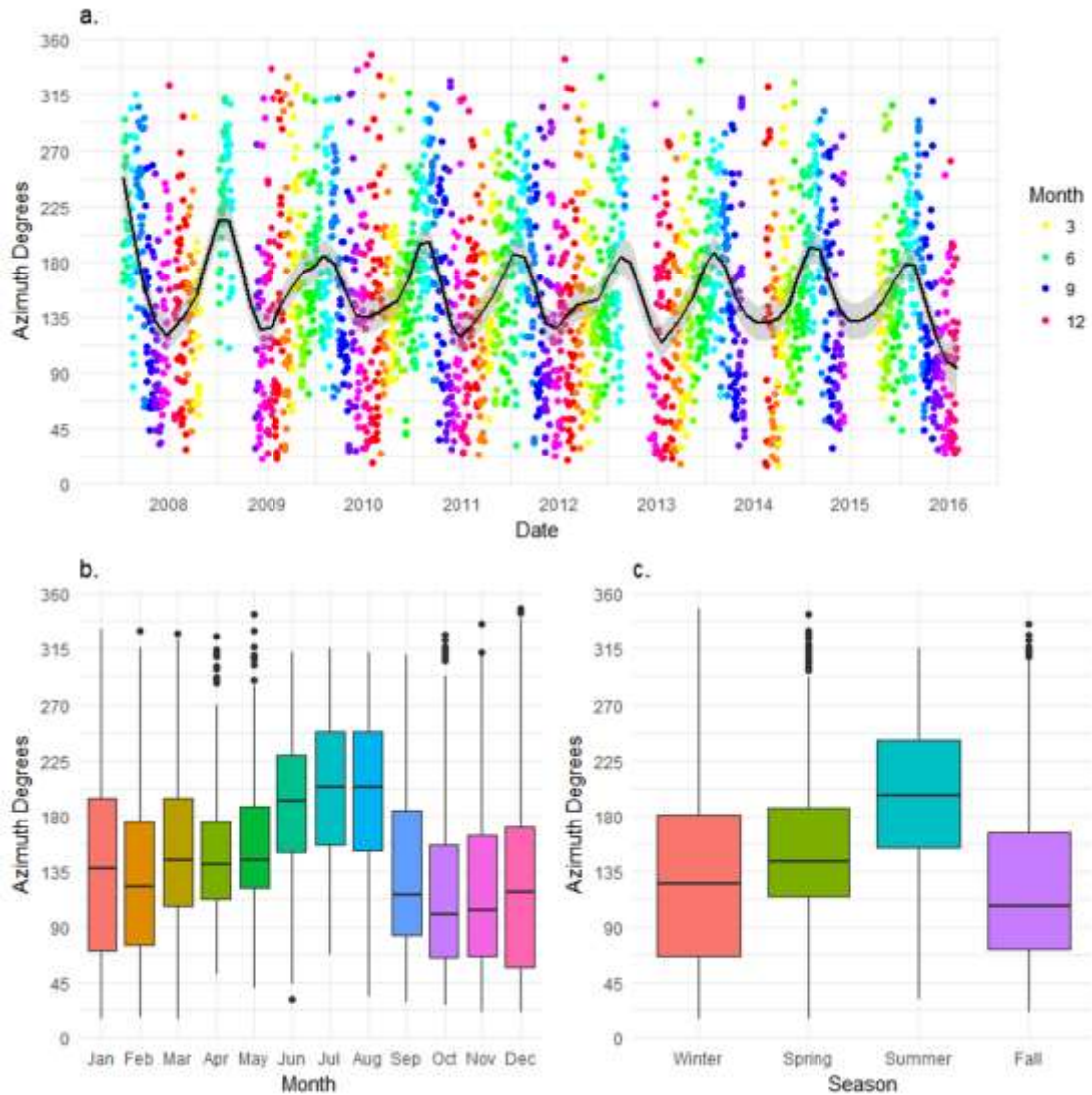


Figure 2.11 Wind direction data from PSTL buoy plotted by day, colored by month, and fitted with a Loess line (a). Wind direction binned by month (b) and season (c). No data has been excluded from these figures.

Table 2.4 Summary of the Wilcoxon Rank sum tests for differences in wind direction by season for PSTL station.

	Spring	Summer	Fall	Winter
Spring	<i>n/a</i>			
Summer	W = 150930, p-value < 2.2 e-16	<i>n/a</i>		
Fall	W = 147040, p-value < 2.2e-16	W = 105280, p-value < 2.2e-16	<i>n/a</i>	
Winter	W = 238040, p-value = 1.585e-09	W = 338020, p-value < 2.2e-16	W = 179780, p-value = 0.1787	<i>n/a</i>

2.3.2 Mississippi River Observations

In addition to significant oscillations in turbidity, dissolved oxygen, and water temperature (not shown), there were substantial seasonal oscillations with respect to the rate of riverine discharge and nitrogen loading at USGS station 07374000 in Baton Rouge, LA. These observations underscore the highly dynamic nature of the lower Mississippi River. The Taylor Energy site, located just 18 km offshore, is likely influenced by some of these same drivers, particularly the discharge and the dissolved nitrogen loading, although there is a multi-day lag between observed levels at USGS station 07374000 and the Taylor Energy site (Rogener, personal communication). The discharge rate of the Mississippi River peaks in the late spring, due to the spring melt upriver, and reaches a minimum in the winter months (Figure 2.12). This discharge carries large amounts of dissolved organic carbon, sediment, and dissolved nutrients, including excess nitrogen (Figure 2.13). The seasonal flux of nitrogen from the Mississippi River is believed to be a primary driver of the annual hypoxic zone in the Gulf of Mexico (Rabalais *et al.* 2002).

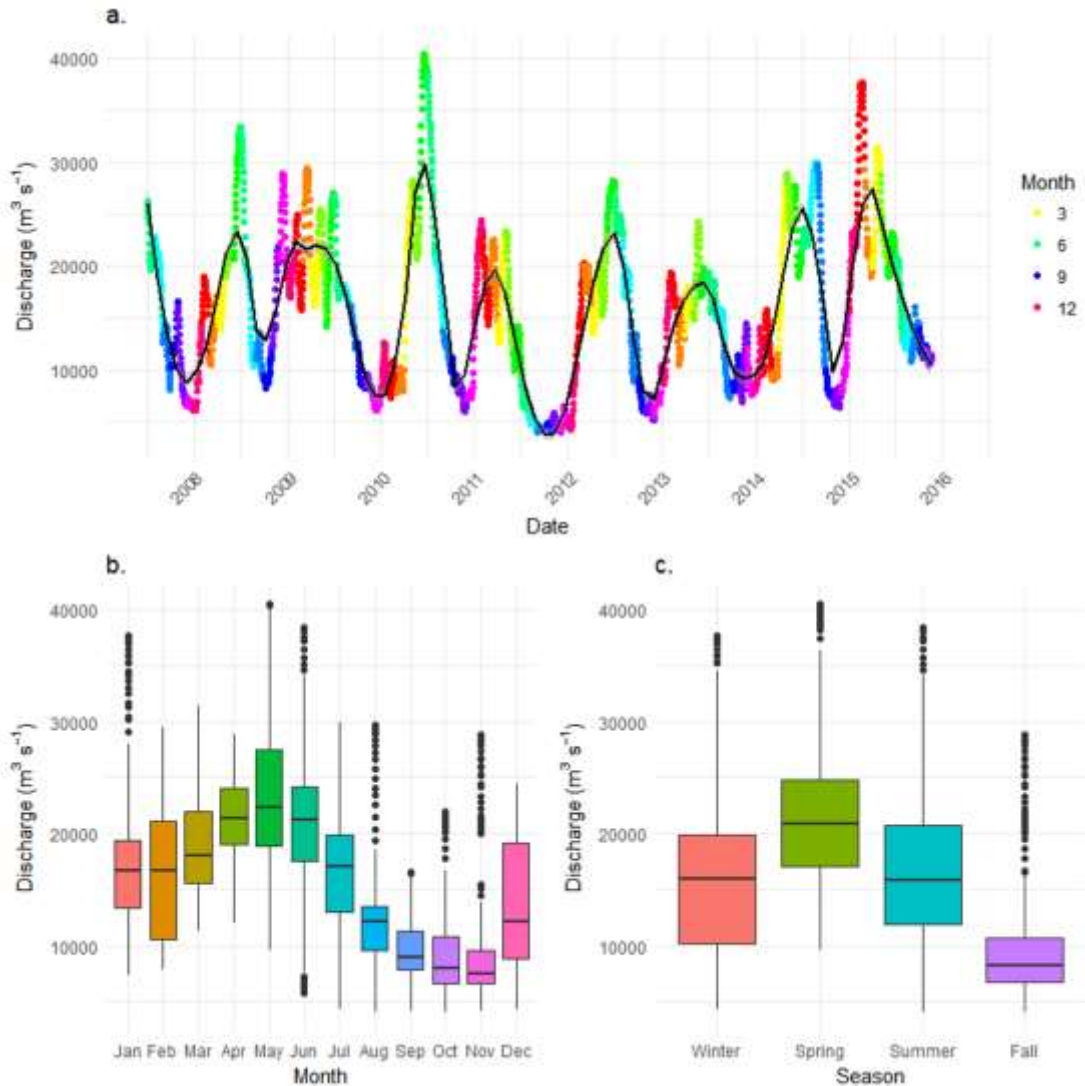


Figure 2.12 Data from USGS 07374000 station plotting riverine discharge of the Mississippi River at Baton Rouge through time (a). Each dot represents the average daily value for each variable, colored to represent the month in which that data point was collected. The black line is a Loess curve, a non-parametric locally weighted regression curve. Discharge data by month (b) and season (c). No data has been excluded from these figures. All data included has been demarcated as 'approved' by the USGS as of March 2017.

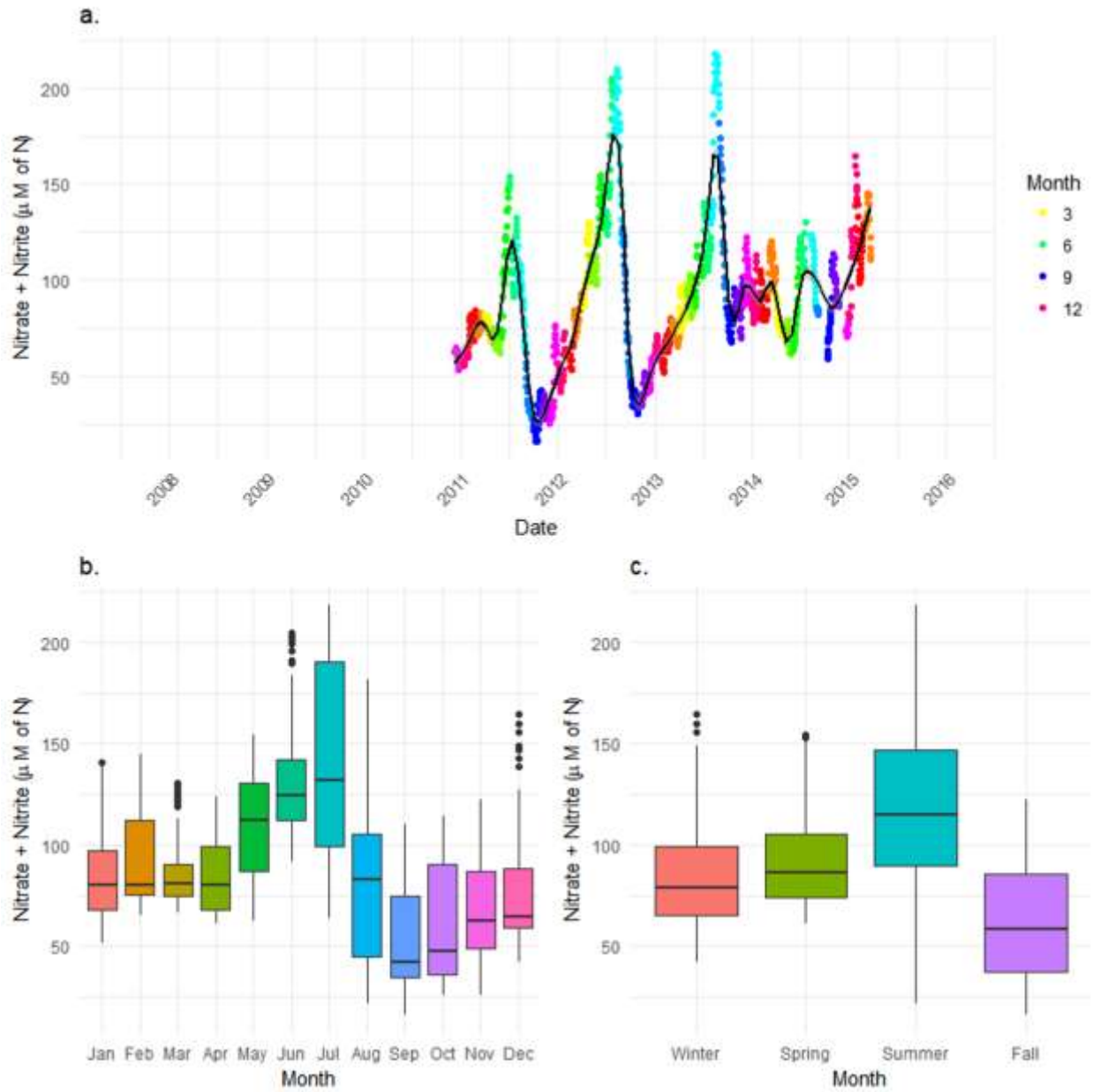


Figure 2.13 Data from USGS 07374000 station plotting dissolved NO_x concentrations of the Mississippi River at Baton Rouge through time (a). Each dot represents the average daily value for each variable, colored to represent the month in which that data point was collected. The black line is a Loess curve, a non-parametric locally weighted regression curve. NO_x data by month (b) and season (c). No data has been excluded from these figures. All data included has been demarcated as 'approved' by the USGS as of March 2017.

2.4 Synthesizing Oil Slick Observations with the Meteorological and Riverine Observations from the Taylor Energy Site

The northern Gulf of Mexico is a seasonally dynamic site, and this seasonality extends to the oil slicks present in surface waters at the Taylor Energy site. From mid-2008-2016, observed oil slicks were statistically longer and more frequently observed in summer months compared to other seasons. Meanwhile, winter months have statistically fewer and smaller slicks observed over the 8.5-year record.

Summer months have statistically lower wind speeds and atmospheric pressures than winter months, and the wind direction also changes during these summer months. Upriver observations of the Mississippi River found that the highest rates of discharge occur in the late spring-early summer months, and nitrogen loading peaks about a month later in mid-summer.

Using a series of Spearman's Rank Correlation tests, we can synthesize how these meteorological and riverine observations relate to the oil slick sightings. While these correlations are not causations, they underscore the site's dynamic seasonality (Figure 2.14 and Table 2.5).

The hierarchical clustering groups the variables such that the agreement between the three buoy stations (BURL1, PSTL, and PILL) is clear and statistically significant, with respect to wind speed, maximum gust velocity, atmospheric pressure, and wind direction.

There is a significant negative relationship between average daily wind speeds and slick length across all three stations, adding evidence that lower wind speeds correlate with longer oil slicks.

There is also a significant negative relationship between atmospheric pressure and slick length across all three offshore stations. Previously we established that the lowest atmospheric pressures

were observed in the summer, and this negative relationship reflects the coincidence of longer slicks in summer months with the lower atmospheric pressures. However, we would argue that the driving force is not the absolute pressure, but the variance in pressure, which is greater in winter months than in summer months.

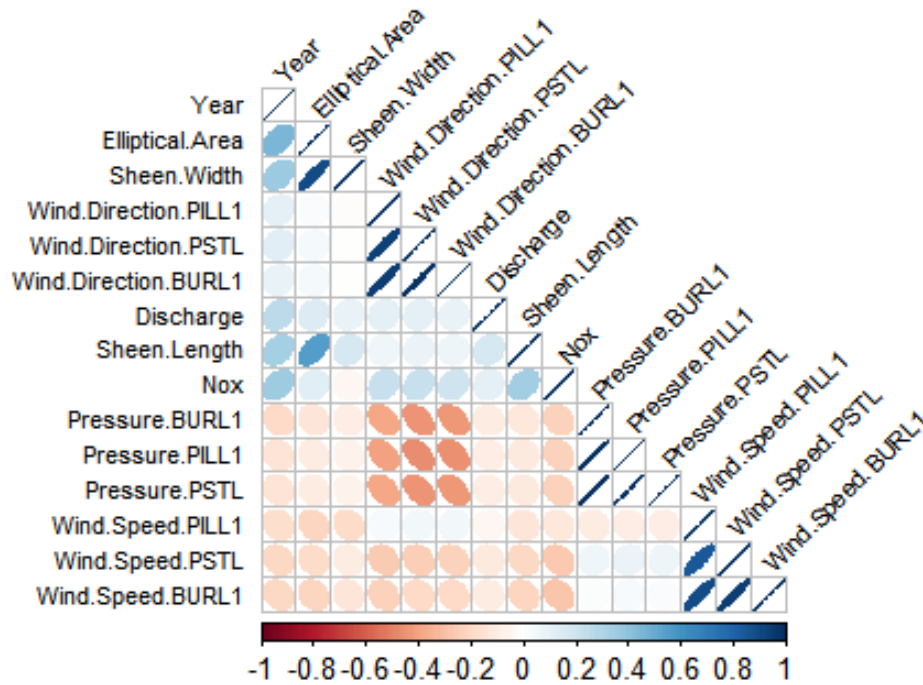


Figure 2.14 Correlogram of all variables from the publicly available record using a Spearman's Rank Correlation Analysis between each variable. The color and shape of each dot on the correlogram is proportional to the size of the correlation coefficient (ρ), with the color dictating whether the monotonic relationship described is positive (blue) or negative (red). Variables are clustered hierarchically.

Table 2.5 Spearman's Rank Correlation Coefficients (ρ) for slick length data and all other significant metadata from the site.

Variable	Rho	p value	Category
Elliptical Area (km ²)	0.5005121	0.0000000	Slick Observation
Sheen Width (km)	0.1304207	0.0000000	Slick Observation
Square Area (km ²)	0.5005121	0.0000000	Slick Observation
Gage Height (m)	0.1457531	0.0000000	Mississippi River
Specific Conductivity	-0.0822708	0.0011114	Mississippi River
Discharge (m ³ s ⁻¹)	0.1476230	0.0000000	Mississippi River
NO _x (μM)	0.2582545	0.0000000	Mississippi River
Dissolved O ₂ (μM)	-0.3367831	0.0000000	Mississippi River
Water Temperature (°C)	0.2883881	0.0000000	Temperature
Max. Temperature (°C)	0.2812940	0.0000000	Temperature
Min. Temperature (°C)	0.2972207	0.0000000	Temperature
PILL1 Wind Direction	0.1328257	0.0000006	Wind
PSTL Wind Direction	0.1356594	0.0000000	Wind
BURL1 Wind Direction	0.0828905	0.0028774	Wind
PILL1 Maximum Gust	-0.0926710	0.0004868	Wind
PSTL Maximum Gust	-0.0979151	0.0000420	Wind
BURL1 Maximum Gust	-0.1009095	0.0000279	Wind
PSTL Wind Speed	-0.1315465	0.0000000	Wind
PILL1 Wind Speed	-0.0887776	0.0008354	Wind
BURL1 Wind speed	-0.1527836	0.0000000	Wind
Average Wind Speed	-0.0880995	0.0000600	Wind
BURL1 Atmospheric Pressure	-0.1114665	0.0000594	Atmospheric Pressure
PSTL Atmospheric Pressure	-0.1048263	0.0000070	Atmospheric Pressure
PILL1 Atmospheric Pressure	-0.1045319	0.0000821	Atmospheric Pressure
Year	0.2957745	0.0000000	Time

Additionally, the Spearman's Rank Test shows that there is a very weak, positive relationship between discharge and observed slick length ($\rho = 0.147623$, $p = 1.661e-11$), as well as a weak, positive relationship between the NO_x and observed slick length ($\rho = 0.25825$, $p < 2.2e-16$). This suggests that there are large seasonal inputs of terrestrial material, including DOC, dissolved nutrients, and perhaps even trace metals, that might be utilized by surface microbial communities responding to oil in the surface waters of the Taylor Energy site. Further research is required to determine how rapidly water from the USGS station reaches the Taylor Energy site.

The meteorological conditions near the Taylor Energy site vary throughout the course of the year with respect to wind speed, atmospheric pressure, and wind direction. These three variables each can uniquely impact the Taylor Energy site and the fate of oil emanating from the seafloor at the site of the felled platform. When oil slicks are likely to be more frequent and larger in size, the Mississippi River can supply high levels of nitrogen, phosphorous, and trace metals that would be required to degrade the hydrocarbons persisting in surface waters. In the fall and winter, the changing atmospheric conditions churn up surface water, physically dispersing oil slicks and dispersing the oil vertically and horizontally in the water column.

References

Bureau of Ocean Energy Management and Bureau of Safety and Environmental Enforcement (BOEM and BSEE; DOI). *2016 Update of Occurrence Rates for Offshore Oil Spills*. Report prepared by ABS Consulting Inc. Arlington, VA. July 13, **2016**.

Coast Guard Maritime Information Exchange (CGMIX), version 5.4.0. United States Coast Guard. Accessed 10/17/2016 from <https://cgmix.uscg.mil/>

MacFayden, A.; Wei, E.; Warren, C.; Henry, C.; Watabayashi, G. Utilization of the Northern Gulf Operational Forecast System to Predict Trajectories of Surface Oil from a Persistent Source Offshore of the Mississippi River Delta. In *2014 International Oil Spill Conference*; **2014**; Vol. 53, pp 1689–1699.

National Data Buoy Center (NDBC). Department of Commerce; National Oceanic and Atmospheric Administration; Center of Excellence in Marine Technology and the National Weather Service. Stennis Space Center, MS. Accessed 3/17/2017 from <http://www.ndbc.noaa.gov/>

National Water Information System (NWIS). Department of the Interior; U.S. Geological Survey; National Streamflow Information Program and National Water-Quality Assessment Project. Baton Rouge, LA. Accessed 3/18/2017 from https://waterdata.usgs.gov/usa/nwis/uv?site_no=07374000

Rabalais, N. N.; Turner, R. E.; Wiseman, W. J. Gulf of Mexico Hypoxia, a.k.a. “The Dead Zone.” *Annu. Rev. Ecol. Syst.* **2002**, 33, 235–263 DOI: 10.1146/annurev.ecolsys.33.010802.150513.

Taylor Energy Company LLC MC20. FRACE: Final Risk Assessment and Cost Estimate. Unified Command Summary. March 25-26, **2014**.

CHAPTER 3

A TALE OF TWO TAYLORS: COMPARISON OF THE TAYLOR ENERGY SITE WITH TWO SEASONALLY DISTINCT TRANSECTS

3.1 Introduction

In the previous chapter, we established that the northern Gulf of Mexico experiences substantial seasonal variations with respect to riverine and meteorological inputs, and that these seasonal oscillations extend to the observed oil slick length and slick frequency at the Taylor Energy site. These seasonal observations of the macro-environment suggest that there might be seasonal oscillations at the microscopic level, potentially impacting hydrocarbon degrading dynamics in surface waters at the Taylor Energy site.

Surface water is of particular interest at the Taylor Energy site, because this is where oil is likely to accumulate after being released into the water column, and the surface is also where a large fraction of oil can be transformed via photo-oxidation, evaporation, and biodegradation by microbial communities. Understanding the long-term fate of oil in marine and coastal communities requires a thorough understanding of the kinds of transformations possible at the sea surface.

To understand the seasonal dynamics and to begin understanding the biogeochemical range of the Taylor Energy site, we conducted two four-point transects of surface water at the Taylor

Energy site. The first transect was conducted in October 2014 and the second transect was conducted in June 2015 (Figure 3.1 and Table 3.1). Surface water was examined along a wide variety of biogeochemical parameters, including dissolved nutrients, dissolved organic carbon, microbial community composition, extractable petroleum hydrocarbons, and potential hydrocarbon oxidation rates. These geochemical parameters were compared within and between transects to determine how the seasonal oscillations at the macro-scale of the northern Gulf of Mexico manifest at the Taylor Energy site, and how those seasonal oscillations impact the surface water's ability to degrade petroleum derived hydrocarbons.

3.2 Methods

3.2.1 Sampling and Sample Storage

Surface waters were collected in October 2014 from stations A-D (Figure 3.1) by the MacDonald Lab. Stations A and D had extensive oiling, while stations B and C were in the vicinity of faint, rainbow sheens (Figure 3.1). Station A was observed to have extensive mousse formation; oil mousse is defined as an emulsion of oil, water, and gas whipped up by wind and wave action (Leahy and Colwell, 1990; reference 45 therein). The oil slick at the Taylor Energy site was described as a rainbow sheen, extending 12.1 km x 0.8 km in size (SEQNOS ID: 1097841; NRC and CGMIX).

Whole surface water was collected and stored in acid-washed collapsible low-density polypropylene cube containers (10L). Oil slick samples were collected into combusted glass jars (120mL) fitted with PTFE lined caps. 1 x 10L whole water sample was taken from each station, and 4 surface grabs of the oil at the surface were collected from each station. Samples were placed out of direct sunlight and stored on ice and shipped overnight to Athens, GA, where

whole water was subsampled for nutrients, microbial community, and potential hydrocarbon oxidation rates. Surface grabs were frozen at -20°C for hydrocarbon extraction and analysis via gas-chromatography mass spectrometry (GC-MS).

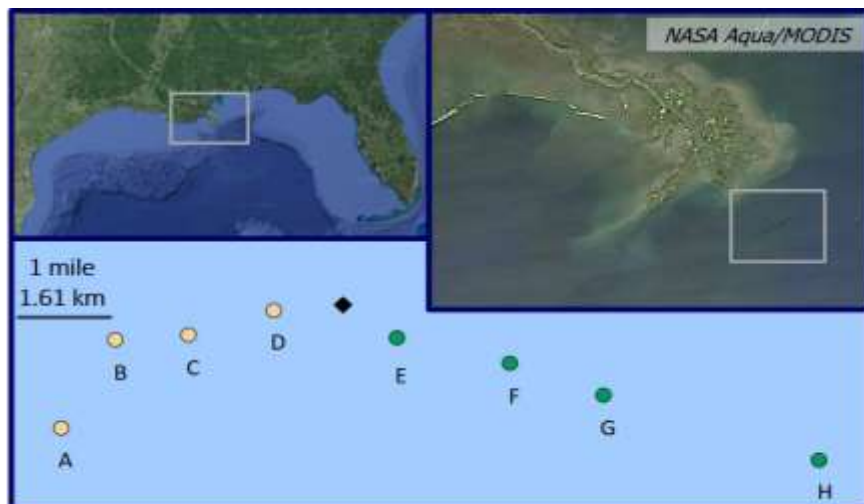


Figure 3.1 Map of (a) the northern Gulf of Mexico, (b) the Taylor Energy site, just 11 miles southeast of the Bird Foot Delta, a slick progressing from the northeast to southwest, and (c) locations of the stations along the 2014 and 2015 transects. Stations A, B, C, and D were sampled on October 9, 2014 by the MacDonald Lab, and are depicted in yellow. Stations E, F, G, and H were sampled on June 10, 2015 from the R/V Endeavor (EN559), are depicted in green. The location of the sunken Taylor Energy platform is depicted by the black diamond.

Table 3.1 Coordinates for the 2014 transect and 2015 transects.

Fall 2014 Transect			Summer 2015 Transect		
Station	Longitude	Latitude	Station	Longitude	Latitude
A	28.91834	-89.0184	E	28.93270	-88.9619
B	28.93243	-89.0093	F	28.92863	-88.9428
C	28.93319	-88.9969	G	28.92365	-88.9270
D	28.93712	-88.9825	H	28.91315	-88.8906

Surface waters were collected in June 2015 from stations E-H (Figure 3.1). According to records from the National Response Center and CMIX database of chemical spills, the oil slick at the Taylor Energy site on the day of the summer 2015 transect was 6.9 km x 1.8 km in size and a

'silvery' sheen (SEQNOS ID: 1119149). However, by the time *R/V Endeavor* arrived on station, no oil sheen was visible or smell detected, as a summer storm had physically dispersed oil from the surface.

1L aliquots from bucket casts were poured into 1L amber bottles, fitted with PTFE lined caps, with 3 x 1L samples taken per site (n= 3/station) and sampled for all analytes within 4 hours of sample collection.

3.2.2 Dissolved Nutrients

Aliquots of whole surface water were filtered (0.2 μm) and preserved at -20°C until analysis of dissolved organic carbon (DOC), ammonium (NH_4^+), NO_x^- ($\text{NO}_3^- + \text{NO}_2^-$), total dissolved nitrogen (TDN), phosphate (HPO_4^{3-}), and total dissolved phosphate (TDP). Dissolved organic nitrogen and total dissolved organic phosphate concentrations were estimated from subtraction of inorganic species from total dissolved species.

Dissolved organic carbon (DOC) was analyzed by high temperature (680°C) combustion catalytic oxidation on a total organic carbon analyzer (Shimadzu TOC-Vcph); concentrations were determined by comparison to a series of potassium hydrogen phthalate standards. Organic carbon was measured as the non-purgeable organic carbon (NPOC) content with an NDIR detector, following sparging with phosphoric acid. Total dissolved nitrogen (TDN) was measured on the same instrument with a TNM-1 module; concentrations were derived from a glycine standard. Samples were not diluted prior to analysis.

Nitrate plus nitrite (NO_x^-) concentrations were quantified by a vanadium reduction method using a vanadium reduction assembly (Antek 745; Braman and Hendrix 1989) coupled with a chemiluminescent nitric acid detector (Antek 7050; Garside 1982).

Nitrite (NO_2^-) was analyzed in parallel by standard colorimetric assay (Bendschneider and Robinson, 1952), while ammonium was measured colorimetrically using the standard phenol hypochlorite method (Solorzano, 1969). Nitrate (NO_3^-) was determined from the subtraction of NO_2^- from NO_x^- .

Dissolved phosphate was measured colorimetrically, using the molybdate blue method (Solorzano and Sharp, 1980). Total dissolved phosphate (TDP) was first precipitated with magnesium sulfate, and heated with acid to convert organic phosphate into orthophosphate. This residue was then subjected to colorimetric analysis using the molybdate blue method (Solorzano and Sharp, 1980). Colorimetric analyses were performed using a Shimadzu UV-1601 spectrophotometer.

3.2.3 Hydrocarbons

Whole unfiltered water was frozen at -20° for analysis of total extractable hydrocarbons using a method adapted from Kleindeinst *et al.* (2015) and Kujawinski *et al.* (2014). Following thawing, sample volume was determined gravimetrically, and spiked with known quantities of three deuterated standards ($5\mu\text{g}/\text{sample}$; fluorene- d_{10} , eicosane- d_{24} , and benzo[a]pyrene- d_{12}). Samples were transferred to combusted 1L glass separation funnels fitted with solvent rinsed PTFE spigots, and extracted with dichloromethane ($2 \times 250\text{ mL}$) and hexane ($1 \times 250\text{ mL}$). Samples from stations A and D required additional hexane and dichloromethane washes as there were still visible sheens of colored oil in the separatory funnel. Organic fractions from each sample were combined and reduced in volume via rotary evaporation (Buchi Corp.) and solvent exchanged into hexane. Samples were further reduced to $500\ \mu\text{L}$ under a gentle stream of Ar.

Organic extracts were analyzed with a gas chromatography with time of flight mass spectrometry (GC-TOF-MS; Pegasus 4D GC, LECO, Michigan). 1 μL of each extract was injected with a 1:10 split injection method, and separated on two in-line columns; the primary column was a Rxi-5 Sil fused silica column (60m x 0.25 mm ID; 0.25 μm df; Restek) joined to an Rxi-17 Sil MS fused silica column (1m x 0.10mm ID x 0.1 μm dr; Restek) housed in a secondary GC oven. The GC oven was held for 3 minutes at 50°C, followed by a 6°C/minute temperature ramp until reaching 320°C, and held for 20 minutes. Time of flight mass spectrometry allowed for the simultaneous monitoring of ions ranging from 50-575 m/z across the entire method, after a 600 s solvent delay. Samples from the 2014 transect were also analyzed via gas chromatography coupled with a flame ionization detector (GC-FID; model 8610C, SRI, California). Briefly, 1 μL of each extract was manually injected into a GC-FID, equipped with a splitless inlet and separated on a MXT-5 fused silica column (30 m x 0.53mm x 0.5 μm ; Restek). The GC oven was held at 45°C for 3 minutes, and the oven temperature was increased at 6°C/min to 120°C, and then increased at 10°C/min to 315°C and held at 315°C for 10 min; the FID detector was held at 315°C. Samples were run alongside a standard curve of n-alkanes (nC7-nC40; heptane- tetracontane), a mixture of 16 parent PAHs, and a dilution of crude oil as an estimation of total petroleum hydrocarbons (TPH).

3.2.4 Potential Hydrocarbon Oxidation Rates

Potential hydrocarbon oxidation rates were quantified as the rate of conversion of a radiolabeled model hydrocarbon into $^{14}\text{CO}_2$ by the microbial community within each bottle (Kleindienst *et al.* 2015; Sibert *et al.* 2016). [1- ^{14}C]-n-hexadecane (American Radiolabeled Chemicals, Missouri) was used as the model aliphatic compound, and [1,4,5,8- ^{14}C] naphthalene (American Radiolabeled Chemicals, Missouri) was used as the model aromatic compound (Figure 3.2).

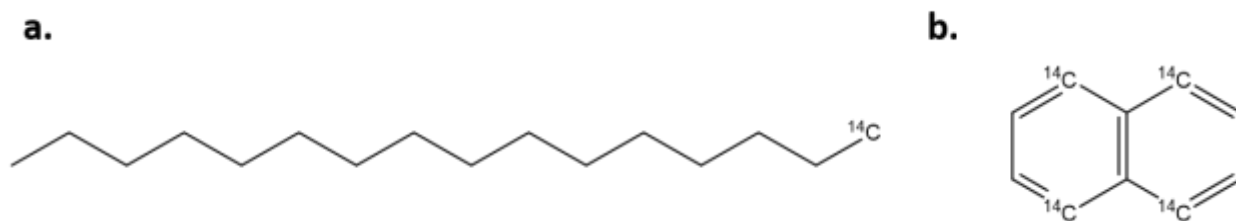


Figure 3.2 Structures of ^{14}C substrates used to quantify hydrocarbon turnover in surface waters. $[1\text{-}^{14}\text{C}]$ -*n*-hexadecane (a) was used as a model linear alkane, and $[1,4,5,8\text{-}^{14}\text{C}]$ naphthalene was used as a model aromatic compound (b).

Homogenized water from station sample was subsampled into headspace-free, 8mL glass scintillation vials capped with a PTFE-lined rubber septum (Supelco, Pennsylvania). Each assay was carried out in triplicate alongside a killed control (2mL of 2M NaOH). ^{14}C -labeled hydrocarbons were each dissolved in molecular grade ethanol and delivered into each scintillation vial with a glass syringe ($0.5\ \mu\text{Ci} = 1.35 \times 10^{-5}\ \text{Bq}$; $10\ \mu\text{L}$) and inverted gently to distribute the tracer. Killed controls were injected with tracer and immediately added to the killing solution (2M NaOH, 2mL) in a 50mL polypropylene conical tube. Incubations were carried out at room temperature in the dark. Incubations were terminated by transferring the contents of the scintillation tube into a 50mL polypropylene conical tube prefilled with the killing solution. Terminated incubations were stored in the basic solution ($\text{pH} > 10$) at room temperature for up to 3 weeks before acidic distillation of the evolved $^{14}\text{CO}_2$.

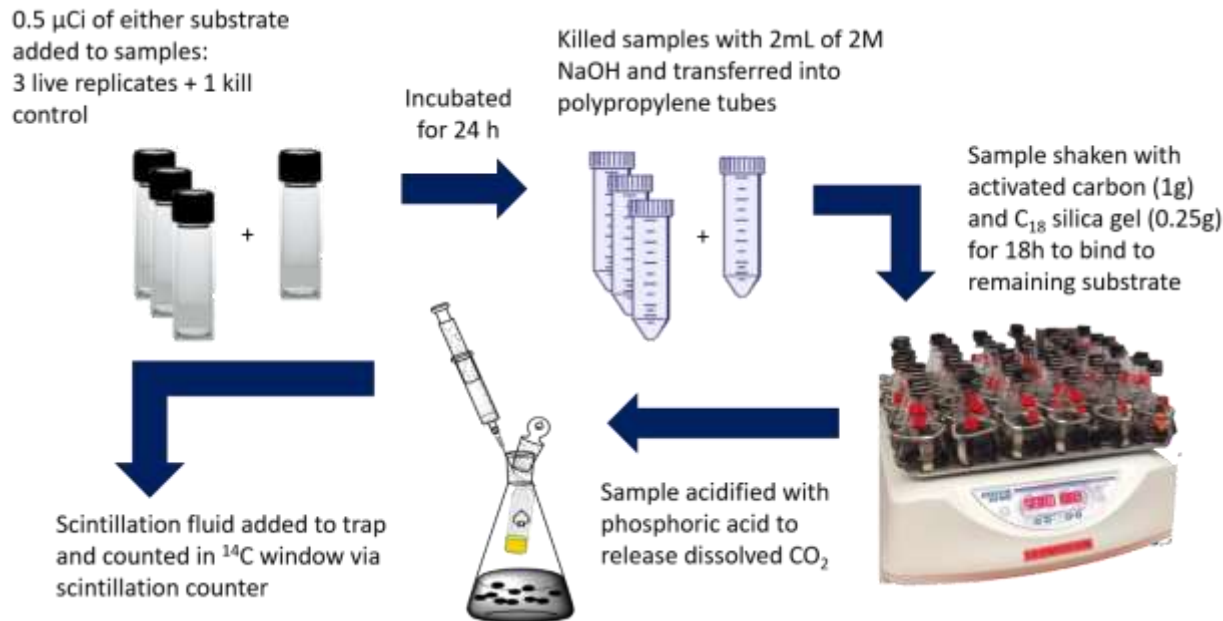


Figure 3.3 Schematic of hydrocarbon oxidation rate method developed by Kleindienst et al. (2015) and Sibert et al. (2016).

Evolved $^{14}\text{CO}_2$ was distilled from the terminated incubation in the following method (Figure 3.3). Samples were transferred to 250mL Erlenmeyer flasks capped with rubber stoppers and clamps and shaken with activated charcoal (1g, Sigma Aldrich) for 6h as a pre-treatment to bind any unused tracer to the charcoal. Hexadecane oxidation assays were further amended with C_{18} reverse phase silica gel (250 mg, Supelco) to more effectively bind unused alkane tracer.

Following this pretreatment, the Erlenmeyer flask was fitted with a carbon dioxide trap (1.5 mL, CarboSorb E®, Perkin Elmer), acidified with concentrated phosphoric acid (5mL), and quickly stoppered to minimize loss of evolved CO_2 . Acidified solutions were then shaken overnight to capture CO_2 . Radioactivity of the carbon dioxide trap was quantified using a Beckman 6500 liquid scintillation counter, after adding scintillation fluid, (4.5mL, Scintisafe®, Fisher Scientific) to each trap. Instrumentation blanks were counted after every 10 samples, and total injected tracer was quantified as the blank corrected average of the 3 injections made into

scintillation fluid at the time of the incubation. All values from the scintillation counter were first blank corrected, and each sample was kill corrected with the value of the kill control for each sample.

Potential rates were calculated using modifications of the following formula (Equation 3.1). k is the rate constant, a term derived from the quotient of α , the fraction of radiotracer turned over, by t , the duration of the incubation. S is the concentration of the substrate.

$$-\frac{d[\text{Hydrocarbon}]}{dt} = k[S] = \frac{\alpha}{t}[S] * \frac{[\text{Radioactivity turned over, dpm}]}{[\text{Radioactivity added, dpm}]} * \frac{[S]}{t}$$

Equation 3.1

Potential Hexadecane Oxidation Rate: $[1\text{-}^{14}\text{C}]\text{-hexadecane} + \text{O}_2 \rightarrow {}^{14}\text{CO}_2 + \text{H}_2\text{O}$

$$-\frac{d[\text{Hexadecane}]}{dt} = k[\text{Hexadecane}] = \frac{\alpha}{t} * [\text{Hexadecane}] = \frac{[{}^{14}\text{CO}_2]}{[{}^{14}\text{C} - \text{Hexadecane} * t]} * [\text{Hexadecane}]$$

Equation 3.2

Potential Naphthalene Oxidation Rate: $[1,4,5,8\text{-}^{14}\text{C}]\text{-naphthalene} + \text{O}_2 \rightarrow {}^{14}\text{CO}_2 + \text{H}_2\text{O}$

$$-\frac{d[\text{Naphthalene}]}{dt} = k[\text{Naphthalene}] = \frac{\alpha}{t} * [\text{Naphthalene}] = \frac{[{}^{14}\text{CO}_2]}{[{}^{14}\text{C} - \text{Naphthalene} * t]} * [\text{Naphthalene}]$$

Equation 3.3

Calculated Concentration of the Radiotracer used in the ^{14}C Incubations

$$[\text{Hexadecane tracer}] = \frac{\text{Radioactivity of added tracer, dpm}}{\text{Volume of incubation vessel, mL}} * \frac{1 \text{ mCi}}{2.22 \times 10^9 \text{ dpm}} * \frac{1 \text{ mmol}}{55 \text{ mCi}}$$

Equation 3.4

$$[\text{Naphthalene tracer}] = \frac{\text{Radioactivity of added tracer, dpm}}{\text{Volume of incubation vessel, mL}} * \frac{1 \text{ mCi}}{2.22 \times 10^9 \text{ dpm}} * \frac{1 \text{ mmol}}{58 \text{ mCi}}$$

Equation 3.5

The concentration of the added tracer is a function of the incubation vessel dimension (7.5 mL) and specific activity of the hexadecane and naphthalene tracer, as determined by the manufacturer (55 Ci/mol and 58 Ci/mol, respectively; Equations 3.2 and 3.3).

Determining which concentration of substrate to use presented a challenge in this study, given the vastly different concentrations of oil across the two transects. The *in situ* concentrations of hexadecane and naphthalene were below the limit of detection via GC-MS for the entire summer 2015 transect and near the limit of detection for stations B and C in the fall 2014 transect (Table 3.3). Additionally, the incubations required a high concentration of radiotracer (1.45 μM for hexadecane, and 1.10 μM for naphthalene), which were above the solubility limit for both compounds. Naphthalene fully saturates water at 25°C under standard atmosphere conditions at 0.248 μM (Pearlman *et al.* 1984), while the measured solubility limit for hexadecane is considerably lower, at 4.06 nM (*Human Metabolome Database* and EPIWEB v4.11). The tracer, then, is a misnomer in this study, as the tracer itself contributes substantially to the concentration of substrate in the incubation vessel. Given these limitations, the estimations made from these assays should be considered as potential rates for the given substrate. Additionally, the potential rates discussed in this study use the sum of the measured substrate in the environment plus the tracer concentration as the total substrate concentration.

3.2.5 Microbial Community Composition

Microorganisms were filtered onto a Sterivex filter cartridge (0.22 μm ; Millipore) and flash frozen in liquid nitrogen. 1L of water was filtered from each station along the fall 2014 transect; in the summer 2015 transect, 250 mL from each bottle was pooled with other station replicates for a total of 750 mL water per station (3 bottles/station * 250 mL/bottle= 750 mL).

Samples from 2014 were stored at -20°C until processing. Samples from 2015 were shipped on dry ice from Gulfport, MS to Athens, GA and stored at -80°C until processing. Sterivex filters were thawed on ice, the tops removed with sterilized pliers, and the filter cut using sterile scalpels; the cut filters were immediately processed for DNA extraction using the DNeasy Powerwater Kit (Qiagen) according to the manufacturer’s directions. Eluted DNA was quantified using the dsDNA assay kit and a Qubit fluorometer (Invitrogen) (Table 3.2).

Barcoded amplicons of the 16S rRNA were generated using primers amplifying the V4 region and the AccuPrime™ Pfx SuperMix kit (Invitrogen) with methods previously described (Kozich *et al.* 2013; Table 3.2). Samples were sequenced on an Illumina MiSeq (Illumina) at the Georgia Genome Facility (GGF, University of Georgia, Athens, GA) resulting in 2x250 paired-end reads.

Transect	Station	Extracted DNA concentration (ng/μL)	Barcoded Primer IDs for 16S Amplification
Oct-14	A	lost during extraction	N/A
Oct-14	B	8.4	SA504/SA702
Oct-14	C	2.08	SA503/SA712
Oct-14	D	0.444	SA504/SA701
Jun-15	E	22	SA501/SA705
Jun-15	F	11.4	SA502/SA701
Jun-15	G	29.4	SA502/SA710
Jun-15	H	53	SA502/SA708
extraction	blank	too low for detection	SA502/SA711

Table 3.2 Table of DNA concentrations for surface water samples from the two Taylor Energy transects and the amplicon barcodes assigned to each sample using the protocol developed by Kozich *et al.* (2013).

At the time of writing, this analysis is still in progress and will not be discussed further.

3.2.6 Statistical Analysis

Data was analyzed using R version 3.2.4 (Copyright © 2016, The R Foundation for Statistical Computing). Due to the small sample size and non-normal distributions of data, non-parametric

tests were used to compare and contrast the biogeochemical data from the two stations. Variance was assessed by the Kruskal-Wallis Rank Sum Test, a non-parametric alternative to an ANOVA. Paired Wilcoxon rank sum tests were used to assess differences within the sample sets, and Spearman's rank coefficients were used to assess correlation between geochemical parameters.

3.3 Results

3.3.1 *Dissolved Nutrients*

Analysis of the dissolved constituents in the water revealed statistically greater differences between the two transects than within each transect. The summer 2015 transect has significantly higher levels of DOC (Wilcoxon rank sum test: p-value = 0.02857), NO_2^- (Wilcoxon rank sum test: p-value = 0.02107), NO_3^- (Wilcoxon rank sum test: p-value = 0.02652), HPO_4^{3-} , (Wilcoxon rank sum test: p-value = 0.02652), and TDP (p-value = 0.02652) compared to the fall 2014 transect. The differences in these dissolved parameters may reflect the seasonal oscillations described previously (Chapter 2 of this project).

There were, however, no significant differences between or within the two transects with respect to NH_4^+ (Wilcoxon rank sum test: p-value = 0.7702). This is surprising, given the overall oligotrophic nature of the fall 2014 transect; however, this relative enrichment of ammonium in the 2014 transect may be due to the rapid cycling of petrogenic material from the nearby oil slick. This significance underscores the intertwined relationship of nutrient dynamics and carbon cycling in surface waters at this coastal site.

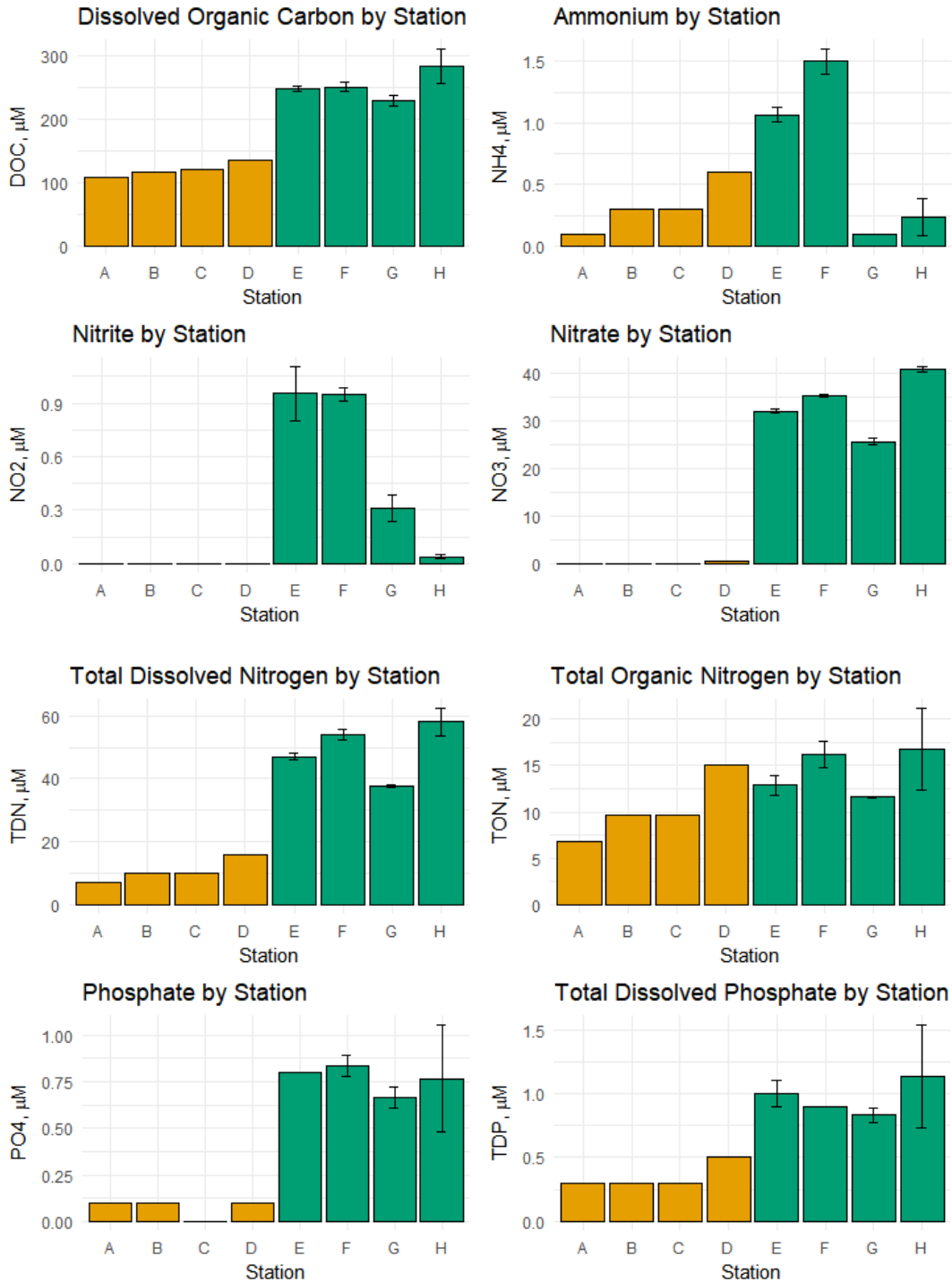


Figure 3.4 Average dissolved nutrient concentrations in surface water for each station. Stations from the fall 2014 transect are represented with gold bars and stations from the summer 2015 transect are represented with green bars. Bars represent the average values from each +/- standard deviations; no error bars are plotted for 2014 samples.

3.3.2 Extractable Hydrocarbons

As anticipated, there were stark differences between the two transects with respect to extractable hydrocarbon concentrations. Stations A and D were the two most heavily oiled stations in the fall 2014 transect. All stations from the 2015 transect contained hydrocarbons below detectable limits via GC-TOF-MS or GC-FID analysis, which was on the order of 1 ng/mL or 1ppm. Average recovery of eicosane-d₂₄ was 74.28% for 2015 samples.

The oil extracted from surface grabs of oil slicks in the 2014 transect revealed a heavily weathered oil at Stations A and D, as demonstrated by the absence of short chain alkanes and the appearance of an unresolved complex mixture forming in the chromatographic window (Figure 3.4). The chromatographs look similar to other heavily oiled surface slicks observed in the Gulf of Mexico and resembles extracts of weathered sand patties found on beaches in the aftermath of the *Deepwater Horizon* oil spill (Aeppli *et al.* 2012; Harrison, 2013).

Table 3.3 Table summarizing extractable hydrocarbons for surface water samples from the two Taylor Energy transects. Results presented are the average of 3 extractions per station. Only naphthalene and hexadecane are presented, as these concentrations were used in calculations for the radiolabeled hydrocarbon turnover assays.

Station	Naphthalene Concentration				Hexadecane Concentration				Oil Concentration	
	Average (ng/mL)	SD	Average (µM)	SD	Average (ng/mL)	SD	Average (µM)	SD	Average (mg/mL)	SD
A	42.77	22.84	0.33	0.18	3151.47	182.89	13.945	0.809	6.485	0.555
B	BDL	n/a	BDL	n/a	0.41	0.35	0.002	0.002	0.009	0.001
C	0.12	0.20	0.0009	0.002	BDL	n/a	BDL	n/a	0.003	0.001
D	69.04	39.28	0.54	0.31	2293.82	1274.26	10.150	5.638	4.725	2.866
E	BDL	n/a	BDL	n/a	BDL	n/a	BDL	n/a	BDL	n/a
F	BDL	n/a	BDL	n/a	BDL	n/a	BDL	n/a	BDL	n/a
G	BDL	n/a	BDL	n/a	BDL	n/a	BDL	n/a	BDL	n/a
H	BDL	n/a	BDL	n/a	BDL	n/a	BDL	n/a	BDL	n/a

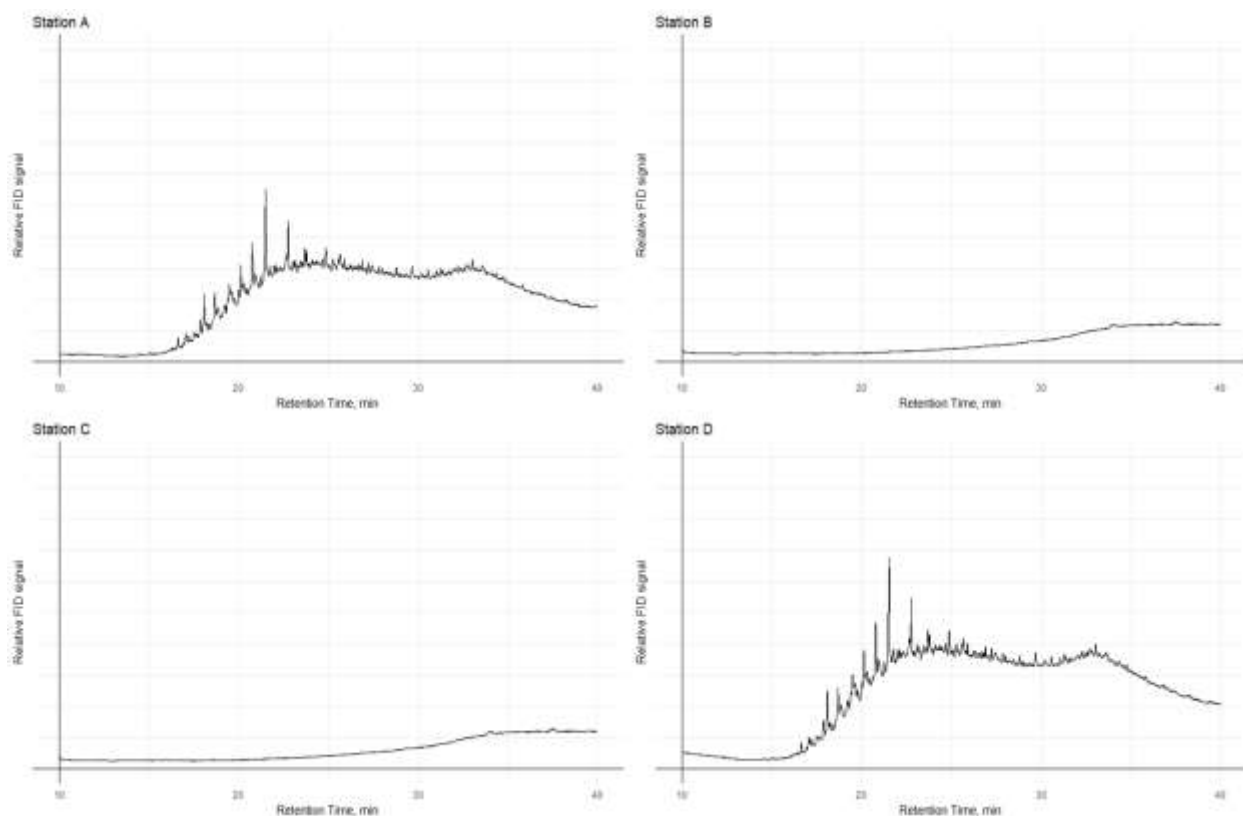


Figure 3.5 GC-FID chromatograms of surface slick samples from each of the stations along the fall 2014 transect.

3.3.3 Potential Rates of Hydrocarbon Oxidation

3.3.3.1 Potential Hexadecane Oxidation Rates

There was robust oxidation of hexadecane at all stations from both transects (mean 13.4 nM/d; SD \pm 17.2). Using this same method, Kleindienst *et al.* measured maximum hexadecane oxidation rates of 0.006 nM/d in a microcosm experiment using mid-water (Kleindienst *et al.* 2015). The highest rates observed at this site were at Station A, a station with large quantities of observable oil mousse, while the lowest observed potential rates were measured in the same transect at Station C, adjacent to a fine oil sheen.

Despite the large range of potential hexadecane oxidation rates observed at the Taylor Energy site (0.06-51 nM/d), no statistical differences were detected (via a series of Kruskal-Wallis rank

sum tests) between individual stations or between the two seasons that hexadecane oxidation was measured. This finding suggests that there is a robust alkane degrading community present within surface waters across seasons.

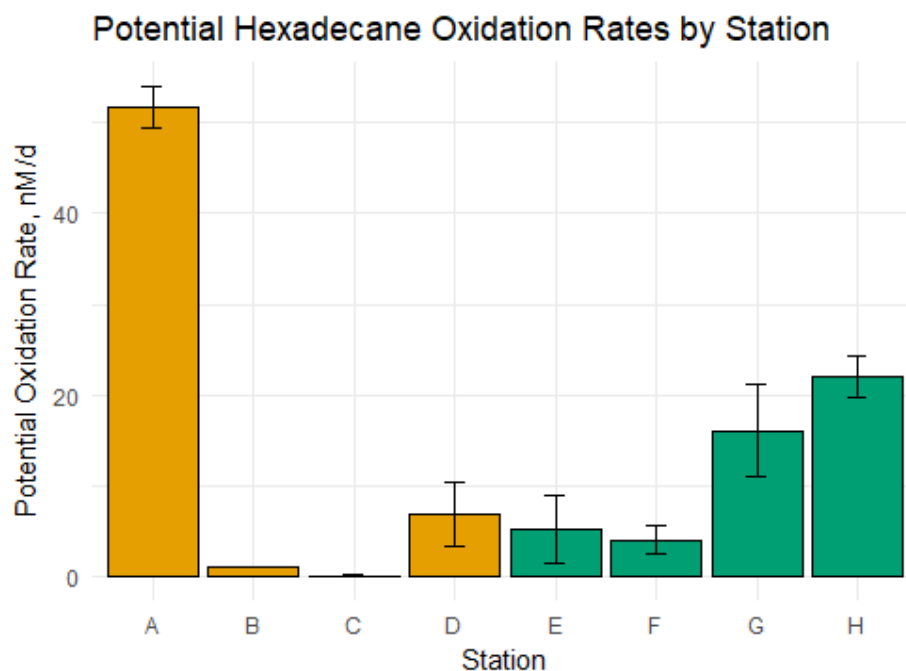


Figure 3.6 Potential hexadecane oxidation rates by station, yellow bars are from the 2014 transect, green from the 2015 transect. Note that the 2014 samples are the average potential rate from 3 replicate rad samples, while the 2015 samples are the overall site average from 3 bottle reps/station, +/- standard deviation. The hexadecane concentration is a sum of the calculated tracer addition (1.5-2 μM) plus the concentration of hexadecane as determined via GC-MS quantification.

3.3.3.2 Potential Naphthalene Oxidation Rates

There were modest rates of naphthalene oxidation measured across the two transects, with a mean. The potential naphthalene oxidation rates were considerably lower than previously measured naphthalene oxidation rates observed by Kleindienst *et al.* using mid-water from the Gulf of Mexico exposed to a water accommodated fraction of oil (2015).

Unlike potential hexadecane oxidation rates across the Taylor Energy site, there was a significant difference between the two transects with respect to the potential rates of naphthalene oxidation (Kruskal-Wallis chi-squared = 5.3976, df = 1, p-value = 0.02016). Despite detectable concentrations of naphthalene at three stations in the fall 2014 transect, there was significantly lower potential rates of naphthalene oxidation compared to the summer 2015 transect (Wilcoxon Rank Sum Test: p-value = 0.0294).

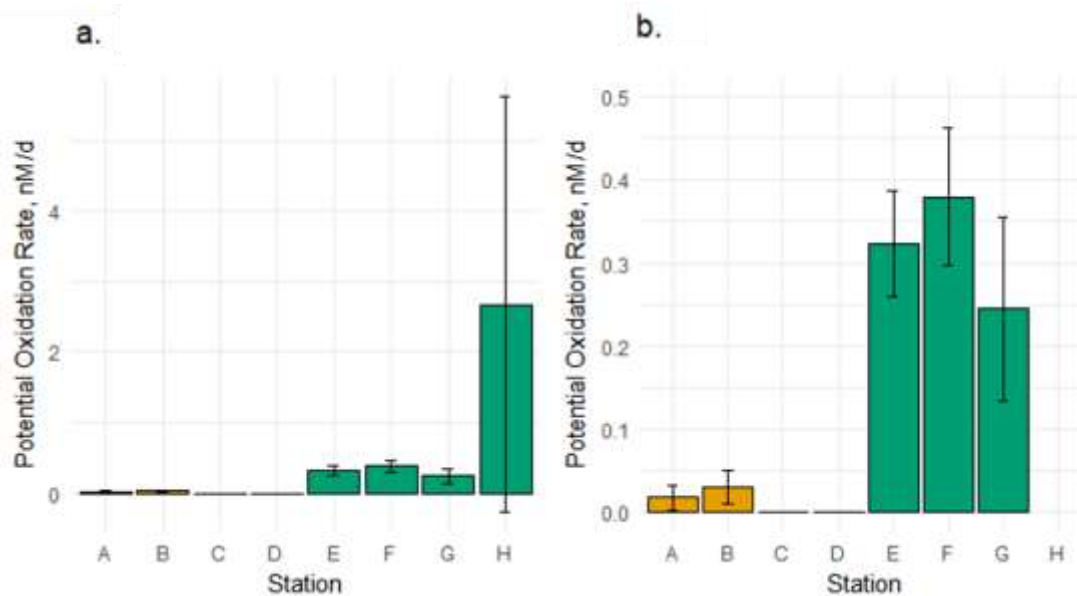


Figure 3.7 Potential naphthalene oxidation rates by station, yellow bars are from the 2014 transect, green from the 2015 transect. All stations are plotted on (a), while the y-axis is limited in (b) to highlight the differences within the 2014 transect. Note that the 2014 samples are the average potential rate from 3 replicate rad samples, while the 2015 samples are the overall site average from 3 bottle reps/station, +/- standard deviation. The naphthalene concentration used to calculate the rate is the sum of the calculated tracer addition (1.5-2 μM) plus the measured naphthalene concentration.

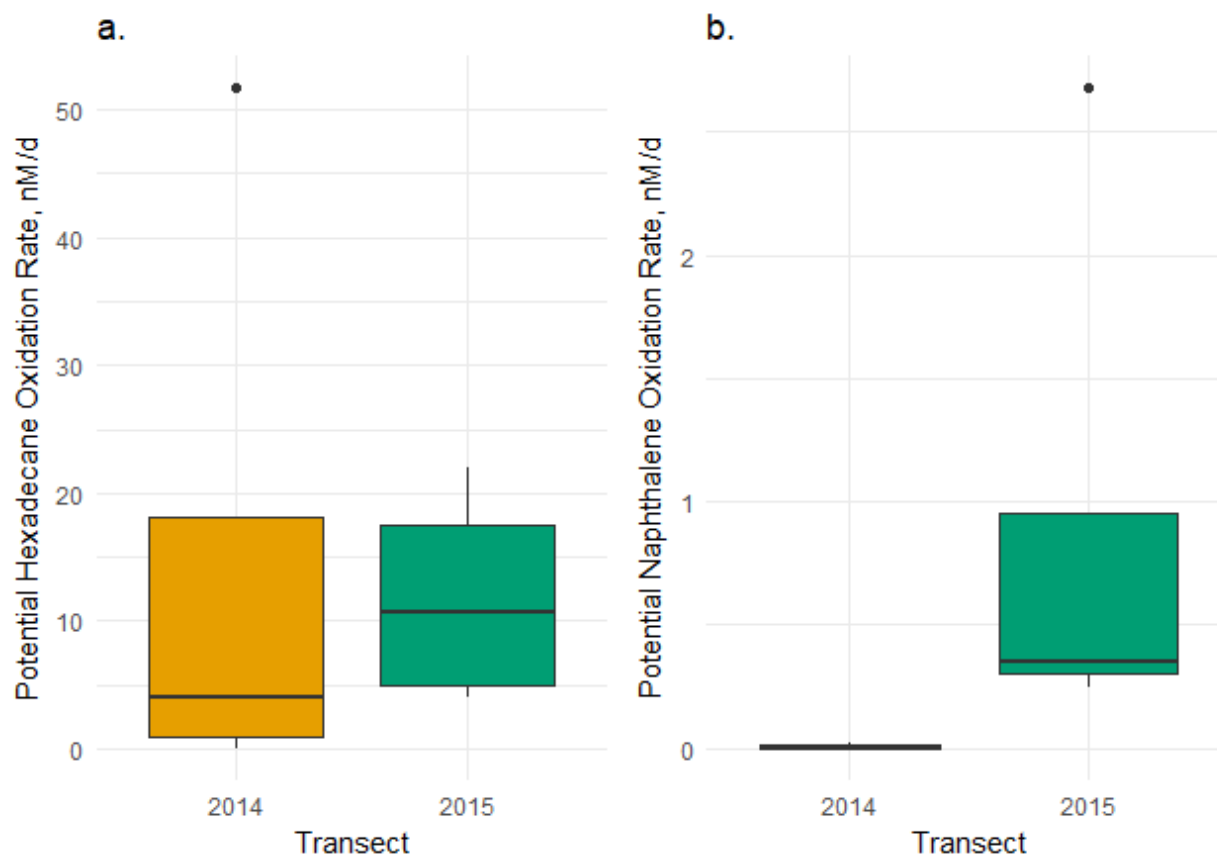


Figure 3.8 Box plots of the potential hexadecane oxidation rate (a) and potential naphthalene oxidation rate (b) aggregated by transect.

Statistical examination of the potential hexadecane oxidation rates failed to detect differences between the two transects (Figure 3.8a), reflecting the year-round presence of a robust aliphatic degrading microbial community in the surface waters surrounding the Taylor Energy site. In contrast, there was a significant difference in the potential rate of naphthalene oxidation between the two transects, (Kruskal-Wallis chi-squared = 5.3333, df = 1, p-value = 0.02092). This seasonal difference could reflect seasonal nutrient limitation for aromatic degrading microbes or seasonal priming by aromatic-rich riverine DOC.

3.3.3.3 Rate Constants for Hydrocarbon Turnover Assays

To further examine the rates, we can also examine the rate constant, k , as measured by the radiotracer assays (Equations 3.2 and 3.3). The rate constant is the quotient of alpha (fraction of total radiotracer turned over to $^{14}\text{CO}_2$ out of the total pool injected into the live incubation, corrected for kill controls and instrument blanks) and incubation time. Examination of the rate constant allows us to compare potential rates across the Taylor Energy site independently of the measured *in situ* substrate concentration.

3.3.3.3.1 Hexadecane Oxidation Rate Constant

Examination of the hexadecane oxidation rate constants revealed a significant difference between the two different transects (Kruskal-Wallis chi-squared = 4.0833, df = 1, p-value = 0.04331); examination by a Wilcoxon rank sum failed to detect a difference between the two transects (Wilcoxon rank sum test; p-value= 0.05714). No significant differences were detected with each transect.

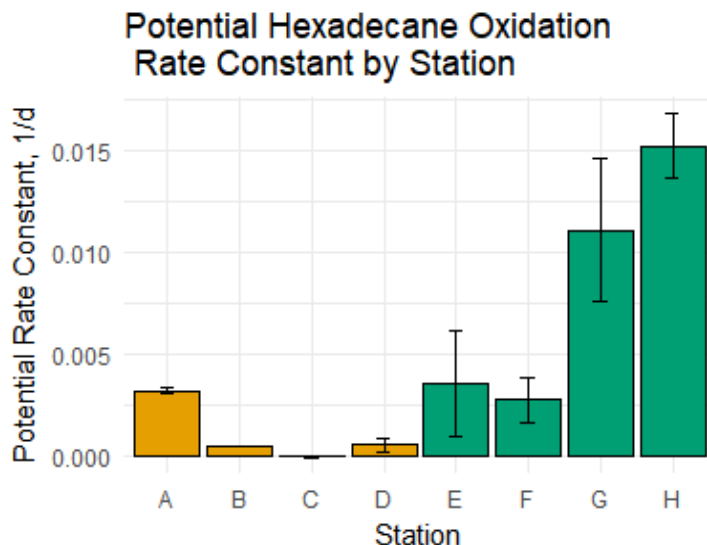


Figure 3.9 Rate constants for hexadecane oxidation, plus or minus the standard deviation among the radiotracer replicates. Bars are colored according to the year the sample was taken.

3.3.3.3.2 Naphthalene Oxidation Rate Constant

The only significant difference across naphthalene oxidation rate constants was detected between the two transects (Kruskal Wallis rank sum test: Kruskal-Wallis chi-squared = 5.4634, df = 1, p-value = 0.01942). A follow up examination with a Wilcoxon rank sum test agreed with this finding (Wilcoxon rank sum test: p-value=0.02843), agreeing with the potential rate finding discussed earlier.

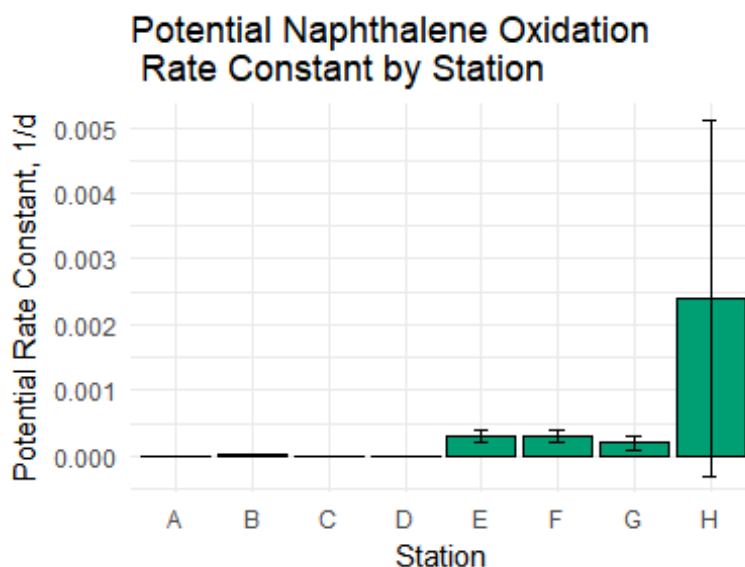


Figure 3.10 Rate constants for naphthalene oxidation, plus or minus the standard deviation among the radiotracer replicates. Bars are colored according to the year the sample was taken.

Analysis of the rate constant largely agrees with the analysis of the full potential rate data. There are significant differences in the microbial community's ability to mineralize hydrocarbons across seasons, but not within each transect. The major difference is with respect to hexadecane oxidation; analysis of the potential rate revealed no significant differences between the autumn 2014 and summer 2015 transect, yet there were significant differences with respect to the rate constant (Kruskal-Wallis chi-squared = 4.0833, df = 1, p-value = 0.04331).

3.4 Discussion

3.4.1 Commentary about post hoc experimental design

The comparison between these two transects is truly a *post hoc* experimental design utilizing samples of opportunity, and there are considerable concerns with this. The sample sizes for each station are different across the years (n=1/ station in 2014; n= 3 /station in 2015).

The 2014 samples included in this project are some of the very first biological and geochemical samples collected from surface waters at the Taylor Energy site. Unfortunately, for this transect, we were water-limited in our sampling, with only one sample taken per station. We were unsure of what kind of variability we might see within these four stations within this single transect. As such, sampling was rethought and redesigned prior to the 2015 transect.

The 2015 transect, again, has some interesting factors to consider. According to the CGMIX database, there was an oil slick (2 km x 0.5 km; SEQNOS report ID 1119149) reported slick at the Taylor Energy site, following a northwest to southeast trajectory the day of sampling.

However, between the time of the slick sighting and getting on station, a storm rolled through, severely limiting any slick visibility and likely breaking up any slicks that had previously set up during the day.

3.4.2 Comparison of Potential Hydrocarbon Oxidation Rates

3.4.2.1 Differences between Substrates

Previously, hydrocarbon oxidation rates were compared amongst each other siloed the rates by the type of rate. However, these rate methods were developed as tools to quantify the biodegradation of a complex mixture of petroleum hydrocarbons in surface water. Ultimately, we

hope to compare these two types of potential rates to better understand the fate of the various fractions of petroleum hydrocarbons in the environment.

Overall, there are higher rates of hexadecane oxidation compared to naphthalene oxidation in surface waters around the Taylor Energy site (Wilcoxon rank sum test: p -value= 0.03226). The mean potential hexadecane oxidation rate is 13.40 nM/d compared to the mean potential naphthalene oxidation rate of 0.46 nM/d. This nearly two orders of magnitude difference agrees with previously work; Aeppli *et al.* described n-alkanes as among the most readily biodegraded classes compounds within oil (Aeppli *et al.* 2014). Moreover, the mineralization of hexadecane requires breaking single carbon-carbon bond, where each carbon is bound to one another across a pair sp^3 hybridized orbitals. The mineralization of naphthalene requires breaking double carbon-carbon bonds, which require enough energy to break both the single bond forged from the two sp^3 hybridized orbitals as well as the pi bond that contributes to the compounds aromaticity. This difference in bond structure is echoed in the energetic costs to break these different kinds of carbon bonds: 348 kJ/mol for saturated carbon bonds, compared to 519 kJ/mol required for a single carbon aromatic bond (Silverstein *et al.*, 2005).

Constraining these hydrocarbon oxidation rates is important to the much larger study of how oil is transformed biologically. While the biodegradation of mid-sized alkanes has long been characterized, it has been assumed that the disappearance of aromatic hydrocarbons from surface slicks was largely the result of physical processes, such as evaporation, photo-oxidation, oxidation, and/or dissolution. It appears, however, that biodegradation of a small aromatic, like naphthalene, is an important sink for these petroleum hydrocarbons.

3.4.2.1 Differences between Fall 2014 and Summer 2015 Transects

Previously, we established that there are seasonal differences in the slick length and frequency at the Taylor Energy site and that the northern Gulf of Mexico is a highly seasonal region. The first installment of this chapter illustrated that these seasonal differences are also apparent at the Taylor Energy site. Closer examination of the rate data has revealed a significant difference with respect to the potential rate of naphthalene oxidation between the two transects (Kruskal-Wallis chi-squared = 5.3333, df = 1, p-value = 0.02092), but not the potential rate of hexadecane (Kruskal-Wallis chi-squared = 1.3333, df = 1, p-value = 0.2482). Unlike hexadecane, the potential rate and the rate constant data agree for naphthalene oxidation.

One question that emerges from this work is whether the rates of hydrocarbon oxidation differ with season at the Taylor Energy site. While the data included in this chapter are not rich enough to definitively describe the seasonal differences for all petroleum hydrocarbons, we can begin to understand how the microbial community and its capacity to degrade broad classes of hydrocarbons changes between the summer and autumn months. If hexadecane is a good model for other mid-sized normal alkanes, then there appears to be no seasonal variation with respect to the potential rate of biodegradation for these compounds. The significant increase in naphthalene oxidation in the summer 2015 transect as compared to the fall 2014 transect suggests that there may be seasonal controls on the biodegradation of small aromatic compounds. While these trends are suggestive, there is not enough information to assess whether oil is biodegraded more rapidly in the autumn or summer based on just these two transects. Sampling the site, with and without oil, across various points of time in the year will be required to ultimately state if there are significant seasonal microbial sinks of petroleum hydrocarbons in the surface waters at the Taylor Energy site. Understanding the seasonal capacity of microbial oxidation of oil in surface

waters around the Taylor Energy site is important for understanding the greater ecological impact of the Taylor Energy oil spill to coastal waters. For instance, economically valuable and large predatory pelagic species, such as blue- and yellowfin tuna, amberjack, sailfish, blue marlin, and cobia spawn offshore in the late spring and summer months, and can be significantly impacted by trace concentrations of crude oil in the water column (Incardona *et al.* 2013; references 5-13 therein).

3.4.3 Correlations between Nutrients and Potential Hydrocarbon Oxidation Rates

Examining the geochemical and potential rate data from across both transects via a Spearman's Rank Correlation test allows us to hypothesize which geochemical parameters could be candidate drivers for hydrocarbon oxidation in surface waters (Figure 3.11).

Given that there were no statistical differences between the two transects with respect to potential hexadecane oxidation rates, it is unsurprising that there were also no significant correlations between potential hexadecane oxidation rates and any of the other geochemical parameters tested that varied significantly. There were, however, significant relationships between parameters used to calculate the rate, including the rate constant (HexaOx.RC) and the potential rate using just tracer concentration (HexaOx.Tracer). There was a strong negative correlation between potential hexadecane oxidation rates and ammonium, but this relationship was not found to be significant (Spearman's rank correlation: $\rho = -0.59$; $p\text{-value} = 0.1233$).

There were several statistically significant relationships between the potential rate of naphthalene oxidation and dissolved nutrients. The potential rate of naphthalene oxidation was positively correlated with nearly every geochemical parameter measured: phosphate concentrations (Spearman's rank correlation: $\rho = 0.88$; $p\text{-value} = 0.00361$), nitrate concentrations (Spearman's

rank correlation: $\rho = 0.86$; p -value = 0.00628), total dissolved nitrogen (Spearman's rank correlation: $\rho = 0.84$; p -value = 0.00949), total dissolved phosphate (Spearman's rank correlation: $\rho = 0.83$; p -value = 0.00997); nitrite (Spearman's rank correlation: $\rho = 0.77$; p -value = 0.02681); and DOC (Spearman's rank correlation: $\rho = 0.80$; p -value = 0.01654). There was no significant relationship between naphthalene oxidation and ammonium concentrations. Meanwhile, there was a negative relationship between naphthalene oxidation and total petroleum hydrocarbon concentration (Spearman's rank correlation: $\rho = -0.79$; p -value = 0.01937) as well as with measured quantities of naphthalene, although the latter correlation was not statistically significant (Spearman's rank correlation: $\rho = -0.59$; p -value = 0.125).

Naphthalene oxidation is significantly correlated with higher concentrations of dissolved nitrogen and phosphate species, indicating that naphthalene oxidation may become nutrient limited in fall and winter months.

Naphthalene oxidation also appears to have a complex relationship with carbon in surface waters. While there is a statistically significant negative relationship between the concentration of oil at a site and the rate of naphthalene oxidation (Spearman's rank correlation: $\rho = -0.79$; p -value = 0.01937), there is also a statistically significant and equally positive correlation with dissolved organic carbon across the site (Spearman's rank correlation: $\rho = 0.80$; p -value = 0.01654). The negative relationship with oil and naphthalene oxidation may stem from synergistic toxicity or higher affinity for smaller aromatic compounds. More likely, this negative relationship reflects that the stations with heavily oiled surface water were also nutrient limited. Further investigations at the Taylor Energy site are needed to understand the relationship between oil concentrations and potential naphthalene oxidation rates.

The significant, positive relationship between DOC and potential rates of naphthalene oxidation is among the most surprising discoveries from this site. This relationship may reflect an underlying influence of the Mississippi River plume on the surface waters at the Taylor Energy site. As conduits of carbon from terrestrial to marine ecosystems, rivers play a key role in the transformation of terrestrial carbon to marine carbon. One important class of terrestrial carbon is lignin, a key component in the support structure of woody plants, comprised of phenolic compounds joined together with aromatic ether bonds. Lignin is heavily degraded along riverine systems, such as the Amazon River (Ward *et al.* 2013), releasing small aromatic compounds, such as phenols, into the DOC pool. Microbial communities along the river-ocean-continuum responsible for this transformation has been implicated as an important sink for these aromatic compounds, especially at a river's mouth (Medeiros *et al.* 2015). The export of degraded terrestrial carbon and the microbial communities responsible for degrading terrestrial material may confer the Taylor Energy site, a site inundated with persistent oil slicks, with a microbial community primed to degrade small aromatic compounds found in oil, such as naphthalene.

Correlation Matrix of Potential Hydrocarbon Oxidation Rates and Geochemical Parameters

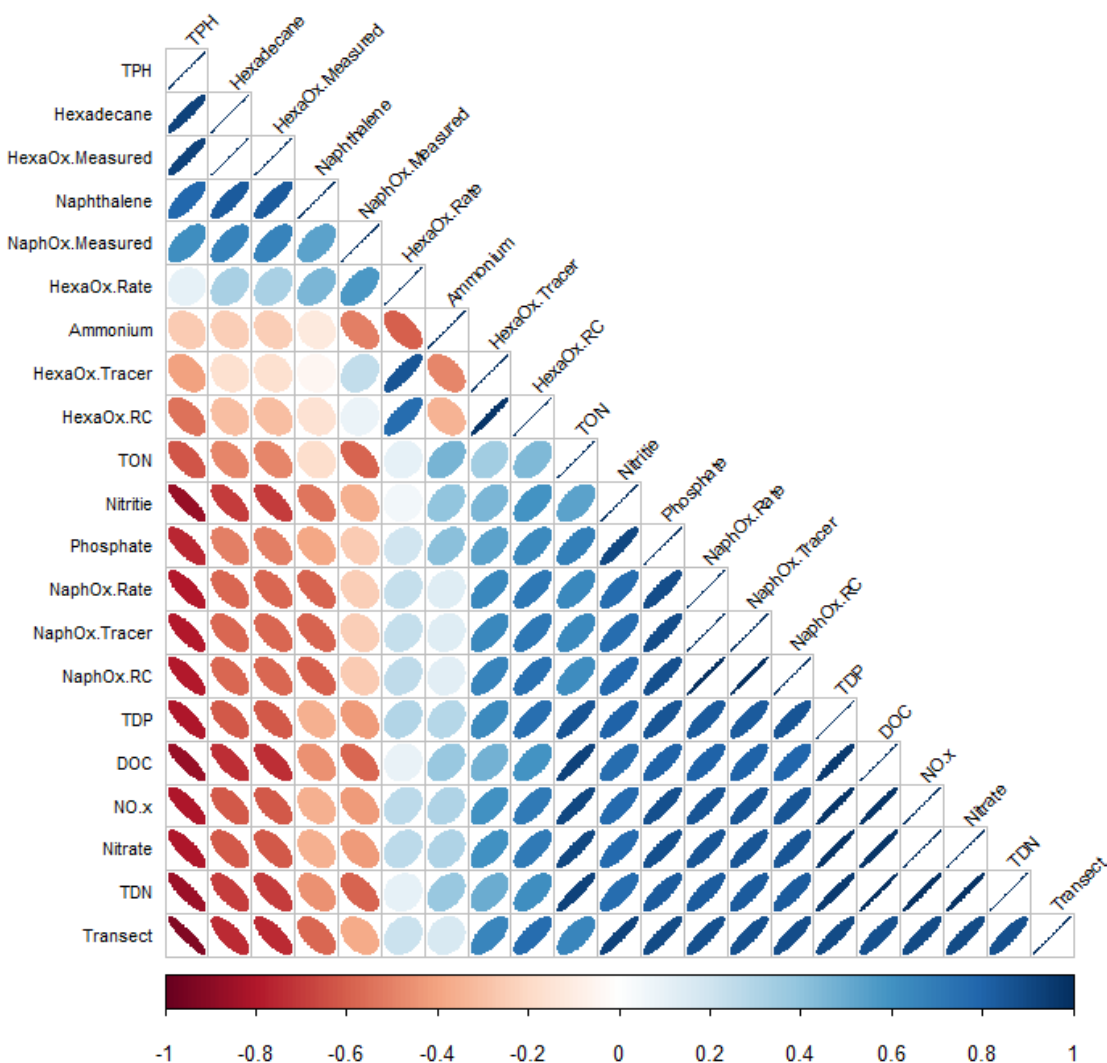


Figure 3.11 Correlogram of all rates and geochemical parameters from the in situ sampling regime of the Taylor Energy site, using a Spearman's rank correlation test. Rho values are depicted as colors; blue values indicate a positive relationship, white bubbles indicate a neutral or minimal relationship, and red values indicate a negative relationship.

3.5 Conclusion

These two transects conducted in the fall and summer represent two extreme ends of the biogeochemical range possible at the Taylor Energy site. While this is not a full factorial exploration of this site (with oil across all four seasons; without oil across all four seasons), these two transects reveal the surface water at the Taylor Energy site to be a highly dynamic and seasonally variant site. There were significant differences with respect to dissolved nutrients and the potential naphthalene oxidation rate between the summer and fall transects, but the potential rate of hexadecane was robust and not significantly different between the two transects. No significant differences were found within transects, but deeper sampling will be required to resolve nutrient and hydrocarbon degrading dynamics within the area of a surface slick. Differences in correlations between dissolved nutrients and potential hydrocarbon oxidation rates suggest that the geochemical controls governing hydrocarbon oxidation in surface waters are highly substrate specific and may be seasonally variant.

References

- Aeppli, C.; Carmichael, C. A.; Nelson, R. K.; Lemkau, K. L.; Graham, W. M.; Redmond, M. C.; Valentine, D. L.; Reddy, C. M. Oil Weathering after the Deepwater Horizon Disaster Led to the Formation of Oxygenated Residues. *Environ. Sci. Technol.* **2012**, *46* (16), 8799–8807 DOI: 10.1021/es3015138.
- Aeppli, C.; Nelson, R. K.; Radovic, J. R.; Carmichael, C. A.; Valentine, D. L.; Reddy, C. M. Recalcitrance and Degradation of Petroleum Biomarkers upon Abiotic and Biotic Natural Weathering of Deepwater Horizon Oil. *Environ. Sci. Technol.* **2014**, *48*, 6726–6734.
- Bendschneider K.; Robinson R.J. A new spectrophotometric method for the determination of nitrite in sea water. *University of Washington Oceanographic Laboratories.* **1952**.
- Braman, R.S.; Hendrix, S.A. Nanogram nitrite and nitrate determination in environmental and biological materials by vanadium (III) reduction with chemiluminescence detection. *Analytical Chemistry.* **1989** Dec 1;61(24):2715-8.
- Garside C. A chemiluminescent technique for the determination of nanomolar concentrations of nitrate and nitrite in seawater. *Marine Chemistry.* **1982** Apr 1;11(2):159-67.
- Harrison, S.J. Investigating the Dynamic Range of Weathered Oil and Chemical Dispersant in the Environment. B.Sc. Thesis, Haverford College, Haverford, PA. **2013**.
- Incardona, J. P.; Gardner, L. D.; Linbo, T. L.; Brown, T. L.; Esbaugh, A. J.; Mager, E. M.; Stieglitz, J. D.; French, B. L.; Labenia, J. S.; Laetz, C. A.; Tagal, M.; Sloan, C. A.; Elizur, A.; Benetti, D. D.; Grosell, M.; Block, B. A.; Scholz, N. L. PNAS Plus: From the Cover: Deepwater Horizon Crude Oil Impacts the Developing Hearts of Large Predatory Pelagic Fish. *Proc. Natl. Acad. Sci.* **2014**, *111* (15), E1510–E1518 DOI: 10.1073/pnas.1320950111.
- Kleindienst, S.; Seidel, M.; Ziervogel, K.; Grim, S.; Loftis, K.; Harrison, S.; Malkin, S. Y.; Perkins, M. J.; Field, J.; Sogin, M. L.; Dittmar, T.; Passow, U.; Medeiros, P. M.; Joye, S. B. Chemical Dispersants Can Suppress the Activity of Natural Oil-Degrading Microorganisms. *Proc. Natl. Acad. Sci.* **2015**, *112* (48) DOI: 10.1073/pnas.1507380112.
- Kozich, J. J.; Westcott, S. L.; Baxter, N. T.; Highlander, S. K.; Schloss, P. D. Development of a Dual-Index Sequencing Strategy and Curation Pipeline for Analyzing Amplicon Sequence Data on the Miseq Illumina Sequencing Platform. *Appl. Environ. Microbiol.* **2013**, *79* (17), 5112–5120 DOI: 10.1128/AEM.01043-13.

- Liu, Y.; Kujawinski, E. B. Chemical Composition and Potential Environmental Impacts of Water-Soluble Polar Crude Oil Components Inferred from ESI FT-ICR MS. *PLoS One* **2015**, *10* (9), e0136376 DOI: 10.1371/journal.pone.0136376.
- Medeiros, P.; Seidel, M.; Ward, N. D.; Carpenter, E.; Gomes, H.; Niggemann, J.; Krusche, A. V.; Richey, J. E.; Yager, P. L.; Dittmar, T. Fate of the Amazon River Dissolved Organic Matter in the Tropical Atlantic Ocean. *Global Biogeochem. Cycles* **2015**, 677–690 DOI: 10.1002/2015GB005115.
- Pearlman R.S.; Yalkowsky, S.H.; Banerjee S. Water solubilities of polynuclear aromatic and heteroaromatic compounds. *Journal of physical and chemical reference data*. **1984** Apr;13(2):555-62.
- Sibert, R. J.; Harrison, S. J.; Joye, S. B. Protocols for Radiotracer Estimation of Primary Hydrocarbon Oxidation in Oxygenated Seawater. In *Hydrocarbon and Lipid Microbiology Protocols*; McGenity, T. J., Timmis, K. N., Nogales, B., Eds.; Humana Press, 2016; pp 263–276.
- Silverstein, R.M.; Webster, F.X.; Kiemle, D.J. *Spectrometric Identification of Organic Compounds*, 7th ed.; John Wiley & Sons, Inc.: Hoboken, **2005**.
- Solorzano L. Determination of ammonia in natural waters by phenolhypochlorite method 1 1. This research was fully supported by US Atomic Energy Commission Contract No. ATS (11-1) GEN 10, PA 20. *Limnology and Oceanography*. **1969** Sep 1;14(5):799-801.
- Solorzano, L.; Sharp, J. H. Determination of Total Dissolved Phosphorous and Particulate Phosphorous in Natural Waters. *Limnol. Ocean.* **1980**, No. 1965, 754–758.
- Ward, N. D.; Keil, R. G.; Medeiros, P. M.; Brito, D. C.; Cunha, A. C.; Dittmar, T.; Yager, P. L.; Krusche, A. V.; Richey, J. E. Degradation of Terrestrially Derived Macromolecules in the Amazon River. *Nat. Geosci.* **2013**, *6* (7), 530–533 DOI: 10.1038/ngeo1817.

CHAPTER 4

AVAILABILITY OF DISSOLVED NUTRIENTS AND CHEMICAL DISPERSANT IMPACTS MICROBIAL COMMUNITIES AND POTENTIAL HYDROCARBON OXIDATION RATES IN SURFACE WATER FROM THE TAYLOR ENERGY SITE

4.1 Introduction

When oil is spilled in a coastal or marine environment, first responders are often left with a selection of difficult choices about how to respond to the spilled oil. Physical efforts to contain and divert the oil from delicate coastal environments can include deploying booms, packed with oil absorbing materials, or skimming sheens off the surface. Responders have also used controlled *in situ* burning of surface slicks to remove surface slicks. The efficacy of these mitigation efforts can be limited by the amount of oil spilled, the location of the spill, the weather conditions at the site of the spill, and the type of oil spilled (e.g. bunker fuel, crude oil, *etc.*) (Daling and Lewis, 2001).

Chemical dispersants, complex mixtures of solvents and surfactants able to physically lower the free energy at the interface between nonpolar and polar molecules, were first applied in the aftermath of the 1967 *Torrey Canyon* oil spill. An estimated 136 million liters of oil washed onshore after an oil tanker ran aground on Seven Stones reef, located off the southwest coast of England. At the time, it was considered the largest oil spill in history. 10,000 tons of first generation dispersants were applied on delicate shoreline ecosystems to clean up the oil, killing

scores of sea birds, threatening the local commercial fisheries, and upsetting the coastal ecosystem for decades (Southward and Southward, 1978).

Since their first use, various formulations of dispersants have been used in the cleanup efforts of many notable oil spills, including the 1977 Ekofisk Bravo blow out in the North Sea, the 1993 Braer spill off the Scottish coast, the 1996 Sea Empress spill off the English coast (Daling and Lewis, 2001), and most recently during the 2010 *Deepwater Horizon* blow out in the northern Gulf of Mexico.

Yet, many questions remain about the impact of these chemical mixtures. There is little dispute that dispersants function well at the molecular level to break up oil slicks and remove oil from the sea surface. Prince *et al.* (2015), however, heralded these mixtures as “bioremediation tool[s]”, which stimulate aerobic oil degradation through the process of dilution, overcoming macronutrient and oxygen limitation in surface waters. McFarlin *et al.* (2014) demonstrated that 0.167 ppm addition of Corexit 9500, the primary chemical dispersant used in the *Deepwater Horizon* oil spill response, enhanced the rate of oil degradation compared to undispersed oil treatment at each time point up until the end of their 60-day incubation of Arctic surface waters (McFarlin *et al.* 2014). Kleindienst *et al.* (2015) demonstrated that chemical dispersants do not stimulate, and in some cases, may suppress the activity of natural oil-degrading microorganisms in Gulf of Mexico mid-waters (Kleindienst *et al.* 2015).

It has long been known that microbial communities in surface waters readily respond to oil (Atlas 1981, Leahy and Colwell, 1990), and dissolved nutrients enhance the capabilities of oil degrading microbial communities (Atlas 1981, Leahy and Colwell 1990, Prince 2010). Without these inorganic nutrients, microbial communities have few resources to breakdown carbon rich oil in surface slicks. Edwards *et al.* (2011) postulated that offshore nutrient limitation inhibited

the degradation of oil in surface slicks in the aftermath of the *Deepwater Horizon* oil spill. Meanwhile, Seidel *et al.* documented the disappearance of heteroatomic compounds from a WAF bottle experiment, indicating some of the metabolic plasticity microbial communities use to work around apparent nutrient limitation to degrade petroleum derived hydrocarbons (Seidel *et al.* 2015).

Moreover, little is known about the nutrient dynamics following application of Corexit to surface waters. In this chapter, we will compare the microbial response of a chemical dispersant, Corexit 9500A (Nalco, Sugar Land, TX), with an inorganic nutrient amendment (NO_3^- , NH_4^+ , HPO_4^{3-} , 20:1 N:P) in surface waters from the Taylor Energy site in the northern Gulf of Mexico. We will explore how inorganic nutrients are utilized in these different treatments, how potential hydrocarbon oxidation rates change, and how microbial communities change after application of chemical dispersant and nutrients.

4.2 Methods and Materials

4.2.1 *Sample Collection*

Surface waters from four stations approaching the Taylor Energy site in the northern Gulf of Mexico were collected via bucket cast on board the *RV Endeavor*, aliquoted into 1L bottles. Although an oil slick had been spotted near the site (SEQNOS ID: 1119149) several hours before we arrived on station, a summer storm had churned up the slick prior to our arrival on station. No oil sheen or smell was visible in any of the four stations along the transect (Figure 4.1).



Figure 4.1 Map of the Taylor Energy Site in the northern Gulf of Mexico. Regional overview from Google Maps (left); satellite image of the site with oil emanating from the source, demarcated with an X (top right); and a map of surface water sampling locations (shades of blue) featured in this chapter (bottom right).

4.2.2 Experimental Design

Water from each station was aliquoted into 1L amber bottles and amended with one of the following treatments: + Nutrients ($10\mu\text{M NH}_4^+$, $10\text{ NO}_3^- \mu\text{M}$, and $1\ \mu\text{M HPO}_4^{3-}$), targeting a 20:1 N:P ratio; + Corexit ($5\ \mu\text{L}$ of Corexit 9500A); or Nutrients + Corexit, in triplicate, with an unamended control for each station. Water was incubated for 24 h at room temperature onboard, and sampled for dissolved nutrients, cell counts, potential hydrocarbon oxidation rates, and hydrocarbon composition. 250 mL of each bottle was pooled with site and treatment replicates for microbial community analysis via 16S rRNA sequencing.

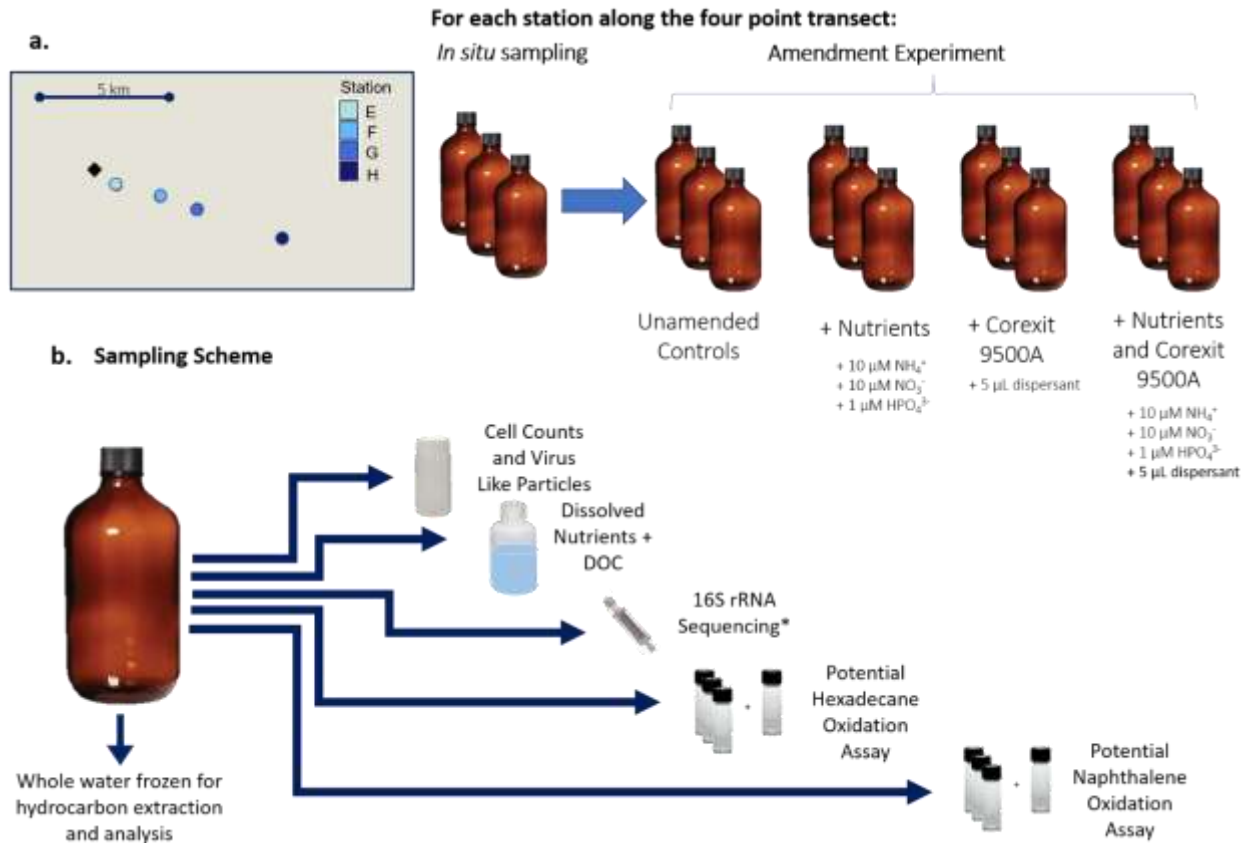


Figure 4.2 Schematic of experimental design (a) and sampling design (b). Surface water was collected from each of the four stations, and was sampled for in situ values and rates. Additional surface water was collected for the amendment experiment discussed here, with each treatment done in triplicate for each station. Each bottle was sampled for cell counts and virus like particle counts, dissolved nutrients, DOC, and water was subsampled for radiotracer assays. Water was pooled from each site and treatment for 16S rRNA analysis (*).

4.2.3 Dissolved Nutrients

Aliquots of whole water were filtered (0.2 μm) and preserved at -20°C for analysis of dissolved organic carbon (DOC), ammonium (NH_4^+), NO_x^- ($\text{NO}_3^- + \text{NO}_2^-$), total dissolved nitrogen (TDN), phosphate (HPO_4^{3-}), and total dissolved phosphate (TDP). Dissolved organic nitrogen and total dissolved organic phosphate concentrations were estimated from subtraction of inorganic species from total dissolved species.

Dissolved organic carbon (DOC) was analyzed by high temperature (680°C) combustion catalytic oxidation on a total organic carbon analyzer (Shimadzu TOC-Vcph); concentrations

were determined by comparison to a series of potassium hydrogen phthalate standards. Organic carbon was measured as the non-purgeable organic carbon (NPOC) content with an NDIR detector, following sparging with phosphoric acid. Total dissolved nitrogen (TDN) was measured on the same instrument with a TNM-1 module; concentrations were derived from a glycine standard. Samples were not diluted prior to analysis.

Nitrate plus nitrite (NO_x^-) concentrations were quantified by a vanadium reduction method using a vanadium reduction assembly (Antek 745; Braman and Hendrix, 1989) coupled with a chemiluminescent nitric acid detector (Antek 7050; Garside *et al.* 1982).

Nitrite (NO_2^-) was analyzed in parallel by standard colorimetric assay (Bendschneider and Robinson, 1952), while ammonium was measured colorimetrically using the standard phenol hypochlorite method (Solorzano, 1969). Nitrate (NO_3^-) was determined from the subtraction of NO_2^- from NO_x^- .

Dissolved phosphate was measured colorimetrically, using the molybdate blue method (Solorzano and Sharp, 1980). Total dissolved phosphate (TDP) was first precipitated with magnesium sulfate, and heated with acid to convert organic phosphate into orthophosphate. This residue was then subjected to colorimetric analysis using the molybdate blue method (Solorzano and Sharp, 1980). Colorimetric analyses were performed using a Shimadzu UV-1601 spectrophotometer. Dissolved organic carbon (DOC) was analyzed by high temperature (680°C) combustion catalytic oxidation on a total organic carbon analyzer (Shimadzu TOC-Vcph), as compared to a series of potassium hydrogen phthalate solution standards. Samples were diluted 2:11 in Milli-Q water. Organic carbon was measured as the non-purgeable organic carbon (NPOC) content with an NDIR detector, following sparging with a strong acid.

4.2.4 Hydrocarbons

Whole unfiltered water was frozen at -20° for analysis of total extractable hydrocarbons using a method adapted from Kleindeisnt *et al.* (2015) and Kujawinski *et al.* (2014). Following thawing, sample volume was determined gravimetrically, and spiked with known quantities of three deuterated standards (5µg/sample; fluorene-d₁₀, eicosane-d₂₄, and benzo[a]pyrene-d₁₂). Samples were transferred to combusted 1L separation funnels fitted with solvent rinsed PTFE spigots, and extracted with dichloromethane (2x 250 mL each) and hexane (1 x 250 mL). Samples from stations A and D required additional hexane and dichloromethane washes as there were still visible sheens of colored oil in the extraction. Organic fractions were combined and reduced in volume via rotary evaporation (Buchi Corp.) and solvent exchanged into hexane. Samples were further reduced to 500 µL under a gentle stream of Ar.

Organic extracts were analyzed with a gas chromatography with time of flight mass spectrometry (GC-TOF-MS; Pegasus 4D GC, LECO, Michigan). 1 µL of each extract was injected with a 1:10 split injection method, and separated on two in-line columns; the primary column was a Rxi-5 Sil fused silica column (60m x 0.25 mm ID; 0.25µm df; Restek) joined to an Rxi-17 Sil MS fused silica column (1m x 0.10mm ID x 0.1µm dr; Restek) housed in a secondary GC oven. The GC oven was held for 3 minutes at 50°C, followed by a 6°C/minute temperature ramp until reaching 320°C, and held for 20 minutes. Time of flight mass spectrometry allowed for the simultaneous monitoring of ions ranging from 50-575 m/z across the entire method, after a 600 s solvent delay. Samples were run alongside a standard curve of n-alkanes (nC7-nC40; heptane- tetracontane), a mixture of 16 parent PAHs, and a dilution of crude oil as an estimation of total petroleum hydrocarbons (TPH).

4.2.5 Potential Hydrocarbon Oxidation Rates

Potential hydrocarbon oxidation rates were quantified as the rate of conversion of a radiolabeled model hydrocarbon into $^{14}\text{CO}_2$ by the microbial community within each bottle (Kleindienst *et al.* 2015; Sibert *et al.* 2016). [$1\text{-}^{14}\text{C}$]-n-hexadecane was used as the model aliphatic compound, and [$1,4,5,8\text{-}^{14}\text{C}$] naphthalene was used as the model aromatic compound.

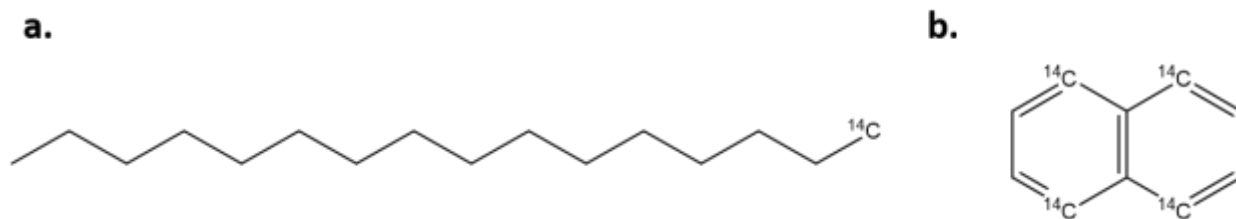


Figure 4.3 Structures of ^{14}C substrates used to quantify hydrocarbon turnover in surface waters. [$1\text{-}^{14}\text{C}$]-n-hexadecane (a) was used as a model linear alkane, and [$1,4,5,8\text{-}^{14}\text{C}$] naphthalene was used as a model aromatic compound (b).

Homogenized water from each microcosm was subsampled into headspace-free, 8mL glass scintillation vials capped with a PTFE-lined rubber septum (Supelco, Pennsylvania). Each assay was carried out in triplicate alongside a NaOH killed control. ^{14}C -labeled hydrocarbons were each dissolved in molecular grade ethanol and delivered into each scintillation vial with a glass syringe ($0.5\ \mu\text{Ci}=1.35 \times 10^{-5}\ \text{Bq}$; $10\ \mu\text{L}$) and shaken gently to distribute the tracer. Killed controls were injected with tracer and immediately added to the killing solution (2M NaOH, 2mL). Incubations were carried out at room temperature in the dark, and stopped in the same manner as killed controls. Assays were stored in the basic solution ($\text{pH} > 10$) at room temperature for up to 3 weeks before acidic distillation of the evolved $^{14}\text{CO}_2$.

Evolved $^{14}\text{CO}_2$ was distilled from the terminated incubation in the following method (Figure 3.3). Samples were transferred to 250mL Erlenmeyer flasks capped with rubber stoppers and

clamps and shaken with activated charcoal (1g, Sigma Aldrich) for 6h as a pre-treatment to bind any unused tracer to the charcoal. Hexadecane oxidation assays were further amended with C₁₈ reverse phase silica gel (250 mg, Supelco) to more effectively bind unused alkane tracer.

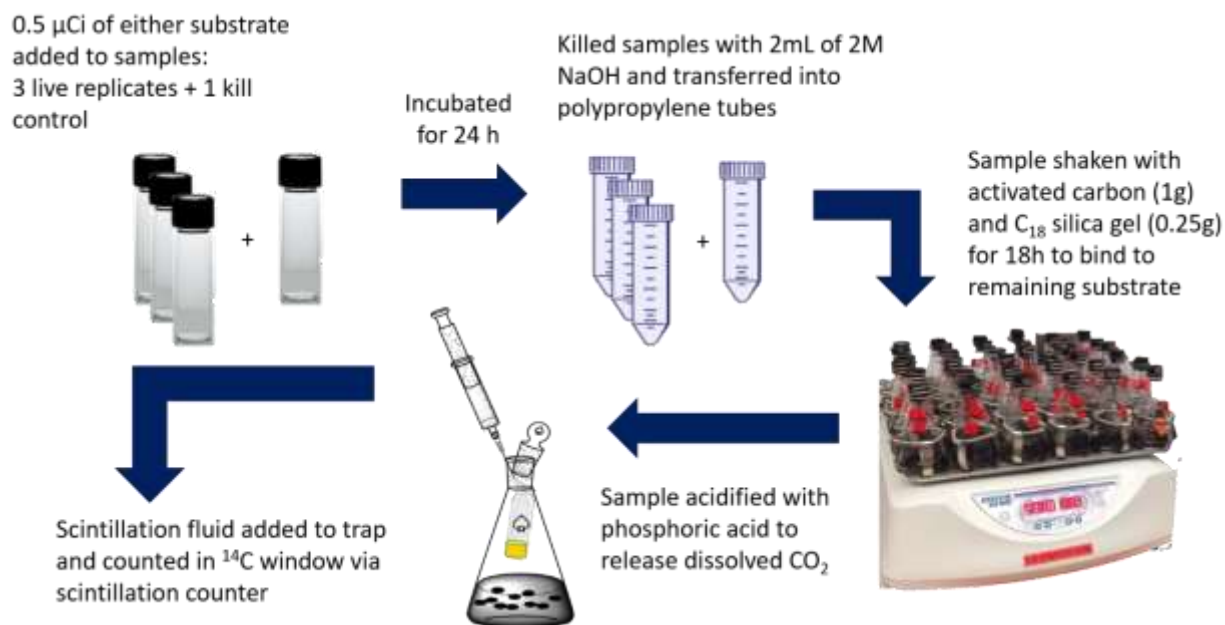


Figure 4.4 Schematic of hydrocarbon oxidation rate method developed by Kleindienst et al. (2015) and Sibert et al. (2016).

Following this pretreatment, the Erlenmeyer flask was fitted with a carbon dioxide trap (1.5 mL, CarboSorb E®, Perkin Elmer), acidified with concentrated phosphoric acid (5mL), and quickly stoppered to minimize loss of evolved CO₂. Acidified solutions were then shaken overnight to capture CO₂. Radioactivity of the carbon dioxide trap was quantified using a Beckman 6500 liquid scintillation counter, after adding scintillation fluid, (4.5mL, Scintisafe®, Fisher Scientific) to each trap. Instrumentation blanks were counted after every 10 samples, and total injected tracer was quantified as the blank corrected average of the 3 injections made into scintillation fluid at the time of the incubation. All values from the scintillation counter were first

blank corrected, and each sample was kill corrected with the value of the kill control for each sample.

Potential rates were calculated using modifications of the following formula (Equation 3.1). k is the rate constant, a term derived from the quotient of α , the fraction of radiotracer turned over, by t , the duration of the incubation. S is the concentration of the substrate.

$$-\frac{d[\text{Hydrocarbon}]}{dt} = k[S] = \frac{\alpha}{t} [S] * \frac{[\text{Radioactivity turned over, dpm}]}{[\text{Radioactivity added, dpm}]} * \frac{[S]}{t}$$

Equation 4.1

Potential Hexadecane Oxidation Rate: $[1\text{-}^{14}\text{C}]\text{-hexadecane} + \text{O}_2 \rightarrow {}^{14}\text{CO}_2 + \text{H}_2\text{O}$

$$-\frac{d[\text{Hexadecane}]}{dt} = k[\text{Hexadecane}] = \frac{\alpha}{t} * [\text{Hexadecane}] = \frac{[{}^{14}\text{CO}_2]}{[{}^{14}\text{C} - \text{Hexadecane} * t]} * [\text{Hexadecane}]$$

Equation 4.2

Potential Naphthalene Oxidation Rate: $[1,4,5,8\text{-}^{14}\text{C}]\text{-naphthalene} + \text{O}_2 \rightarrow {}^{14}\text{CO}_2 + \text{H}_2\text{O}$

$$-\frac{d[\text{Naphthalene}]}{dt} = k[\text{Naphthalene}] = \frac{\alpha}{t} * [\text{Naphthalene}] = \frac{[{}^{14}\text{CO}_2]}{[{}^{14}\text{C} - \text{Naphthalene} * t]} * [\text{Naphthalene}]$$

Equation 4.3

Calculated Concentration of the Radiotracer used in the ^{14}C Incubations

The concentration of the added tracer is a function of the incubation vessel dimension (7.5 mL) and specific activity of the hexadecane and naphthalene tracer, as determined by the manufacturer (55 Ci/mol and 58 Ci/mol, respectively; Equations 4.2 and 4.3).

$$[\text{Hexadecane tracer}] = \frac{\text{Radioactivity of added tracer, dpm}}{\text{Volume of incubation vessel, mL}} * \frac{1 \text{ mCi}}{2.22 \times 10^9 \text{ dpm}} * \frac{1 \text{ mmol}}{55 \text{ mCi}}$$

Equation 4.4

$$[\text{Naphthalene tracer}] = \frac{\text{Radioactivity of added tracer, dpm}}{\text{Volume of incubation vessel, mL}} * \frac{1 \text{ mCi}}{2.22 \times 10^9 \text{ dpm}} * \frac{1 \text{ mmol}}{58 \text{ mCi}}$$

Equation 4.5

The *in situ* concentrations of hexadecane and naphthalene were below the limit of detection via GC-MS for the entire summer 2015 transect, and so the concentration of the tracer was used in the radiotracer incubations was used to calculate the potential rate of hydrocarbon oxidation.

4.2.6 Microbial Community

Microorganism were filtered onto a Sterivex filter cartridge (0.22 μ m; Millipore) and flash frozen in liquid nitrogen. Homogenized water from each biological replicate was pooled with other station replicates for a total of 750 mL water per station (3 bottles/station * 250 mL/bottle= 750 mL). Samples were shipped on dry ice from Gulfport, MS to Athens, GA, and stored at -80°C until processing. Sterivex filters were thawed on ice, the tops removed with sterilized pliers, and the filter cut using sterile scalpels; the cut filters were immediately processed for DNA extraction using the DNeasy Powerwater Kit (Qiagen) according to the manufacturer's directions. Eluted DNA was quantified using the dsDNA assay kit and a Qubit fluorometer (Invitrogen) (Table 4.1).

Barcoded amplicons of the 16S rRNA were generated using primers amplifying the V4 region and the AccuPrime™ Pfx SuperMix kit (Invitrogen) with methods previously described (Kozich *et al.* 2013; Table 3.2). Samples were sequenced on an Illumina MiSeq (Illumina) at the Georgia Genome Facility (GGF, University of Georgia, Athens, GA) resulting in 2x250 paired-end reads.

At the time of writing, analyses of these data were still underway and will not be discussed further.

4.2.7 Statistical Analysis

Data was analyzed using R version 3.2.4 (Copyright (C) 2016, The R Foundation for Statistical Computing). Due to the small sample size and non-normal distributions of data, non-parametric tests were used to compare and contrast the biogeochemical data from the two stations. Variance was assessed by the Kruskal-Wallis Rank Sum Test, a non-parametric alternative to an ANOVA. Paired Wilcoxon rank sum tests were used to assess differences within the sample sets, and Spearman's rank coefficients were used to assess correlation between geochemical parameters.

4.3 Results

4.3.1 Dissolved Nutrients

4.3.1.2 Dissolved Nitrogen

As a coastal station 18 km the mouth of the Mississippi River, there are high levels of total dissolved nitrogen (TDN) at this station during the spring-summer months compared with farther offshore (Edwards *et al.* 2011 and Pomeroy *et al.* 1995).

A Kruskal-Wallis rank sum test detected a difference in ammonium drawdown by treatment (Kruskal-Wallis chi-squared = 10.201, df = 3, p-value = 0.01693), and a series of Wilcoxon rank sum tests detected a significant difference in the drawdown of ammonium in the Nutrient + Corexit treatment compared to the unamended treatment (p-value = 0.02021). In the Nutrient + Corexit treatments, nearly the entire ammonium addition (10 μ M) was depleted over the 24 h incubation.

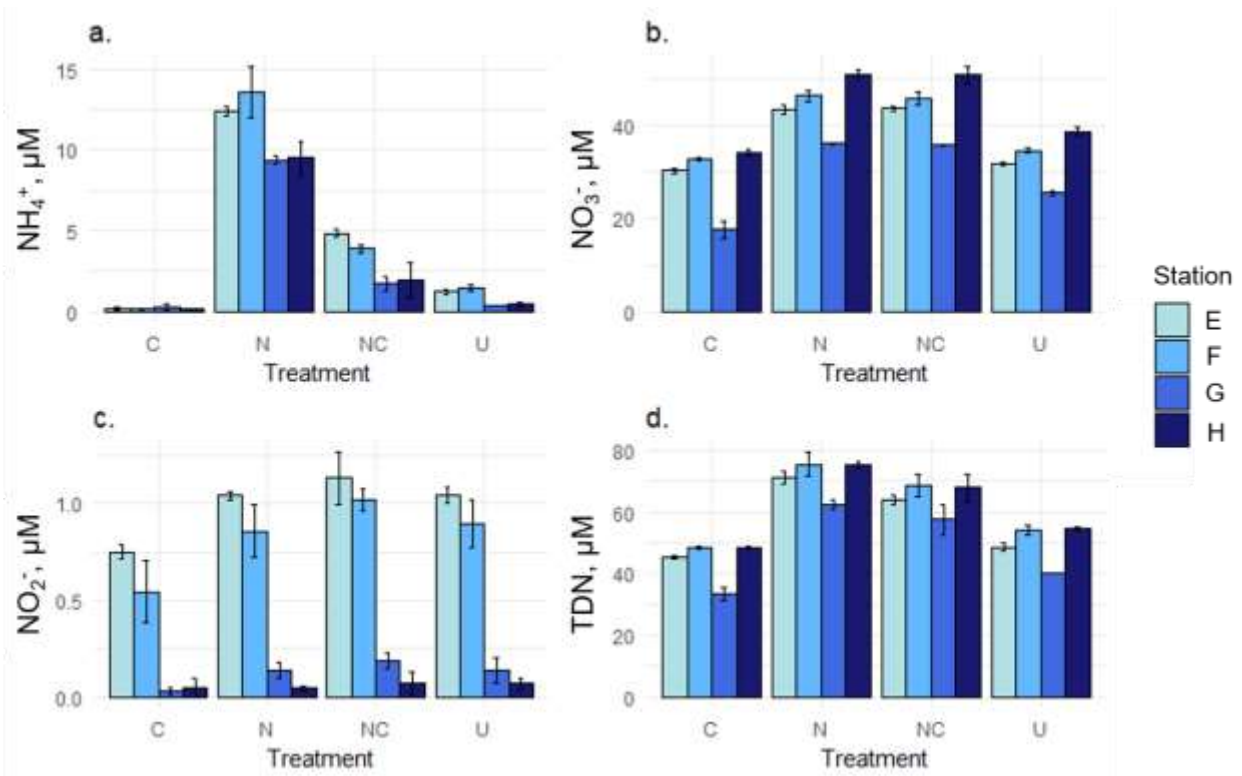


Figure 4.5 Bar plots of the dissolved nitrogen species grouped by treatments and shaded by station after incubation for 24h with each respective treatment. C= Corexit alone, N= + Nutrients, NC= Corexit + Nutrients, U= unamended controls. Colors progressing from pale blue to dark blue as a function of moving away from the Taylor Energy site.

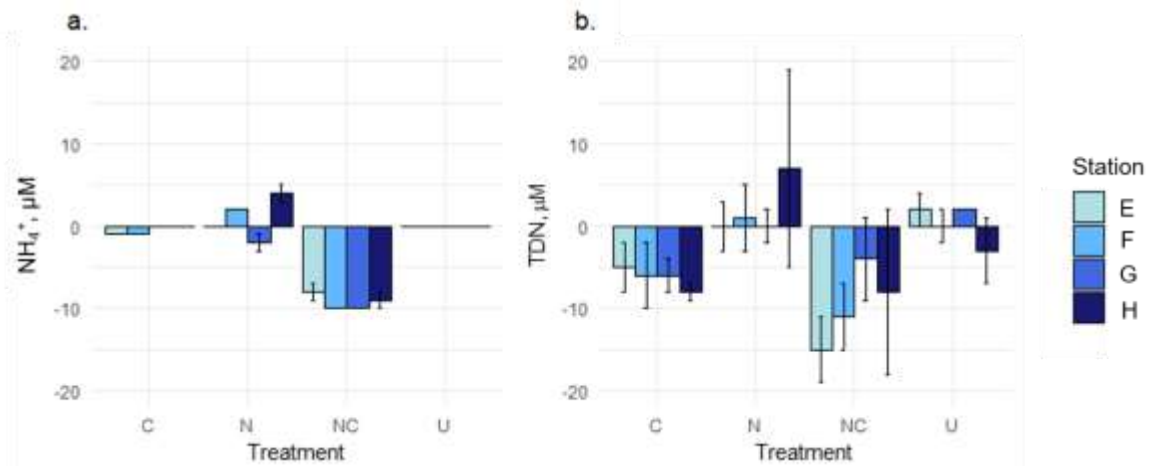


Figure 4.6 Bar plots of ammonium drawdown (a) and total dissolved nitrogen drawdown (b) grouped by treatments and shaded by sites after incubation for 24h with each respective treatment. C= Corexit alone, N= + Nutrients, NC= Corexit + Nutrients, U= unamended controls. Colors progressing from pale blue to dark blue as a function of moving away from the Taylor Energy site.

A Kruskal-Wallis rank sum test detected a difference in the drawdown of total dissolved nitrogen by treatment (Kruskal-Wallis chi-squared = 11.707, df = 3, p-value = 0.008458), and a series of Wilcoxon rank sum tests detected a significant difference in the drawdown of total nitrogen in the Nutrient+ Corexit treatments compared to the unamended controls (p-value = 0.0294) as well as in the Corexit amended treatments ($W = 0$, p-value = 0.02843). No significant difference was observed between the nutrient amended treatment and the unamended controls.

Dissolved nitrogen species were significantly removed in all Corexit-amended treatments, and ammonium was significantly depleted in the nutrient + Corexit treatments.

4.3.1.2 Dissolved Organic Species

A Kruskal-Wallis rank sum test detected that there was a significant difference in the size of the dissolved organic pool by treatment, and a follow up analysis with a Wilcoxon rank sum detected significantly higher levels of DOC both Corexit amended treatments compared to unamended treatments (Corexit alone: $W = 144$, p-value = $3.63e-05$; Nutrients + Corexit: $W = 144$, p-value = $3.63e-05$), a difference of about 100 μM on average. Analysis of the dissolved organic nitrogen pool failed to reveal differences by treatment, indicating that the pool of dissolved organic species is carbon rich. Given the dynamic range of compounds within the Corexit formulation and its predominant hydrocarbon formulation (Harrison, 2013; Baelum *et al.* 2012), it is unsurprising that many of these compounds enter the pool of dissolved organic carbon.

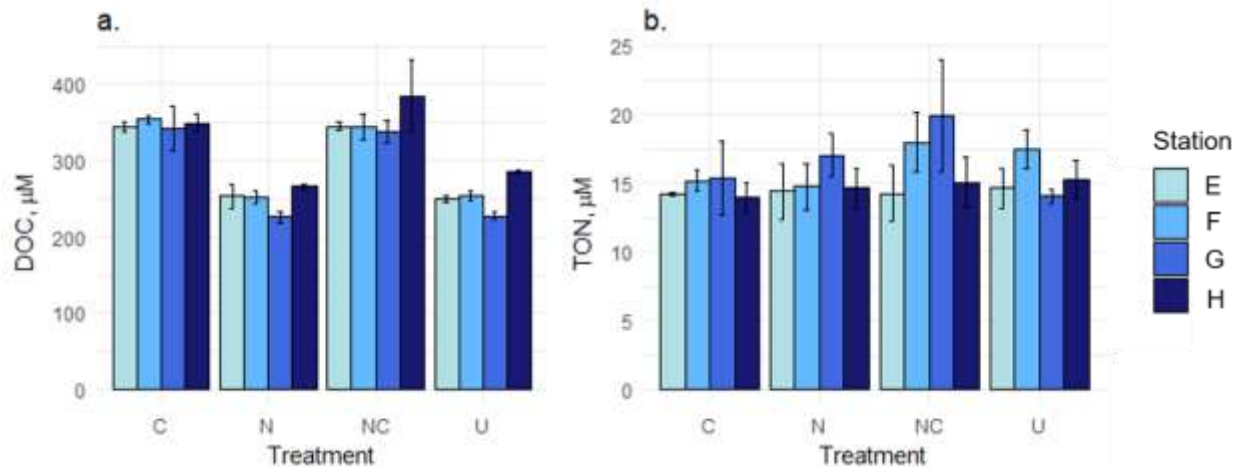


Figure 4.7 Bar plots of the dissolved organic carbon (DOC) and dissolved organic nitrogen (DON) concentrations following 24h incubation with each respective treatment. Plots are grouped by treatments and shaded by site. C= Corexit alone, N= + Nutrients, NC= Corexit + Nutrients, U= unamended controls. Colors progressing from pale blue to dark blue as a function of moving away from the Taylor Energy site.

4.3.1.3 Dissolved Phosphorous Species

As expected for surface waters, the background levels of orthophosphate and total dissolved phosphate were close to 1µM, with no significant differences detected across the four stations (Figure 4.4). A Kruskal-Wallis rank sum test detected a significant difference in the drawdown of phosphate by treatment (Kruskal-Wallis chi-squared = 12.812, df = 3, p-value = 0.005061). Follow-up analysis of the drawdown of phosphate revealed a significant difference in the drawdown of phosphate in both Corexit-amended treatments compared to unamended treatments (p-value = 0.02857; p-value = 0.02857; Figure 4.5). No significant difference in the drawdown of phosphate was detected in the nutrient amended treatments.

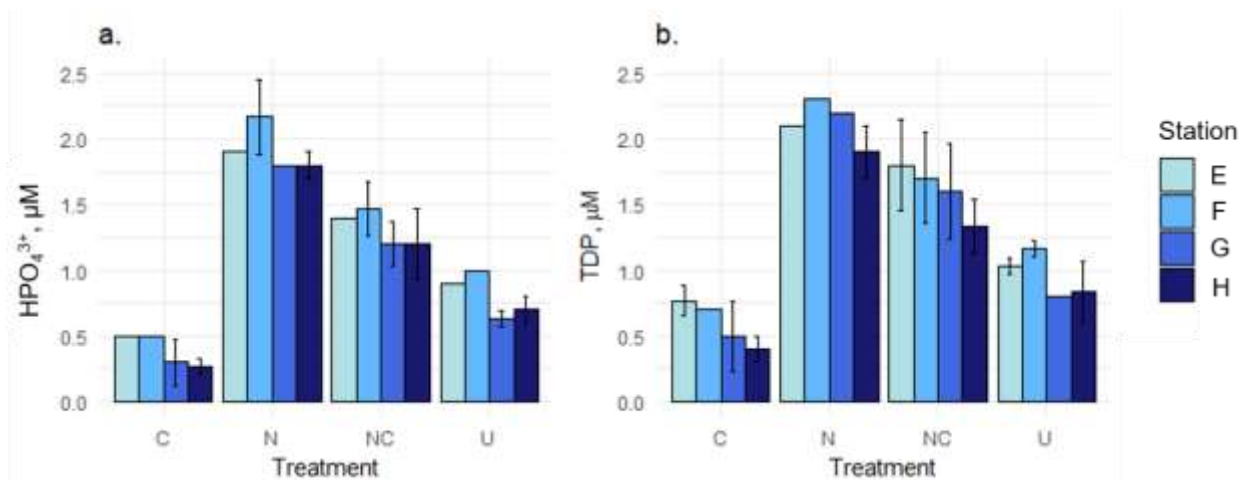


Figure 4.8 Bar plots of phosphate (a) and total dissolved phosphate (TDP) species (b) grouped by treatments and shaded by sites. C= Corexit alone, N= + Nutrients, NC= Corexit + Nutrients, U= unamended controls. Colors progressing from pale blue to dark blue as a function of moving away from the Taylor Energy site.

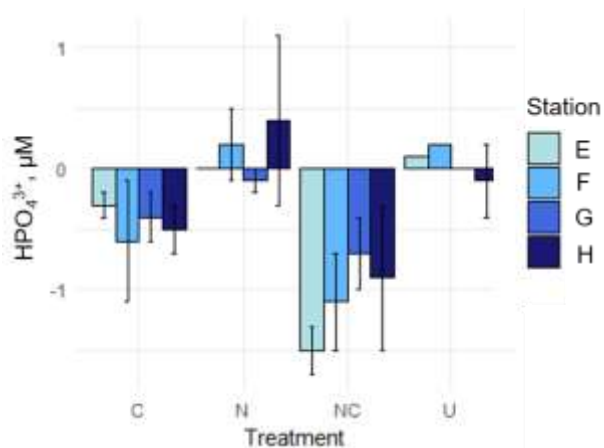


Figure 4.9 Bar plots of the phosphate drawdown grouped by treatments and shaded by sites. C= Corexit alone, N= + Nutrients, NC= Corexit + Nutrients, U= unamended controls. Colors progressing from pale blue to dark blue as a function of moving away from the Taylor Energy site.

4.3.4 Nutrient Summary

Taken together, the Corexit amendments (5 $\mu\text{L}/1\text{L}$; 5 ppm) significantly changed the size of the dissolved organic carbon pool in these surface water incubations. It is important to note that this concentration of Corexit is well below the estimated critical micelle concentration (CMC) of Corexit estimated by Steffy *et al.* (2011) and in the same order of magnitude as the trace levels of DOSS detected in midwater depths from 2010 in the aftermath of the *Deepwater Horizon* oil spill (Kujawinski *et al.* 2011), if DOSS is ~10% by mass.

Over the course of the 24h incubation in the dark, there were significant differences in the amount of total dissolved nitrogen and phosphate utilized in both Corexit-amended treatments compared to the unamended treatment. This observation was not seen in the nutrient-only treatments. This suggests that adding low amounts of Corexit changes the pool of carbon in surface waters, which dramatically alters the way that nutrients are utilized, and that the change is rapid, changing on timescales of hours. This change in nutrient use could make these communities that are already at risk of being nutrient limited (Pomeroy 1995; Edwards 2011) even more so and could limit the ability of these microbial communities to degrade petroleum hydrocarbons found in surface waters.

4.3.2 Microbial Community Composition

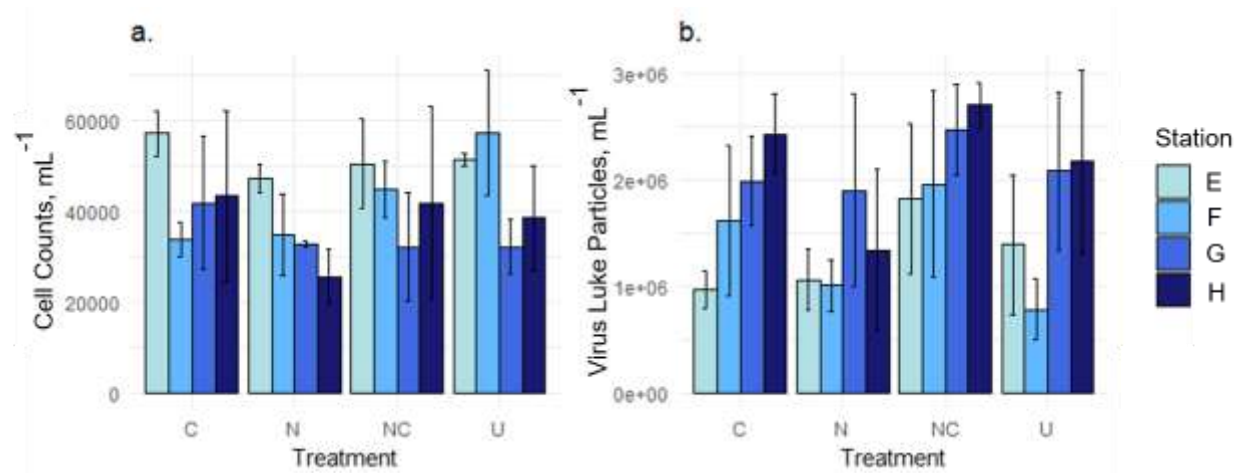


Figure 4.10 Bar plots of the cell counts (a) and virus like particles (b) grouped by treatments and shaded by sites. C= Corexit alone, N= + Nutrients, NC= Corexit + Nutrients, U= unamended controls. Colors progressing from pale blue to dark blue as a function of moving away from the Taylor Energy site.

No significant differences in cell counts were detected across sites or treatments, and the only significant difference with respect to virus like particles was detected between the nutrient amended treatments and nutrient + Corexit amended treatments ($W = 21$, p -value = 0.003535). However, given that neither treatment was significantly different from the controls, this is not a treatment effect and may reflect a subtle shift in the dynamic responses to nutrients and dispersant.

Analyses of the 16S rRNA data is still underway and is to be featured in future work.

4.3.3 Potential Hydrocarbon Oxidation Rates

4.3.3.1 Potential Hexadecane Oxidation Rates

There was robust oxidation of the hexadecane tracer across the whole Taylor transect, especially compared to offshore stations in the Gulf of Mexico (Shepherd and Joye, unpublished results from EN586). The nutrient amendment had the most dramatic impact at station G, which was the most oligotrophic station among those featured in this study.

A Kruskal-Wallis rank sum test detected differences among the hexadecane oxidation rate by treatment (Kruskal-Wallis chi-squared = 10.004, df = 3, p-value = 0.01853), however, there were no significant differences in potential hexadecane oxidation were observed between the unamended controls and the amended samples. Therefore, there is no treatment effect of Corexit or nutrients on the potential rate of hexadecane oxidation after a 24 h exposure.

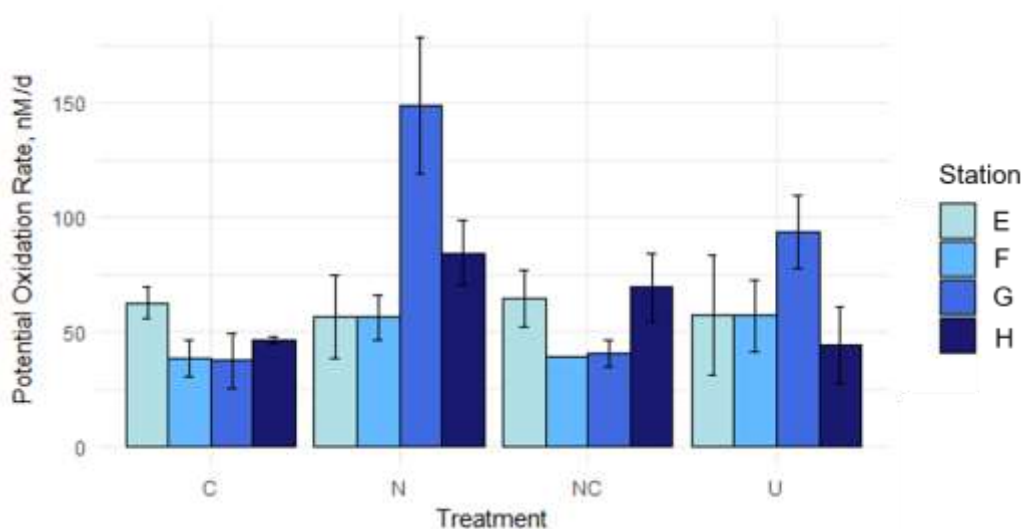


Figure 4.11 Bar plots of the potential hexadecane oxidation grouped by treatments and shaded by sites. C= Corexit alone, N= + Nutrients, NC= Corexit + Nutrients, U= unamended controls. Colors progressing from pale blue to dark blue as a function of moving away from the Taylor Energy site.

However, there were no significant differences between the amendment treatments. Between nutrient only amendments and Corexit-only amendments, potential hexadecane oxidation rates were higher in the nutrient amended samples ($W = 21$, p-value = 0.002316). Between the two nutrient amended treatments, potential rates were higher among the nutrient-only amended samples compared to the nutrient and dispersant treatment ($W = 109$, p-value = 0.03324). This indicates that Corexit and dissolved nutrients have diverging impacts on the potential rate of hexadecane oxidation in surface waters. In agreement with previous findings in mid-water (Kleindeinst *et al.* 2015), Corexit does not enhance the rate of potential hexadecane oxidation in

surface waters, but, perhaps more importantly to oil spill responders, Corexit does not appear to depress the potential rate of alkane degradation either. However, a longer incubation may be required to detect significant differences from the unamended control treatments.

These findings can be explained for several reasons: Corexit, itself, has n-alkanes within its formulation (Harrison, 2013; Baelum *et al.* 2013; Nalco MSDS, 2012), and so microorganisms may prefer to degrade these shorter, more labile n-alkanes over the radiolabeled n-hexadecane. Alternatively, it is possible that the added substrate, hexadecane, was intermolecularly bound to components of the dispersant (e.g. surfactants and solvents) through alkyl-alkyl interactions, which become important intermolecular forces in the presence of increasingly polar solvents (Yang *et al.* 2013). Nutrient data from this data set, however, suggests the former, given the significant drawdown of nutrients in Corexit-amended treatments suggests that something is being degraded.

4.3.3.2 Potential Naphthalene Oxidation Rates

The potential oxidation rates of naphthalene, the simplest polycyclic aromatic hydrocarbon, are highly variable by treatment and station. When compared to potential hexadecane oxidation rates for the same sites and treatments, the rate is roughly two orders of magnitude lower than the hexadecane oxidation rate.

A Kruskal-Wallis rank sum test detected a significant difference in potential naphthalene oxidation rates by treatment (Kruskal-Wallis chi-squared = 8.2891, df = 3, p-value = 0.0404). A series of Wilcoxon rank sum tests detected a significantly higher potential rates of naphthalene oxidation in the Corexit-amended treatments compared to the control treatments (W = 109, p-value = 0.03324) and in the Corexit and nutrient amended treatments compared to the unamended controls (W = 112, p-value = 0.02049). No significance was detected between the

nutrient treatments and unamended controls ($W = 83$, $p\text{-value} = 0.5512$) or between any other treatment pairings.

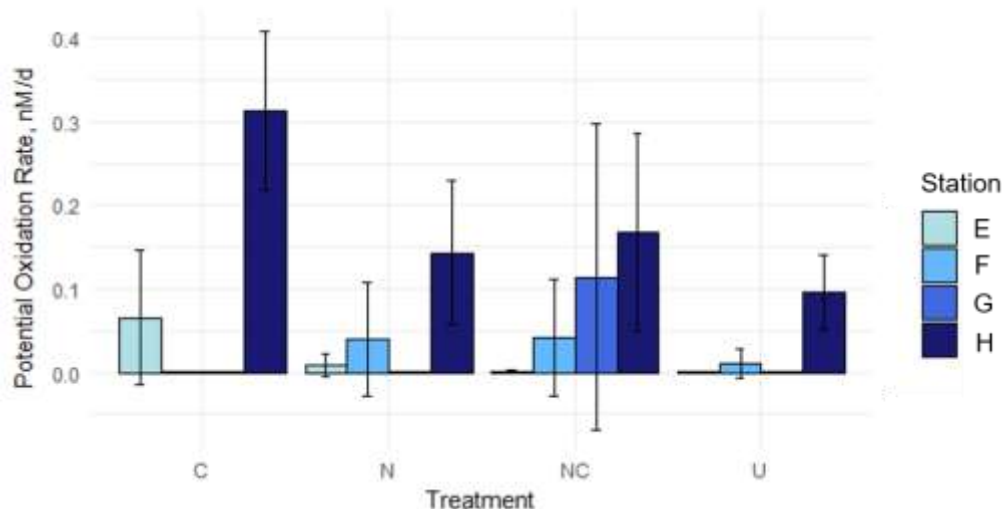


Figure 4.12 Bar plots of potential naphthalene oxidation rates grouped by treatments and shaded by sites. C= Corexit, N= Nutrients, NC= Corexit + Nutrients, U= unamended controls. Colors progressing from pale blue to dark blue as a function of moving away from the Taylor Energy site.

Although this trend appears to be site specific, the increased degradation of naphthalene in the presence of Corexit is surprising. Previous findings using this method (Kleindienst *et al.* 2015) did not observe this trend in deep sea waters from the Gulf of Mexico. Moreover, Corexit has only one aromatic constituent, trace amounts of a phthalic acid described by Major and colleagues (2012), and so it is unlikely that the increased rate is reflection of an enrichment in aromatic hydrocarbon degraders. Finally, the degradation of an aromatic compound is a metabolically expensive endeavor, as the carbon-carbon bonds found in naphthalene require about twice the energy to break compared to the single carbon bonds found in hexadecane (Blanksby and Ellison, 2003).

However, the larger ecological context is important to understanding this result. The surface microbial community at the Taylor Energy site is likely primed to degrade small aromatics,

given its proximity to the Mississippi River. Riverine DOC is rich in phenol-like compounds, which are formed in the degradation of lignin (e.g. Ward et al. 2013). This priming, however, does not fully explain why the Corexit appears to enhance the potential rate of naphthalene.

Aromatic compounds, including polycyclic aromatic hydrocarbons, have a halo of electrons sandwiching the planar hydrophobic core (Figure 4.10). The high electron density on either side of the compound's face confers the compound with a slight electronegative field, which allows for interactions with cations, in what is known as a cation- π interaction, first described by Sunner *et al.* (1981). In a saltwater matrix, this molecular interaction would allow naphthalene to truly dissolve into the aqueous phase and be shielded by cations, thereby limiting the ability of dispersants to interact with aromatic compounds. Essentially, we hypothesize that Corexit does not work to disperse the more water-soluble components within oil; it was not designed to disperse those compounds. In these radiotracer assays, the effective concentration of naphthalene is higher compared to other carbon substrates, and so aromatic degraders likely flourish under these conditions.

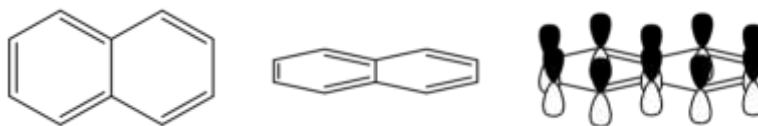


Figure 4.13 Structure of naphthalene from above and the side with the sp^2 hybrid orbitals in view.

This promiscuous finding suggests that Corexit may enhance the biodegradation of a small, but important class of compounds within crude oil. Polycyclic aromatic hydrocarbons (PAHs) are among the most toxic constituents of crude oil. While long known to be carcinogenic, PAHs

have recently been discovered to be uniquely cardiotoxic to developing fish embryos (Incardona *et al.* 2004, 2005, and 2011) and phenanthrene, a tricyclic PAH, can disrupt ion channels integral to the normal function of cardiac muscle in fish (Brette *et al.* 2017).

4.4 Discussion

4.4.1 *Commentary on Potential Rate Measurements*

In the wake of the *Deepwater Horizon* oil spill, there was great interest in constraining the rate of biodegradation to better calculate the oil budget. The hydrocarbon oxidation rate method used for this study was first developed by Kleindienst *et al.* (2015) and refined by Sibert *et al.* (2016).

This method can estimate the rate of oil biodegradation using a small volume of water, and due to the short incubation time required, it can be done without as many risks of bottle effects.

Additionally, because the method traces the conversion of a hydrocarbon to carbon dioxide, it can uniquely isolate and quantify the rate of biodegradation separate from other weathering processes. The amount of available substrate in the environment, however, remains a considerable obstacle in the optimization and continued use of this radiotracer methodology in the wider oil spill response community, as will be discussed below. However, if this uncertainty can be constrained and better characterized, then this technique may eventually be used to estimate oil degradation in the same way that ^3H -leucine incorporation is used to estimate bacterial production (Kirchman *et al.*, 2001), an established and critical tool for biogeochemists.

At the time of this writing, the only other published data utilizing model radiolabeled hydrocarbons to approximate the rate of hydrocarbon degradation is from Kleindienst *et al.* (2015). In that microcosm study, water collected from a natural seep in the Gulf of Mexico was exposed to various hydrocarbon and nutrient treatments to understand how dispersant application

impacted the rate of hydrocarbon oxidation and hydrocarbon degrading microbial communities, using 16S rRNA genotyping and hydrocarbon oxidation rates as key end members, among a host of other geochemical parameters.

Table 4.1 Table of potential rates between the Kleindienst et al. (2015) and this study. Substrate rates are calculated using the concentration of the substrate measured in the sample as the substrate concentration; potential rates are calculated using the concentration of the tracer as the substrate concentration; and full rates are calculated using the sum of the measured compound and the tracer as the substrate concentration (Equation 4.1). Kleindienst et al. (2015) used the substrate rates for publication.

	Kleindienst et al. 2015		
	Substrate Rates (nM/d)	Potential Rates (nM/d)	Full Rate (nM/d)
Hexadecane Oxidation	0.000397 ± 0.001	0.877 ± 1.45	0.877 ± 1.45 nM/d
Naphthalene Oxidation	4.34 ± 15.03	1.86 ± 2.20	6.20 ± 16.04 nM/d
	This Study		
	Substrate Rates (nM/d)	Potential Rates (nM/d)	Full Rate (nM/d)
Hexadecane Oxidation	0.00 ± 0	62.43 ± 30.22	62.43 ± 30.22
Naphthalene Oxidation	0.00 ± 0	69.15 ± 114.16	69.15 ± 114.16

It is challenging to directly compare the potential rates from this study to the published rates from the previous works, given that the calculations were done differently (Table 4.1). While this study uses the concentration of the tracer as the concentration of the substrate available (a potential rate), Kleindienst *et al.* used the concentration of the extracted hydrocarbons as the concentration of the substrate available to the microbial consortia. However, the concentration of tracer, in some instances, can overwhelm the concentration of the substrate, sometimes by several orders of magnitude. The rate observed in the radiotracer assay is therefore much larger than what is occurring in the bottle (as in the case of the published potential rates of hexadecane oxidation). In other instances, this route of calculating the rate fails to encapsulate the whole pool of the substrate available and therefore underestimates the rate (as in the case of the published potential rates of naphthalene oxidation). Therefore, to compare these studies, the rates from

Kleindienst *et al.* were recalculated, using the sum of the tracer and the detected substrate in the bottle, in what henceforth is known as the full rate (Table 4.1).

The magnitude of the potential rates in the present study is much higher than those observed by Kleindienst *et al.*, despite the absence of detectable levels of petroleum derived hydrocarbons in surface waters from the Taylor Energy site (Table 4.1). One key reason for this difference may be the temperature at which these studies were conducted (4°C versus 25°C), suggesting an important role for temperature in governing the rate of hydrocarbon oxidation in surface and mid-water. Additionally, Kleindienst *e al.* (2015) observed higher full rates of naphthalene oxidation compared to hexadecane oxidation. This difference is surprising, given the energy required to break aromatic rings is nearly double that required to break single carbon bonds. However, Kleindienst *et al.* used a water accommodated fraction (WAF) to deliver oil to incubations, which is more enriched in hydrophilic compounds like naphthalene than hydrophobic compounds like hexadecane.

4.4.2 The relationship between inorganic nutrients and the DOC pool

The addition of chemical dispersant significantly changes the size and lability of the DOC pool in surface waters, adding roughly 100 µM of labile carbon to surface water following a single 5µL addition of Corexit 9500A. This dispersant addition coincided with a significant drawdown in concentrations of ammonium, total dissolved nitrogen, and phosphate after 24h, reflecting that chemical dispersant may be readily degraded by microorganisms in surface water. This nutrient drawdown, however, leaves the microbial community more vulnerable to nutrient limitation, and may impact the community's ability to degrade hydrocarbons over longer time scales than those observed in this study. Further analysis of the microbial community through 16S rRNA analysis is required to understand this relationship further.

4.4.3 Potential rates, dispersant, nutrients, and implications for oil spill response

Hexadecane, our model alkane, is rapidly degraded in these surface waters. There was no treatment effect for inorganic nutrients or chemical dispersant on the rate of hexadecane oxidation compared to the unamended after a 24h incubation at room temperature in the dark. Although n-alkanes are largely considered to be the most easily biodegraded fraction of hydrocarbons from crude oil, the rate observed in this study is impressive, and much larger than what has previously been reported using this method (Kleindienst *et al.* 2015). Furthermore, these data provide evidence for the “phytoplankton priming” hypothesis posited by Valentine and Reddy (2014) after Lea-Smith *et al.* discovered that the two most abundant cyanobacteria in surface waters, *Prochlorococcus* sp. and *Synechococcus* sp. produce and accumulate alkanes intracellularly (n-C15 and n-C17 predominantly) (Lea-Smith *et al.* 2015). However, a significant difference in the rate of nutrient amended and Corexit amended treatments suggest that a longer incubation may be required to see if the hexadecane oxidation rate is sustainable and to determine how excess inorganic nutrients or chemical dispersant impact this rate.

Naphthalene, the simplest PAH and model aromatic compound in this study, was degraded significantly faster in the presence of a small quantity of the chemical dispersant, Corexit 9500A. This promiscuous finding suggests that Corexit may enhance the biodegradation of a small, but important class of compounds within crude oil. PAHs are among the most toxic constituents of crude oil. While long known to be carcinogenic, PAHs have recently been discovered to be cardiotoxic to developing fish embryos (Incardona *et al.* 2004, 2005, 2011, and 2014) and phenanthrene, a tricyclic PAH, can disrupt ion channels integral to the normal function of cardiac muscle in fish (Brette *et al.* 2017). While statistically significant in this study, this trend was

driven by two stations at a site that has significant seasonal variations, and so further work is required to understand the ecological significance of this finding.

Although inorganic nutrients are essential for surface microbial communities, additional inorganic nutrients did not enhance the potential rates of either model hydrocarbon. Nutrient limitation, however, may become a more important driver in more oligotrophic waters (as observed by Edwards *et al.* 2011) or during fall and winter months when the input of nutrients of the Mississippi River become less significant forces for the Taylor Energy site.

The findings from this study do not support the findings of Kleindienst *et al.* (2015), which stated that chemical dispersant suppressed the microbial community's ability to degrade oil. The choice to use chemical dispersants in the aftermath of an oil spill must be informed by the highest quality science that scales and is able to encompass multi-trophic levels of the marine and coastal ecosystem.

4.5 Conclusion

Following the *Deepwater Horizon* oil spill, many questions remain about the microbial response to oil in surface waters and about how mitigation efforts might impact their biological response to oil. This small incubation study observed a significant drawdown in ammonium, total dissolved nitrogen, and phosphate in all Corexit-amended treatments. Neither inorganic nutrient addition nor dispersant addition altered the robust rate of hexadecane oxidation in surface waters, although a longer experiment may be required to understand this response. Surprisingly, Corexit stimulated the potential rate of naphthalene oxidation in surface waters, suggesting a unique

interaction between Corexit and the water-soluble fraction of oil, including PAHs. This small incubation study follows the example of MacFayden *et al.* 2014 in using the Taylor Energy site in the northern Gulf of Mexico to inform critical oil spill response research at scale.

References

- Atlas, R. M. Measurement of Hydrocarbon Biodegradation Potentials and Enumeration of Hydrocarbon-Utilizing Microorganisms Using Carbon-14 Hydrocarbon-Spiked Crude Oil. *Nativ. Aquat. Bact. Enumeration, Act. Ecol.* **1979**, 196–204.
- Baelum, J.; Borglin, S.; Chakraborty, R.; Fortney, J. L.; Lamendella, R.; Mason, O. U.; Auer, M.; Zemla, M.; Bill, M.; Conrad, M. E.; Malfatti, S. a; Tringe, S. G.; Holman, H.-Y.; Hazen, T. C.; Jansson, J. K. Deep-Sea Bacteria Enriched by Oil and Dispersant from the Deepwater Horizon Spill. *Environ. Microbiol.* **2012**, *14*, 2405–2416 DOI: 10.1111/j.1462-2920.2012.02780.x.
- Bendschneider K.; Robinson R.J. A new spectrophotometric method for the determination of nitrite in sea water. *University of Washington Oceanographic Laboratories.* **1952**.
- Blanksby, S. J.; Ellison, G. B. Bond Dissociation Energies of Organic Molecules. *Acc. Chem. Res.* **2003**, *36* (4), 255–263 DOI: 10.1021/ar020230d.
- Braman, R.S.; Hendrix, S.A. Nanogram nitrite and nitrate determination in environmental and biological materials by vanadium (III) reduction with chemiluminescence detection. *Analytical Chemistry.* **1989** Dec 1;61(24):2715-8.
- Brette, F.; Shiels, H. A.; Galli, G. L. J.; Cros, C.; Incardona, J. P.; Scholz, N. L.; Block, B. A. A Novel Cardiotoxic Mechanism for a Pervasive Global Pollutant. *Sci. Rep.* **2017**, *7*, 41476 DOI: 10.1038/srep41476.
- Corexit®9500; Material Safety Data Sheet, No 3057221. Nalco Energy Services: Sugar Land, TX, June 14, 2005. http://lmrk.org/corexit_9500_uscueg.539287.pdf. Accessed September 17, 2012.
- Edwards, B. R.; Reddy, C. M.; Camilli, R.; Carmichael, C. a; Longnecker, K.; Van Mooy, B. a S. Rapid Microbial Respiration of Oil from the Deepwater Horizon Spill in Offshore Surface Waters of the Gulf of Mexico. *Environ. Res. Lett.* **2011**, *6* (3), 35301 DOI: 10.1088/1748-9326/6/3/035301.
- Garside C. A chemiluminescent technique for the determination of nanomolar concentrations of nitrate and nitrite in seawater. *Marine Chemistry.* **1982** Apr 1;11(2):159-67.
- Harrison, S.J. Investigating the Dynamic Range of Weathered Oil and Chemical Dispersant in the Environment. B.Sc. Thesis, Haverford College, Haverford, PA. **2013**.
- Incardona, J. P.; Carls, M. G.; Teraoka, H.; Sloan, C. A.; Tracy, K.; Scholz, N. L. Aryl Hydrocarbon Receptor-Independent Toxicity of Weathered Crude Oil during Fish Development Published by : The National Institute of Environmental Health Sciences Linked References Are Available on JSTOR for This Article : Aryl Hydroc. *Environ. Health Perspect.* **2005**, *113* (12), 1755–1762.

- Incardona, J. P.; Collier, T. K.; Scholz, N. L. Defects in Cardiac Function Precede Morphological Abnormalities in Fish Embryos Exposed to Polycyclic Aromatic Hydrocarbons. *Toxicol. Appl. Pharmacol.* **2004**, *196* (2), 191–205 DOI: 10.1016/j.taap.2003.11.026.
- Incardona, J. P.; Collier, T. K.; Scholz, N. L. Oil Spills and Fish Health: Exposing the Heart of the Matter. *J. Expo. Sci. Environ. Epidemiol.* **2011**, *21* (1), 3–4 DOI: 10.1038/jes.2010.51.
- Incardona, J. P.; Gardner, L. D.; Linbo, T. L.; Brown, T. L.; Esbaugh, A. J.; Mager, E. M.; Stieglitz, J. D.; French, B. L.; Labenia, J. S.; Laetz, C. A.; Tagal, M.; Sloan, C. A.; Elizur, A.; Benetti, D. D.; Grosell, M.; Block, B. A.; Scholz, N. L. PNAS Plus: From the Cover: Deepwater Horizon Crude Oil Impacts the Developing Hearts of Large Predatory Pelagic Fish. *Proc. Natl. Acad. Sci.* **2014**, *111* (15), E1510–E1518 DOI: 10.1073/pnas.1320950111.
- Kirchman, D. Measuring Bacterial Biomass Production and Growth Rates from Leucine Incorporation in Natural Aquatic Environments. *Methods Microbiol.* **2001**, *30*, 227–237.
- Kleindienst, S.; Seidel, M.; Ziervogel, K.; Grim, S.; Loftis, K.; Harrison, S.; Malkin, S. Y.; Perkins, M. J.; Field, J.; Sogin, M. L.; Dittmar, T.; Passow, U.; Medeiros, P. M.; Joye, S. B. Chemical Dispersants Can Suppress the Activity of Natural Oil-Degrading Microorganisms. *Proc. Natl. Acad. Sci.* **2015**, *112* (48) DOI: 10.1073/pnas.1507380112.
- Kozich, J. J.; Westcott, S. L.; Baxter, N. T.; Highlander, S. K.; Schloss, P. D. Development of a Dual-Index Sequencing Strategy and Curation Pipeline for Analyzing Amplicon Sequence Data on the Miseq Illumina Sequencing Platform. *Appl. Environ. Microbiol.* **2013**, *79* (17), 5112–5120 DOI: 10.1128/AEM.01043-13.
- Kujawinski, E. B.; Kido Soule, M. C.; Valentine, D. L.; Boysen, A. K.; Longnecker, K.; Redmond, M. C. Fate of Dispersants Associated with the Deepwater Horizon Oil Spill. *Environ. Sci. Technol.* **2011**, *45* (4), 1298–1306 DOI: 10.1021/es103838p.
- Leahy, J. G.; Colwell, R. R. Microbial Degradation of Hydrocarbons in the Environment. *Microbiol. Rev.* **1990**, *54* (3), 305–315.
- Lewis, A.; Daling, P.S. Oil spill dispersants. Guidelines on the Planning and Effective Use of Oil Spill Dispersants to Minimise the Effects of Oil Spills. AMOS Report. SINTEF, Trondheim. **2001**:1-13.
- Liu, Y.; Kujawinski, E. B. Chemical Composition and Potential Environmental Impacts of Water-Soluble Polar Crude Oil Components Inferred from ESI FT-ICR MS. *PLoS One* **2015**, *10* (9), e0136376 DOI: 10.1371/journal.pone.0136376.

- Major, D.; Zhang, Q.; Wang, G.; Wang, H. Oil-Dispersant Mixtures: Understanding Chemical Composition and Its Relation to Human Toxicity. *Toxicol. Environ. Chem.* **2012**, *94* (9), 1832–1845.
- McFarlin, K. M.; Prince, R. C.; Perkins, R.; Leigh, M. B. Biodegradation of Dispersed Oil in Arctic Seawater at -1°C. *PLoS One* **2014**, *9* (1), e84297 DOI: 10.1371/journal.pone.0084297.
- Pomeroy, L. R.; Sheldon, J. E.; Sheldon, W. M.; Peters, F. C. Limits to Growth and Respiration of Bacterioplankton in the Gulf of Mexico. *Mar. Ecol. Prog. Ser.* **1995**, *117*, 259–268.
- Prince, R. C. Oil Spill Dispersants: Boon or Bane? *Environ. Sci. Technol.* **2015**, *49* (11), 6376–6384 DOI: 10.1021/acs.est.5b00961.
- Prince, R. C.; McFarlin, K. M.; Butler, J. D.; Febbo, E. J.; Wang, F. C. Y.; Nedwed, T. J. The Primary Biodegradation of Dispersed Crude Oil in the Sea. *Chemosphere* **2013**, *90* (2), 521–526 DOI: 10.1016/j.chemosphere.2012.08.020.
- Seidel, M.; Kleindienst, S.; Dittmar, T.; Joye, S. B.; Medeiros, P. M. Biodegradation of Crude Oil and Dispersants in Deep Seawater from the Gulf of Mexico: Insights from Ultra-High Resolution Mass Spectrometry. *Deep Sea Res. Part II Top. Stud. Oceanogr.* **2015**, 1–11 DOI: 10.1016/j.dsr2.2015.05.012.
- Sibert, R. J.; Harrison, S. J.; Joye, S. B. Protocols for Radiotracer Estimation of Primary Hydrocarbon Oxidation in Oxygenated Seawater. In *Hydrocarbon and Lipid Microbiology Protocols*; McGenity, T. J., Timmis, K. N., Nogales, B., Eds.; Humana Press, **2016**; pp 263–276.
- Solorzano L. Determination of ammonia in natural waters by phenolhypochlorite method 1 1. This research was fully supported by US Atomic Energy Commission Contract No. ATS (11-1) GEN 10, PA 20. *Limnology and Oceanography.* **1969** Sep 1;14(5):799-801.
- Solorzano, L.; Sharp, J. H. Determination of Total Dissolved Phosphorous and Particulate Phosphorous in Natural Waters. *Limnol. Ocean.* **1980**, No. 1965, 754–758.
- Southward, A. J.; Southward, E. C. Recolonization of Rocky Shores in Cornwall after Use of Toxic Dispersants to Clean up the Torrey Canyon Spill. *J. Fish. Res. Board Canada* **1978**, *35* (5), 682–706 DOI: 10.1139/f78-120.
- Steffy, D. A.; Nichols, A. C.; Kiplagat, G. Investigating the Effectiveness of the Surfactant Dioctyl Sodium Sulfosuccinate to Disperse Oil in a Changing Marine Environment. *Ocean Sci. J.* **2012**, *46* (4), 299–305 DOI: 10.1007/s12601-011-0023-x.

Sunner, J.; Nishizawa, K.; Kebarle, P. Ion-Solvent Molecule Interactions in the Gas Phase. The Potassium Ion and Benzene. *J. Phys. Chem.* **1981**, *85*, 1814–1820.

Yang, L.; Adam, C.; Nichol, G. S.; Cockroft, S. L. How Much Do van Der Waals Dispersion Forces Contribute to Molecular Recognition in Solution? *Nat. Chem.* **2013**, *5* (12), 1006–1010 DOI: 10.1038/nchem.1779.

CHAPTER 5

LESSONS FROM THE TAYLOR ENERGY SITE

5.1 Take Home Lessons from this Study

The Taylor Energy site remains a haunting example for the offshore oil and gas industry, which as of 2012, had 2,996 oil and gas platforms in the Gulf of Mexico. The Taylor Energy oil spill has lasted for over 13 years and is expected to continue through the next century. Well capping, dome installation, and pipeline repair have cost TEC \$435 million, and yet oil continues to be spotted in the area. While this spill has largely escaped public notice, it remains, as of this writing, ongoing and the longest offshore oil spill in history.

In Chapter 2, we examined the historical record of oil slicks attributed to TEC in MC20 and found that oil slicks are larger and more frequently observed in summer months compared to winter months. Significant seasonal correlations between slick length with riverine and meteorological parameters suggest possible mechanisms for the size and frequency of surface slicks at the site.

In Chapter 3, we explored how these seasonal dynamics manifest in surface waters around the Taylor Energy site. In two small transects, we observed significant differences with respect to dissolved nutrient and DOC concentrations. While potential naphthalene oxidation rates were significantly higher in the summer transect compared to the fall transect, the potential rate of

hexadecane was found to be robust and not statistically different within the 8 stations sampled. While further investigation of the site is needed to untangle the influence of seasonal nutrient limitation and oil concentration on these rates, there is evidence of a robust and seasonally persistent hydrocarbon degrading community in these waters.

Chapter 4 is an early example of the kind of oil spill research that can be done at the Taylor Energy site. This short, microcosm amendment experiment compared how hydrocarbon oxidation rates changed in response to inorganic nutrient and/or chemical dispersant additions. This study found that there were no significant differences in the potential rate of hexadecane oxidation after 24 h of exposure to all treatments, but did find a significant increase in the potential rate of naphthalene oxidation in the presence of the chemical dispersant, Corexit. Corexit-amended treatments were found to have significant drawdowns of ammonium, total dissolved nitrogen, and phosphate, suggesting that Corexit makes surface communities more vulnerable to nutrient limitation.

5.2 Recognizing a Dynamic and Changing Gulf of Mexico

As petroleum exploration and production on the outer continental shelf (OCS) of the Gulf of Mexico has exponentially increased since the mid-1960s, the frequency of oil spills associated with offshore drilling has declined precipitously as both technology and safety have advanced. Between 1964-1970, one barrel of oil was spilled for every 4,000 barrels of oil produced; by the turn of the century, the ratio had dropped to 1 barrel for every 155,600 barrels produced, even as wells were drilled deeper and farther offshore (BOEM & BSEE, 2012). Having mastered the science and precision drilling in the Gulf demands, the oil and gas industry faces a new kind of challenge as it moves forward: a changing climate.

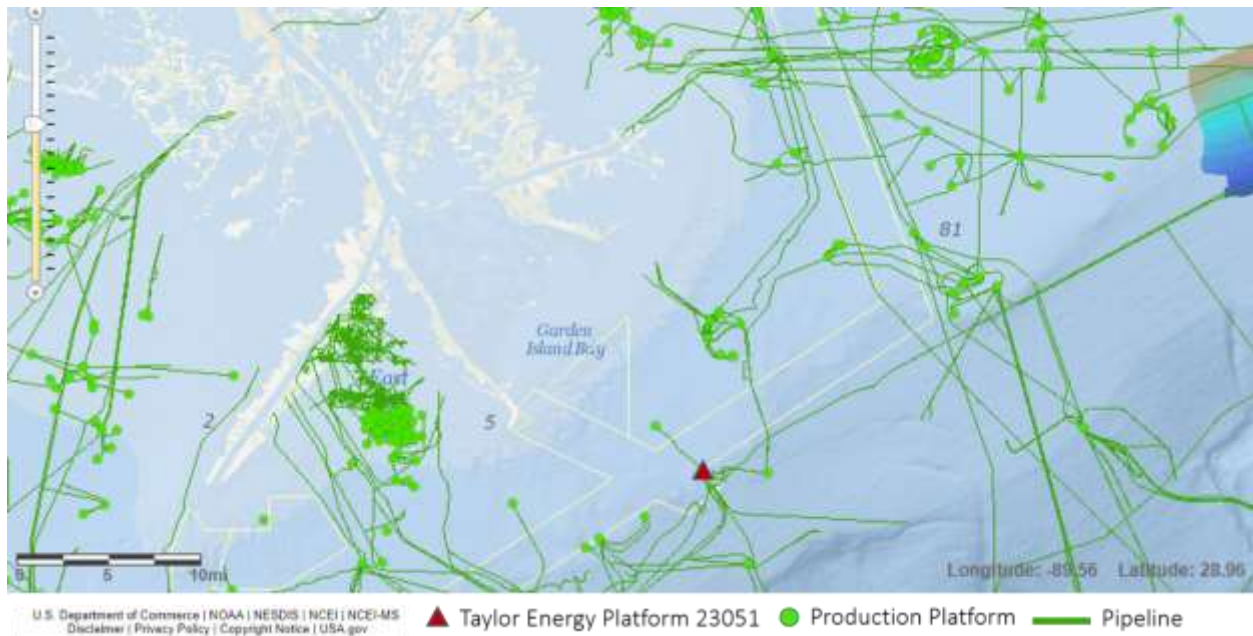


Figure 5.1 Map of oil production platforms and pipelines in the northern Gulf of Mexico; Taylor Energy platform 23051 is marked as a red triangle, while other production platforms are marked as green dots and pipelines as green lines.

Taylor Energy platform 23051 was one of seven production platforms destroyed and twenty-four production platforms significantly damaged by Hurricane Ivan as it approached the Gulf Coast. While this event has been described as an ‘Act of God’ in the courts, the Taylor Energy oil spill is perhaps a new kind of disaster, a chimeric anthropogenic natural disaster threatening our industrialized coasts in the Anthropocene. BOEM estimated that almost half of the 51,000 barrels of oil spilled on the OCS from 1995-2009 was lost during just six storms: Lili (2002), Ivan (2004), Katrina (2005), Rita (2005), Gustav (2008) and Ike (2008) (BOEM, 2016). Some of loss can be attributed to better record keeping; prior to 2004, oil lost from an OCS structure during a storm was not reported. Yet, this is a significant source of oil to coastal waters, given the estimated flux of oil from natural seeps in the Gulf of Mexico is estimated to be only 3,800 barrels/year or 604,150 L/year, diffusing from over 22,000 seeps (MacDonald *et al.* 1998; Joye *et al.* 2014). BSEE has estimated that the rate of oil leaking from the Taylor Energy site

could range from 1-55 barrels of oil per day, or 365-20,075 barrels per year, making it a sizable source of oil into the great Gulf of Mexico environment (Figure 5.2).

As the frequency of strong storms in the Gulf increases, and the long-used infrastructure along the coast and on the OCS continues to age, spills in the wake of large storms are destined to become more frequent and more dangerous. In August 2017, Hurricane Harvey inundated Houston, the seat of the petrochemical industry, with a record amount of rainfall, displacing thousands from their homes, and killing nearly 100 people. While the full cost of this hurricane has yet to be fully tabulated, early estimates range from \$70-109 billion (Quealy, 2017). This unprecedented storm, another chimeric anthropogenic-natural disaster, has released an untold amount of crude and refined products into neighborhoods and streams, which will run downriver to Galveston Bay, and ultimately back to the Gulf.

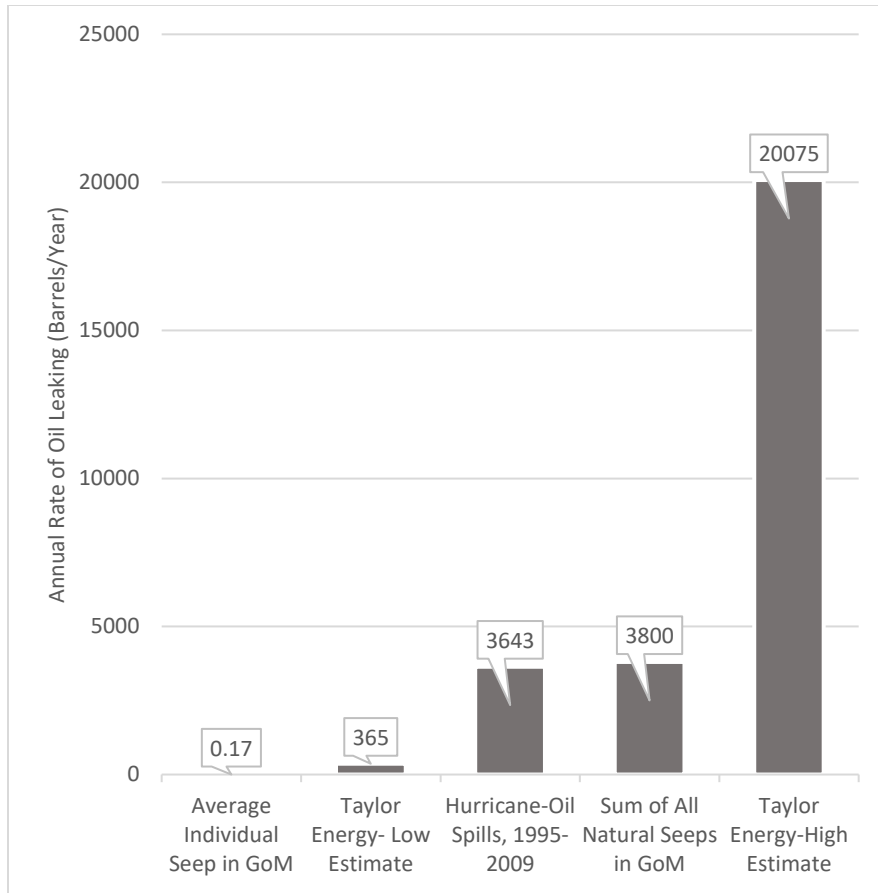


Figure 5.2 Comparison of annual oil fluxes from various sources in the Gulf of Mexico in barrels of oil per year.

References

Anderson, C. M.; Mayes, M.; Labelle, R. Update of Occurrence Rates for Offshore Oil Spills. **2012**, 87.

Bureau of Safety and Environmental Enforcement (BSEE) and Bureau of Ocean Energy Management (BOEM). Incident Archive- Taylor Energy Oil Discharge at MC-20 Site and Ongoing Response Efforts. Retrieved 5/1/2017 from <https://www.bsee.gov/newsroom/library/inc>. **2017**

Joye, S.B., Teske, A.P., Kotska, J.E. Microbial dynamics following the Macondo oil well blowout across Gulf of Mexico environments. *BioScience* **2014**, 64, 766-777.

Kaiser, M. J. Hurricane Clean-up Activity in the Gulf of Mexico, 2004 – 2013. **2015**, 51, 512–526.

MacDonald, I.R. Natural oil spills. *Sci. Amer.* **1998**, 279, 51-66.

Quealy, K. “The Cost of Hurricane Harvey: Only One Recent Storm Comes Close”, *New York Times: The Upshot*. Accessed from <https://www.nytimes.com/interactive/2017/09/01/upshot/cost-of-hurricane-harvey-only-one-storm-comes-close.html> on October 1, 2017.

APPENDIX

1. List of Abbreviations

BDL	Below detection limit
BOEM	Bureau of Ocean Energy Management
Bq	Becquerel, unit of radioactivity
BSEE	Bureau of Safety and Environmental Enforcement
CGMIX	U.S. Coast Guard Maritime Information Exchange
Ci	Curie, unit of radioactivity
CO ₂	Carbon dioxide
DOC	Dissolved organic carbon
DOI	Department of the Interior
DWH	<i>Deepwater Horizon</i>
FRACE	Final risk assessment and cost estimate
F _s	Slick Frequency
GC-FID	Gas chromatography-flame ionization detector
GC-MS	Gas chromatography-mass spectrometry
GC-TOF-MS	Gas chromatography-time of flight-mass spectrometry
GoM	Gulf of Mexico
HPO ₄ ³⁻	Ortho-phosphate
MC	Mississippi Canyon
MC20	Mississippi Canyon Lease Block 20, site of the Taylor Energy oil spill
MC252	Mississippi Canyon Lease Block 252, site of the <i>Deepwater Horizon</i> oil spill
MMS	Minerals Management Service
MOS	Marine oil-snow
MOSSFA	Marine oil-snow sedimentation and flocculation accumulation
NAVD	North American Vertical Datum of 1988
NDBC	National Data Buoy Center
NH ₄ ⁺	Ammonium
NO ₂ ⁻	Nitrite
NO ₃ ⁻	Nitrate
NOAA	National Oceanic and Atmospheric Administration
NO _x ⁻	Nitrate + Nitrite
NPOC	Non-purgeable organic carbon
NRC	National Response Center

NWS	National Weather Service
O ₂	Oxygen
OCS	Outer continental shelf
OPA	Oil Pollution Act of 1990
PAH	Polycyclic aromatic hydrocarbon
RC	Rate Constant
TDN	Total dissolved nitrogen
TDP	Total dissolved phosphate
TEC	Taylor Energy Company
TPH	Total petroleum hydrocarbon
UC	Unified Command
USCG	U.S. Coast Guard
USGS	U.S. Geological Survey
WAF	Water accommodated fraction

2. Statistical Analyses

Shapiro Wilk Normality Test

A Shapiro-Wilk normality test tests for normality of a given population. If the p-value is less than the chosen α level, then the null hypothesis (that the data are normally distributed) is rejected.

Kruskal-Wallis Rank Sum Test as a nonparametric analysis of variance

The Kruskal-Wallis rank sum test is a non-parametric test to determine if there is/are significant differences between two (or more) groups of an independent variable on a continuous or ordinal dependent variable.

Wilcoxon Rank Sum Test for Differences between Groups

The Wilcoxon rank-sum test is a nonparametric alternative to the t-test, which only works for normally distributed data. The Wilcoxon rank-sum test scores individual data points based on their rank, rather than their true value. While it is not as sensitive as a t-test, this test can be applied to determine the significant difference between two groups. A series of pairwise Wilcoxon rank sum tests were run to determine how the observed length varies within a single year.

Spearman's Rank for Correlation Analysis

Spearman's Rank Coefficient is denoted as ρ (rho) and measures the monotonic relationship of the variables, making the Spearman's correlation coefficient more reliable with non-linear data compared to Pearson's r value.

To interpret the value of ρ , the sign is indicative of whether the relationship between the two variables is negative (-) or positive (+). The value of ρ determines the strength of that relationship.

- 00-.19 :“very weak”
- .20-.39 :“weak”
- .40-.59: “moderate”
- .60-.79: “strong”
- .80-1.0: “very strong”

3. Equations

Slick Frequency: The number of reported slicks per days of the month in which the slicks were reported.

$$\text{Equation 2.1: } F_s = \frac{[\text{number of days with reported slick(s) in the month}]}{[\text{total number of days in the month}]} = n_s/n_{\text{total}}$$

For example: In January 2009, there were three days where a report was filed with the NRC reporting that oil slicks were sighted at the Taylor Energy site; therefore, the slick frequency for January 2009 is 0.09677419 (3 days with reports/31 days in January).

$$-\frac{d[\text{Hydrocarbon}]}{dt} = k[S] = \frac{\alpha}{t} [S] * \frac{[\text{Radioactivity turned over, dpm}]}{[\text{Radioactivity added, dpm}]} * \frac{[S]}{t}$$

Equation 3.1

Potential Hexadecane Oxidation Rate: [1-¹⁴C]-hexadecane + O₂ → ¹⁴CO₂ + H₂O

$$-\frac{d[\text{Hexadecane}]}{dt} = k[\text{Hexadecane}] = \frac{\alpha}{t} * [\text{Hexadecane}] = \frac{[^{14}\text{CO}_2]}{[^{14}\text{C} - \text{Hexadecane} * t]} * [\text{Hexadecane}]$$

Equation 3.2

Potential Naphthalene Oxidation Rate: [1,4,5,8-¹⁴C]-naphthalene + O₂ → ¹⁴CO₂ + H₂O

$$-\frac{d[\text{Naphthalene}]}{dt} = k[\text{Naphthalene}] = \frac{\alpha}{t} * [\text{Naphthalene}] = \frac{[^{14}\text{CO}_2]}{[^{14}\text{C} - \text{Naphthalene} * t]} * [\text{Naphthalene}]$$

Equation 3.3

$$[\text{Hexadecane tracer}] = \frac{\text{Radioactivity of added tracer, dpm}}{\text{Volume of incubation vessel, mL}} * \frac{1 \text{ mCi}}{2.22 \times 10^9 \text{ dpm}} * \frac{1 \text{ mmol}}{55 \text{ mCi}}$$

Equation 3.4

$$[\text{Naphthalene tracer}] = \frac{\text{Radioactivity of added tracer, dpm}}{\text{Volume of incubation vessel, mL}} * \frac{1 \text{ mCi}}{2.22 \times 10^9 \text{ dpm}} * \frac{1 \text{ mmol}}{58 \text{ mCi}}$$

Equation 3.5

$$-\frac{d[\text{Hydrocarbon}]}{dt} = k[S] = \frac{\alpha}{t} [S] * \frac{[\text{Radioactivity turned over, dpm}]}{[\text{Radioactivity added, dpm}]} * \frac{[S]}{t}$$

Equation 4.1

Potential Hexadecane Oxidation Rate: [1-¹⁴C]-hexadecane + O₂ → ¹⁴CO₂ + H₂O

$$-\frac{d[\text{Hexadecane}]}{dt} = k[\text{Hexadecane}] = \frac{\alpha}{t} * [\text{Hexadecane}] = \frac{[^{14}\text{CO}_2]}{[^{14}\text{C} - \text{Hexadecane} * t]} * [\text{Hexadecane}]$$

Equation 4.2

Potential Naphthalene Oxidation Rate: $[1,4,5,8-^{14}\text{C}]\text{-naphthalene} + \text{O}_2 \rightarrow ^{14}\text{CO}_2 + \text{H}_2\text{O}$

$$-\frac{d[\text{Naphthalene}]}{dt} = k[\text{Naphthalene}] = \frac{\alpha}{t} * [\text{Naphthalene}] = \frac{[^{14}\text{CO}_2]}{[^{14}\text{C} - \text{Naphthalene} * t]} * [\text{Naphthalene}]$$

Equation 4.3

$$[\text{Hexadecane tracer}] = \frac{\text{Radioactivity of added tracer, dpm}}{\text{Volume of incubation vessel, mL}} * \frac{1 \text{ mCi}}{2.22 \times 10^9 \text{ dpm}} * \frac{1 \text{ mmol}}{55 \text{ mCi}}$$

Equation 4.4

$$[\text{Naphthalene tracer}] = \frac{\text{Radioactivity of added tracer, dpm}}{\text{Volume of incubation vessel, mL}} * \frac{1 \text{ mCi}}{2.22 \times 10^9 \text{ dpm}} * \frac{1 \text{ mmol}}{58 \text{ mCi}}$$

Equation 4.5